Wearable System with Integrated Passive Microfluidics for Real-Time Electrolyte Sensing in Human Sweat

THÈSE N^O 8849 (2018)

PRÉSENTÉE LE 21 SEPTEMBRE 2018
À LA FACULTÉ DES SCIENCES ET TECHNIQUES DE L'INGÉNIEUR
LABORATOIRE DES DISPOSITIFS NANOÉLECTRONIQUES
PROGRAMME DOCTORAL EN MICROSYSTÈMES ET MICROÉLECTRONIQUE

ÉCOLE POLYTECHNIQUE FÉDÉRALE DE LAUSANNE

POUR L'OBTENTION DU GRADE DE DOCTEUR ÈS SCIENCES

PAR

Erick Antonio GARCIA CORDERO

acceptée sur proposition du jury:

Dr J.-M. Sallese, président du jury
Prof. M. A. Ionescu, directeur de thèse
Dr L. Gervais, rapporteur
Prof. G. Fagas, rapporteur
Prof. A. Radenovic, rapporteuse

Todo aquel que tenga el honor de disponer de una pluma, de una tribuna o de una cátedra, tiene la obligación de consultar la salud de la sociedad en la que vive.

Justo Sierra, 1893

To my parents and siblings…

Acknowledgments

This thesis is the result of the teachings, and help from people I had the pleasure to work with during these last four years in Switzerland. My special gratitude to Professor Ionescu for his continuous support and patience during my PhD. I am thankful he let me orient my research path with a lot of freedom while keeping me on track of the high level requirements of my project. Adrian has given me the chance to work in a very interesting multidisciplinary PhD, indeed, the most exciting and challenging project I have ever worked in.

I would like to acknowledge the members of the jury that have accepted to review this thesis: Prof. Georgios Fagas from Tyndall University in Ireland, Dr. Luc Gervais, CEO of the 1Drop Diagnostics in Switzerland, Dr. Jean Michelle-Sallèse, President of the Jury, and Prof. Aleksandra Radenovic, head of the Laboratory of Nanoscale Biology in EPFL. I would like to thank Prof. Radenovic for trusting me and for encouraging me to pursue my career in EPFL all those years ago.

I have had the chance to work with a lot of people in this project, I would like to express my most sincere gratitude with all of you. Sara, thank you for being the greatest mentor for me when I was a rookie, for all of those great memories we built, and for bringing me into this project. Alex, thanks for all the "come on man, we can make this" during my first year, eventually it became a skill that helped me survive the deadlines. Hoël, thanks for taking care of me during the rest of my PhD! I don't know if I'd have made it without your advice and mentoring.

Fabien & Johan, thank you both for teaching me so much on your respective domains, and for the great energy you guys have brought into the group. I am really glad I got to build a team with you. To the rest of the Xsensio family, Negar, Clementine, Rafaelle, Pietro, Guillaume, Amira, & Esmeralda, this has been a great journey with you all. To my office mates: you guys are family. Francesco, thanks

for having my back all these years bro. Manee, thanks for keeping an eye on me! & JunRui, thanks for being such a great teammate.

Thanks to Karin, Isabelle, Raymond & Lucie, that have had the patience to deal with my administrative procedures. I am also thankful with the CMi staff for their support during my time in the cleanroom. Special mention to Giancarlo Corradini, whom received me with last minute requirements more times than I can count. I'd like to thank also Prof. Salvador Venegas in Mexico for being so supportive in my process to obtain the PhD position.

To the people that made my life in Lausanne very joyful. Thanks to my Italian godparents Marco & Fabri, that gladly adopted me when I got in Lausanne. Thanks to Pablo for the great talks, advices and laughs we have had together. Thanks to Pau, Gustavo & Nadia, for all the encouragement I get from you. To my friends Migrolino, Ileana, & Fernando, for all the good times we spent together.

Last but not least, I'd like to thank my dear family. Mamá, papá, no tengo cómo agradecerles todos los sacrificios que han hecho por mí. Les doy las gracias por todas sus enseñanzas, su apoyo y su cariño. Pepe, gracias por haberme llevado de la mano desde pequeño y por inspirarme a hacer carrera en la ciencia. Dianita, muchas gracias por estar siempre al pendiente de mí y por todos los consejos y ánimos que me has dado para salir adelante. Sin el apoyo de ustedes y sin su ejemplo, no estaría en donde estoy. Los amo.

Lausanne, 11 Juin 2018

Abstract

Wearable systems embodied as patches could offer noninvasive and real-time solutions for monitoring of biomarkers in human sweat as an alternative to blood testing, with applications in personalized and preventive healthcare. Sweat is considered to be a biofluid of foremost interest for analysis due the numerous biomarkers it contains. Recent studies have demonstrated that the concentration of some of these biomarkers in sweat, such as the electrolytes studied in this work, can be directly correlated to their concentrations in blood, making sweat a trusted biofluid candidate for non-invasive diagnostics.

Until now, the biggest impediment to on-body sweat monitoring was the lack of technology to analyze sweat composition in real-time and mainly to continuously collect it. The goal of this work was to develop the building blocks of such wearable system for sweat electrolyte monitoring, with main emphasis on the passive microfluidics, the integrated miniaturized quasi-reference electrode and the functionalization of the sensing devices. The basic sensor technology is formed by Ion Sensitive Field Effect Transistors (ISFET) realized in FinFET and ultra-thin body Silicon on Insulator technology.

This thesis shows the development of a state-of-the-art microsystem that allows multisensing of pH, Na^+, K^+ electrolyte concentrations in sweat, with high selectivity and high sensitivities (≈ 50 mV/dec for all electrolytes), in a wearable fashion. The microsystem comprises a biocompatible skin interface that collects even infinitesimal quantities of sweat (of the order of hundreds of picoliters to tenths of nanoliters), which the body produces in periods of low physical effort. One of the main achievements of this work is the integration of Ion Sensing Fully Depleted FETs and zero power consumption microfluidics, enabling low power (less than 50 nWatts/sensor) wearable biosensing. The thesis presents the needed technological processes and optimizations, together with their characterization, in order to achieve a Lab-On-Skin system.

Résumé

Un système portatif sous la forme d'un patch offrirait une solution pour mesurer des bio-marqueurs dans la sueur humaine en temps réel and de manière non-invasive, comme alternative aux tests sanguins, avec des applications en médecine personnalisée et préventive. La sueur est considérée comme un bio-fluide d'intérêt primordial pour l'analyse au vu des nombreux bio-marqueurs qu'elle contient. Des études récentes ont démontré que les concentrations de certains bio-marqueurs dans la sueur, comme les électrolytes étudiés dans ce travail, peuvent être directement corrélées à leurs concentrations dans le sang, faisant de la sueur un candidat fiable comme bio-fluide pour des diagnostiques non-invasifs.

Jusqu'à présent, le plus grand obstacle pour une mesure de la sueur sur le corps était le manque de technologie pour analyser la composition de la sueur en temps-réel, et principalement pour la collecter en continu. Le but de ce travail consiste à développer les modules constituant un tel système portatif pour la mesure d'électrolytes dans la sueur, avec une emphase particulière sur la micro-fluidique passive, l'électrode de référence miniaturisée intégrée, et la fonctionnalisation des dispositifs de capteurs. La technologie des capteurs est basée sur des transistors à effet de champs (field effet transistors, FET) sensibles aux ions (Ion sensitive FET, ISFET) réalisés sous forme de FET à ailerons (FinFET) ou de FET en silicium sur isolant (silicon on insulator, SOI) ultra-mince.

Cette thèse présente le développement d'un microsystème prêt à porter à la pointe de la technologie permettant la mesure simultanée du pH ainsi que de différents analytes tels le sodium et le potassium dans la sueur avec une grande sensibilité (50mV/dec) et sélectivité. Le microsystème comporte une interface de collecte de la sueur compatible avec la peau afin de récolter des quantités infinitésimales de sueur de l'ordre d'une centaine de picolitres à quelques dizaines de nanolitres produits lorsque le corps est au repos. L'un des principaux accomplissements de ce travail est l'intégration d'un système basé sur des transistors à effet de champ

sensible à différents analytes couplé à une interface microfluidique permettant la création d'un système portable de suivi de bio-marqueurs basse consommation (moins de 50nW par senseur). Cette thèse présente les processus technologiques et optimisations nécessaires ainsi que leurs caractérisations dans le but d'obtenir un système Lab-on-skin.

Mots-clés: capteur portable; analyse de la transpiration; FinFET; FD SOI ISFET; microfluidique cutanée; microfluidique avec la SU-8; microfluidique passive; capteur sans étiquette; détection biochimique; intégration hétérogène; électrode Ag/AgCl de quasi-référence miniaturisée.

Contents

List of Figures

xviii

List of Tables

List of equations

Nomenclature

Acronym/Abbreviation	Description
A	Cross section Area
Ag	Silver
Ag/AgCl	Silver/Silver Chloride
Al	Aluminium
Al_2O_3	Aluminium Oxide
ALD	Atomic Layer Deposition
AlSi	Aluminium-Silicon
APTES	(3-aminopropyl)triethoxysilane
Au	Gold
CA	Contact Angle
Ca	Adsorption Capacitance
C_{acc}	Accumulation Capacitance
C_{dep}	Depletion Capacitance
C_{dif}	Diffuse Layer Capacitance
C_{DL}	Double Layer Capacitance
C_{MAX}	Maximum Capacitance
CMOS	Complementary Metal-Oxide-Conductor
Cox	Oxide Capacitance
C_P	Parasitic Capacitance
Cr	Chromium
C_S	Semiconductor Capacitance
C_{Si}	Silicon Capacitance
DI	deionized
E_G	Energy Band Gap
E_{OS}	Electric-Oxide-Semiconductor
E_{REF}	Reference Electrode Potential
FD	Fully Depleted
FDA	U.S. Food and Drug Administration
$FeCl_2$	Iron Chloride
$FeCl_3$	Ferric Chloride
FET	Field Effect Transistor
g_{DS}	Output conductance
g_m	Transconductance

H	Hydrogen
H_2O_2	Hydrogen Peroxide
H_2SO_4	Sulfuric Acid
HCl	Hydrogen Chloride
H_{fin}	Fin Height
HfO_2	Hafnium Oxide
IC	Integrated Circuit
I_D	Drain current
I_G	Gate current
IPA	Isopropanol Alcohol
ISE	Ion Selective Electrode
ISFET	Ion Sensitive Field Effect Transistor
ISM	Ion Sensitive Membrane
I_{TH}	Threshold current
K	Potassium
k	Boltzmann Constant
Ka	Acid dissociation Constant
Kb	Base dissociation Constant
KCl	Potassium Chloride
L	Length
La_2O_3	Lanthanum Oxide
L_{fin}	Fin Length
LPCVD	Low Pressure Chemical Vapor Deposition
ml	milliliter
mM	milimolar
MOSFET	Metal-Oxide-Silicon Field Effect Transistor
N2	Nitrogen
Na	Sodium
nA	Acceptor Dopant Dose
NA	Acceptor Dopant Concentration
NaCl	Sodium Chloride
ND	Donor Donant Concentration
n_i	Intrinsic Carrier concentration
nl	nanoliter
NS	Surface Site Density
OCP	Open Circuit Potential
OH	Hydroxide
P	Power

P_C	Interfacial Pressure
PCB	Printed Circuit Board
PDMS	Polydimethylsiloxane
PGMEA	Propylene Glycol Monomethyl Ether Acetate
pH	Hydrogen Potential
pl	picoliter
PSA	Pressure Sensitive Adhesive
Pt	Platinum
PVB	Polyvinyl Butyral
q	Elementary Charge
Q	Volumetric Flow Rate
Q_D	Depletion Charge
Q_{OX}	Oxidation Quality Factor
Q_{RE}	Quasi Reference Electrode
S	Sensitivity
S/V	Surface to Volume Ratio
SAMs	Self-Assembled Monolayers
SEM	Scanning Electron Microscopy
SHE	Standard Hydrogen Electrode
Si	Silicon
Si_3N_4	Silicon Nitride
SiO_2	Silicon Oxide
Si_{Ox}	IL Oxide
SOI	Silicon On Insulator
S_{out}	Readout Sensitivity
SS	Subthreshold Slope
T	Temperature
Ta_2O_5	Tantalum Oxide
TFin	Fin Thickness
t_{HfO2}	Hafnium Oxide Thickness
Ti	Titanium
TiO_2	Titanium Oxide
UT	Ultra-Thin
UV	Ultra Violet
V_D	Drain Voltage
V_{DS}	Source to Drain Voltage
V_G	Gate Voltage
V_H	Hysteresis Amplitude

xxvii

V_{IN}	Input Voltage
V_{REF}	Reference Voltage
V_S	Source Voltage
V_{TH}	Threshold Voltage
W	Width
ZrO_2	Zirconium Oxide

Greek letters

Acronym/Abbreviation	Description
α	Sensitivity Parameter
β	Surface Buffer Capacitance
β	Substrate Correction for EBL
ε_0	Vacuum Permittivity
ε_{ins}	Insulator Dielectric Constant
ε_{Ox}	Oxide Dielectric Constant
ε_{Si}	Silicon Dielectric Constant
ε_{SiO2}	Silicon Oxide Dielectric Constant
ε_{SiOx}	IL Oxide Dielectric Constant
η_e	Density Correction for EBL
λ_D	Debye Length
μ	Fluid Viscosity
μ_n	Electron Mobility
μ_0	Maximum Mobility
μ_S	Surface Mobility
σ	Standard Deviation
χ_{sol}	Surface Dipole Potential
ψ	Oxide-Electrolyte Potential
φ_M	Metal Work Function
φ_{Si}	Silicon Work Function
φ_s	Surface Potential
φ_f	Fermi Potential
Υ	Surface Tension

Chapter 1   Introduction

In this chapter the motivations and goals of this work are presented. A brief introduction to sweat analysis is given in order for the reader to get immersed into the importance of the analysis of this biofluid. Afterwards, the structure of this thesis is presented.

1.1 Rationale & objectives

Personalized and preventive healthcare could be revolutionized through real-time analysis of biochemical markers in biofluids. Access to the biochemical information of a person could provide a more accurate picture of health and wellness parameters. Today, this typically means a blood test in laboratory: a process that is precise, but invasive, and offering only a snapshot at a given point in time. Furthermore, pressure to reduce medical expenditure [1] have incited the healthcare ecosystem to look into preventive health and look for alternatives to blood testing, notably wearable, noninvasive and continuous sweat monitoring [2] [3].

The field of wearable technologies aims to offer individuals information about their evolving physiology. Continuous collection of data could be used to generate statistics that, parsed with big data techniques, would help to generate personalized baselines with indications of the user's health status [4] [5] [6]. Today, wearable technology available in the market is focused on tracking physical activity and vital signs like heart rate and blood oxygen saturation [7], but they fail to provide molecular-level information related to the body's dynamic chemistry [8]. This is where sweat analysis becomes extremely relevant.

Many of the biomarkers available in blood are also available in sweat, and particular conditions (cystic fibrosis [9], dehydration [10] [11] [12] [13],

hyponatremia [14]) have been associated with changes in biomarkers available in sweat. Until now, the biggest impediment to on-body sweat monitoring was the lack of technology to analyze sweat composition in real-time and mainly to continuously collect it [15], but the recent advances in nanosensors and the development of microfluidic biochips pave the way towards full biochemical microsystems.

The objective of this thesis is to develop of a zero-power, intelligent, autonomous wearable system to track biochemical information at the surface of the skin in real time. This system heterogeneously integrates state-of-the-art ISFET sensor technology, with a biocompatible microfluidic interface, to deliver the first "Lab-on-skin" sensing platform. The full process for fabrication of this system is achieved by standard semiconductor fabrication procedures.

This work gives first an introduction to sweat analysis, the reasons behind the research and a state-of-the-art investigation of wearable devices for sweat available today. Afterwards, the modules of the wearable system are presented: chapter 3 presents the sensing technology and chapter 4 the wearable microfluidic system. Chapter 5 presents the heterogeneous integration of the modules with a miniaturized quasi reference electrode. In addition, three functionalization methods are proposed for the detection of Sodium and Potassium sensing with ISFETs. Chapter 6 presents the electrical characterization of the system for both Sodium and Potassium sensing in an analyte.

This project has been developed with a funding from the Swiss National Science Foundation via the Flag-Era CONVERGENCE project and in collaboration with the Swiss start-up XSensio.

1.2 Thesis outline

This thesis is divided in seven chapters including this one.

Chapter 1: Thesis overview

The current chapter presented the background of the research, and the motivations and goals of this thesis.

Chapter 2: Sweat analysis

This chapter explains the attractiveness of monitoring the biochemical composition of sweat. The main biomarkers present in sweat are mentioned and thus, the advantages of using sweat as a tool for monitoring physiological information relevant to the health and wellness of an individual. In addition, this chapter describes human skin as a microfluidic system, allowing to extract critical parameters for the design of a biocompatible microfluidic system, capable of collecting even infinitesimally small sweat droplets directly from skin.

Chapter 3: Sensing with computing technology
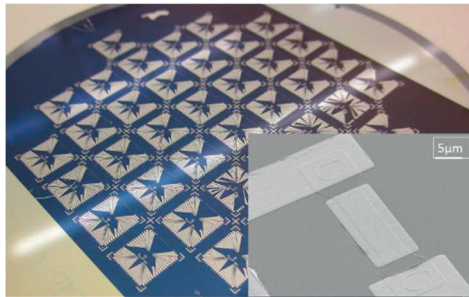
This chapter introduces high-k dielectric Ion Sensitive Field Effect Transistors (ISFETs) as the main sensing technology for the wearable system. The chapter describes the advantages of using Complementary Metal-Oxide Semiconductor (CMOS) compatible technology in a system as a step forward to low power robust sensing system. Two main architectures of high-k ISFETs technology were used in the validation of the wearable system: FinFET in Silicon Bulk and Fully Depleted Silicon-On-Insulator (FD SOI) nanoribbon ISFETs. A description of both architectures is given and a discussion is developed on the advantages of using these devices as pH sensing devices.

Chapter 4: Wearable passive microfluidics for sweat collection and analysis
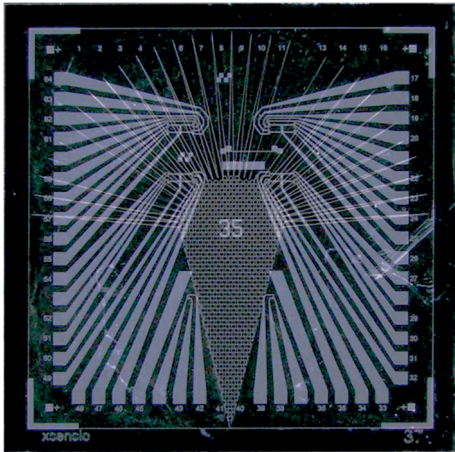
The development of a wearable microfluidic interface compatible with skin is presented. The microfluidic system presents an optimized design of capillary channels for a fully passive flow control of the sweat collected on the skin and delivered to the sensors. Materials and fabrication processes are fully compatible with post-processing of silicon wafer for direct on-chip integration for the wearable sensing technology.

Chapter 5: Heterogeneous Integration of functionalized ISFETs with embedded passive capillary microfluidics and miniaturized Ag/AgCl Q.R.E
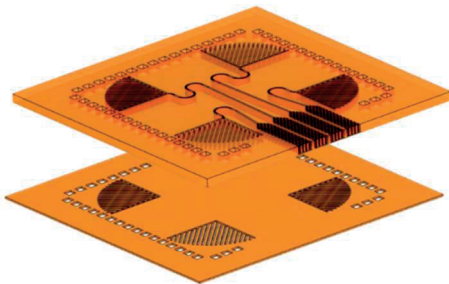
The research presented in this chapter shows the integration of the microfluidic interface with ISFETs. The chapter presents a proposal for a miniaturized Quasi Reference Electrode to be used in the miniaturized system. This R.E. is capable to offer stable and fully calibrated measurements of the biomarkers in the analyte with long term stable operation (13 days). In addition, three methods for ISFET functionalization are proposed and discussed. After experimentation it was possible to observe that the most reliable functionalization method is to use a polymeric membrane on top of a gold metallic gate to sense K^+ and Na^+ electrolytes.

4

Chapter 6: Experimental results: Fully integrated system for wearable multi sensing sweat applications
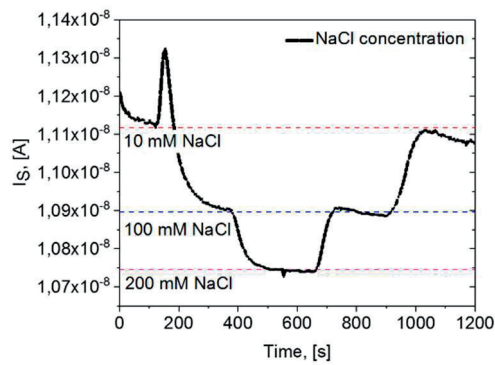
The sensing performance characterization results for Sodium and Potassium sensing under transient conditions are finally given in this chapter. The FD SOI nanoribbon ISFET with a polymeric membrane is successfully demonstrated here as a highly robust, sensitive, and selective sensor for pH, Na^+ and K^+ ($\approx$50 mV/dec for all electrolytes).

Chapter 7: Conclusions and outlook

The last chapter summarizes the main technical contributions and achievements reported in the manuscript. It provides a brief outlook and suggests topics of interest for further work.
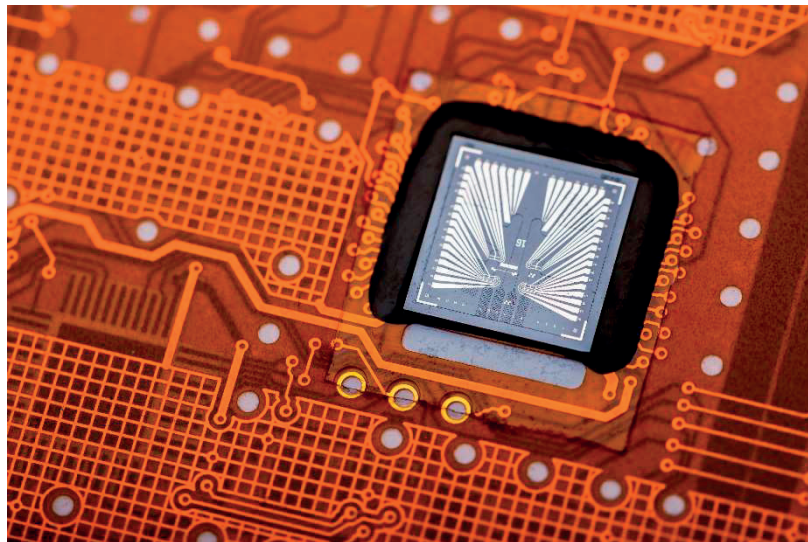
Chapter 2 Sweat sensing

This chapter explores the possibilities that continuous sweat sensing offers for healthcare and wellness applications. Sweat could become a very relevant biofluid as its biochemical composition is interrelated with several blood biomarkers. Proper understanding on how blood and sweat biomarkers are correlated could provide tools for preventive healthcare and disease diagnostics. This chapter provides a list of these biomarkers. In addition, this chapter summarizes efforts in literature to describe human skin as a microfluidic system. This is a relevant study for this work as its sets a foundational guide for further development of wearables for sweat.

2.1 Biomarkers in human sweat

Sweat is produced in the skin by a collection of glands and serves as a thermal regulation system for the body. There are two main types of sweat glands, eccrine and apocrine. Eccrine glands are distributed almost all over the human body whereas apocrine are mostly limited to the axilla and perianal areas in humans [16] [17] [18]. Further discussion in this thesis is limited to the sweat produced by the eccrine sweat gland. Apocrine glands have a different secretion process that goes beyond the scope of this work.

The rich composition of biomarkers in eccrine sweat, altogether with the fact that it can be collected in a noninvasive fashion, makes it a very interesting biofluid for analysis. Sweat sensing technologies then have enormous potential to be used for wellness and healthcare applications [19] [20] [21]. Enabling continuous biomonitoring of sweat could trigger a paradigm shift in the biomedical community.

Sweat is mainly composed of water (usually 99%) [22], with moderately acidic to neutral pH levels (4.5-6) [23]. It also contains minerals, specifically electrolytes, like Sodium, Potassium, Chloride (in mM concentration), and Ammonia, which ionizes with high sweat pH reaching milimolar concentrations (several times higher than in blood) [19] [24]. In addition, other organic substances can be traced in transpiration, like aminoacids [25] [26] [27], lactic acid and butyric acid [28] [29]. Urea and lactate can be generated from blood or directly from the sweat gland and are also found in milimolar concentrations in sweat. Glucose can be traced in a μM range of concentration. Proteins like hormones and neuropeptides can be traced in nano molar or pico molar range of concentrations [24]. Table 2.1 summarizes the analytes found in sweat and their typical concentration levels, altogether with typical sensing layers found in literature, which is data that is relevant for the discussion in the subsequent chapters of this thesis.

Today, sweat analysis is mainly used for detection of cystic fibrosis [30]. Patients with cystic fibrosis have a very high concentration of chloride in their sweat, showing a malfunction in the sweat glands. Sweat has also been used for detection of illicit drugs, as drug metabolites are expelled by sweat [31] [32]. These tests are still performed in laboratories and in the clinic [19]. The main limitations of sweat as a clinical sample are the difficulty to produce enough sweat for analysis, sample evaporation, lack of appropriate sampling devices [33]. Wearable devices can solve many of these issues as the sweat is collected and analyzed in real time, directly from the skin.

2.1.1 Sweat biomarkers' correlation with blood biomarkers

Recent studies show that sweat contains many of the same biomarkers as blood. The correlation between the biomarkers in both biofluids may lead to the development of better diagnostics tools. However, there is still a lack of biomarker partitioning models between sweat and blood [19]. Further understanding of

partitioning models will help to obtain better opportunities for sweat-based diagnostics.

As of today, studies of biomarker partitioning have been done for some electrolytes (Sodium, Potassium, Chloride and Ammonia), and small molecules like ethanol, cortisol, urea and lactate. Biomarker partitioning models with sweat are based on the direct correlation with blood, plasma or serum. It is important to make the distinction as concentrations of biomarkers in blood do not represent the concentration in serum or plasma [19].

Table 2.1. Summary of studied biomarkers in sweat. Adapted from [24].

Sensing modality	*Targeted Analyte*	*Concentration in sweat*	*Sensing layer*	*References*
Potentiometry	pH	3-8	polyaniline	[34] [35]
	Na^+	10-100 mM	Na ionophore	[34] [36]
	K^+	1-18.5 mM	K ionophore	[36]
	Cl^-	10-100 mM	Ag/AgCl	[36]
	Ca^{2+}	.41-12.4 mM	Ca ionophore	[35] [36]
	NH^{4+}	0.1-1 mM	NH^{4+} ionophore	[37]
Chrono-amperometry	Glucose	100-200 μM	Glucose oxidase	[38]
	Lactate	5-20 mM	Lactate oxidase	[34]
	Ethanol	2.5-22.5 mM	Alcohol oxidase	[39] [40]
Cyclic Voltammetry	Uric acid	2-10 mM	Carbon	[41]
	Ascorbic acid	10-50 M	Carbon	[41] [42]

Sensing modality	Targeted Analyte	Concentration in sweat	Sensing layer	References
	Zn^{2+}	100-1560 µg l^{-1}	Bi	[43]
	Cd^{2+}	<100 µg l^{-1}	Bi	[43]
Square wave stripping voltammetry	Pb^{2+}	<100 µg l^{-1}	Bi, Au	[43]
	Cu^{2+}	<100-1000 µg l^{-1}	Au	[43]
	Hg^{+}	<100 µg l^{-1}	Au	[43]
Electrochemical impedance spectroscopy	Cortisol	8-140 ng ml^{-1}	ZnO, MoS$_2$	[44] [45]

2.1.2 Case study for sodium and potassium levels in sweat

This thesis shows the development of a wearable sensor that is able to detect concentrations of sodium and potassium in an analyte. This section explains the applications that can be targeted with the detection of these markers.

Measurements of sodium chloride in sweat can be used to predict hormonal changes that lead to ovulation [46] and could be used for predicting sweat rates [19]. This is especially important as it has been proven that some biomarkers are rate dependent (like lactate and chloride). This is possible since Sodium and Chloride are the dominantly abundant ions in sweat.

Potassium is an interesting ion in sweat as it is proportional to blood concentration and completely independent from the sweat rate. Concentration in plasma predicts muscle activity [47] and certain conditions related to hypo or hypherkalemia [48].

2.2 Microfluidics of the sweat gland

The human eccrine gland is constituted of different components (Fig 2.1), which are the secretory coil, the dermal duct and the upper coiled duct. In the upper duct, the sweat duct expands in diameter, until it arrives to the surface of the skin as a pore. The physical dimensions of these components can vary depending on gender, age, and race [22] [49]. The secretary coil can measure up to 700 µm in diameter, with a length that can measure up to 5 millimeters. The inner diameter of the secretary coil and the dermal ducts have diameters ranging from 5-10 µm. Different parts of the body have different gland densities [50]. Densities across the body are summarized in the table 2.2.
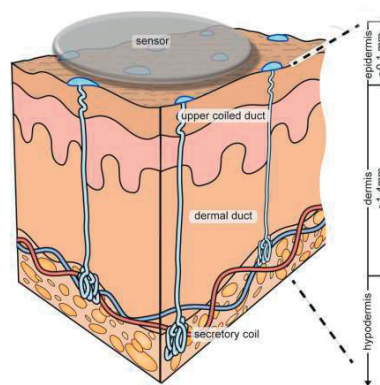
Figure 2.1 Structure of the human sweat glands [19].

Regarding the hydraulic capabilities of the sweat glands, sweat rates can go as high as 5-10 nl/min/gland. Considering a wearable device to be attached in the forearm, the sweat rate would go up to 1.5 µliters per cm^2 per minute. This number is to be considered in periods of physical activities. On the other hand, in steady-state, the volume of sweat produced reduces dramatically, reaching values in the order to 20 nanoliters per cm^2 per minute [50] [19].

Table 2.2. Gland density approximation per location in the body. Adapted from [19]

Location	Approximately gland density (per cm²)
Abdomen/back/legs	100
Forehead/forearm	150
Palm/finger	250
Toe	550

2.3 State-of-the-Art of wearable sweat sensing

In this introductory state-of-the-art, the latest wearable sweat sensors are briefly described. These wearable sweat sensors combine different substrates and detection mechanisms. The wearable sweat devices vary in form depending on the targeted application. For sports application the preferred wearable design focuses on wrist or head bands, whereas for medical purposes, a patch seem to be more attractive [24].

One of the latest wearable sweat sensors (Fig 2.4a) was designed by Gao et al [3]. It shows a system of electrochemical sensors packaged in a wristband capable of measuring metabolites (glucose and lactate), and electrolytes (sodium and potassium), as well as skin temperature. Sodium and potassium sensors showed sensitivities of 62.5 mV and 59.5 mV per decade of concentration, respectively, in ambient conditions. The detection of the analytes is done with two electrodes (3mm diameter) coated with a selective membrane consisting of an ionophore (for Na^+ and K^+). Large amounts of sweat are required to perform the biochemical analysis (minimum 30 microliters to cover the whole surface of a single electrode).

Rose and Heikenfeld proposed an adhesive RFID sensor patch (Fig 2.4b) for electrolyte monitoring on sweat [51]. The patch offers a read out dynamic range with 20-70 mM range in the detection of Sodium, using a potentiometric modality for detection of the biomarker. Values of 57mV/dec of Na^+ were measured in the laboratory (25mV/dec in wearable format). In posterior works, Sonner and Heikenfeld developed a wearable sweat sensing system which induce sweating with iontophoresis. The new system included an Ag/AgCl chloride sensor [52]. The works by Choi et al., also propose the use of an Ag/AgCl for chloride sensing in a wearable system [53]. The works by Kim et al. [54] proposes the use of a patch that employs an amperometric detection method of alcohol in sweat with a sensitivity of 0.36 µA/dec.

Koh and Rodgers propose a colorimetric approach for analyte detection in sweat [55]. It is composed of electrochemical electrodes printed in a temporary tattoo paper (Fig 2.4c). The device is design to detect lactate, glucose, pH and chloride. This device is designed for single use, although, it is the only wearable system (besides the one presented in this work) considering the use of a controlled microfluidic environment on skin.

To our knowledge, there are only 3 publications in which ISFETs are used as the sensing unit for sweat analysis. The work of Nagata and Takei, propose a wearable device (Fig 2.4d) based on ISFETs for pH measurements and skin temperature monitoring [56]. They report a sensitivity for pH of 51 mV/dec with an Al_2O_3 gate oxide. The work of Cazale et al [57] successfully used functionalized ISFETs to quantify sodium levels in sweat with a sensitivity of 57 mV/dec, however this was not tested in a wearable format. The works of Douthwaite [58] present a wearable sweat pH sensor with CMOS ISFETs with a sensitivity of approximately 50 mV/pH. This work is the only sweat sensing system, besides our own, that considers and quantifies the low power consumption of the sensing devices in a sweat sensing system.
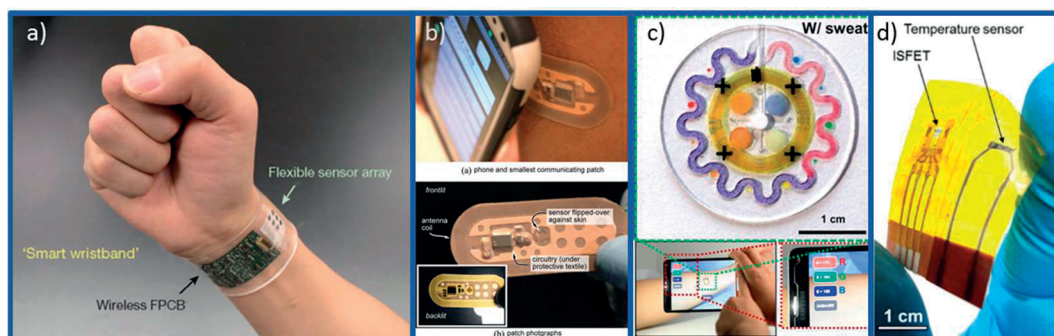
Figure 2.2 State-of-the-art wearable sweat sensors. a) Multiplexed electrochemical system for sweat monitoring in a wrist band [3]. b) Band aid patch for continuous monitoring of ions in sweat [51]. c) Wearable stamp for colorimetric detection of sweat analytes [55]. d) Patch for pH monitoring on sweat [56].

2.4 Alternative biofluids

The most studied biofluid is blood. Blood and interstitial fluid can be probed by implantable devices, but it is hard to access them in a noninvasive fashion through a wearable platform. Serum and urine share the same disadvantage. In literature, besides sweat, two other candidates are proposed as interesting biofluids for healthcare and diagnostics, tears and saliva [59].

Tears are produced by lacrimal glands. They comprise proteins, peptides, electrolytes, goblet cells and blood. The rich composition of biomarkers in tears, make them an interesting biofluid to be considered for continuous analysis. Glucose detection in tears is particularly important as it shows a direct correlation with glucose levels in blood [60]. In addition, aminoacids, antioxidants and metabolites have been detected in tears [61] [62] [63]. Nonetheless, there are several limitations for tear collection as human eyes are very delicate and easy to irritate. Fig 2.2 shows a prototype for tear analysis developed by Yao et al, designed to quantify tears glucose levels.
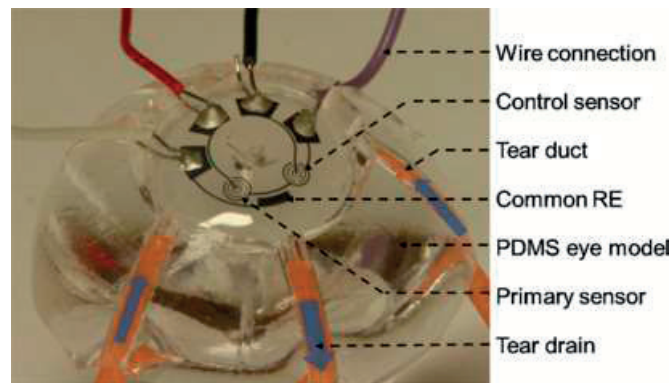
Figure 2.3 Example showing a wearable sensor for tear collection and analysis. Retrieved from [64].

Saliva comprises several elements permeating from blood through transcellular paths. Therefore, it is an optimal alternative to blood analysis for monitoring the metabolic state of the human body [65]. Current research is making efforts in developing portable salivary diagnostics tools [66]. Some of the biomarkers currently tested in a wearable fashion are pH, and fluoride activity. pH in saliva is tested to study the acidogenecity of the plaques [67], whereas fluoride monitoring provides information about the fluoride dentifrice efficacy [68]. Lactate and bacteria has also been measured in undiluted human saliva samples [69] [70]. Figure 2.3 shows a prototype from Mannoor et al, designed to quantify bacteria.

Figure 2.4 Examples of wearable sensors for saliva sampling. Adapted from [70].

2.5 Summary & discussion

This chapter explains why sweat is an interesting biofluid for healthcare applications. The diversity of biomarkers contained in sweat, and the possibility to quantify each of them offers the possibility to monitor in real time biochemical information of a person. This chapter summarizes the different biomarkers in sweat that have been studied in the literature and shows the latest wearable sweat sensors. A brief summary of other biofluids for wearable sensing applications has been discussed too.

Bariya and Javey [24], enlist 5 different challenges for body sweat sensing with the actual wearable devices. This discussion is relevant for this work as it directly focuses on resolving these issues, as will be demonstrated in the following sections of this thesis.

Low sweat rates. Sweat rates vary with factors including activity intensity and hydration level, and highly depend on individuals. In the case of sedentary sweat rates (in the order of tenths of nanoliters per cm^2 per minute), wearable devices must employ microfluidic techniques to be able to manipulate such limited volumes of liquid.

Sample evaporation. Evaporation and chemical degradation between sweat collection and testing can become a problem for the sensitivity. Concentration of the constituent biomarkers in sweat can vary with evaporation of the biofluid.

Obtaining fresh sweat. New sweat secreted onto the skin could mix with older sweat. Therefore techniques to control the sweat flow should be put in the systems so that detection only occurs in the freshest sweat.

Contamination from skin. Irregular sweating has led to the use of chemicals (such as pilocarpine) in order to stimulate the sweat to come out of the glands. This could have an undesired effect in the concentration of the biochemical markers in sweat.

Sweat rate effects. There is a need to compensate sweat rate effects as the concentration of certain biomarkers in sweat can be directly linked to it. This has already been proven for Sodium, Chloride and Lactate [19].

This thesis proposes in the following chapters a system that addresses these limitations. The use of ISFETs as sensing units provide a miniaturization of the sensing area of one order of magnitude (from millimeter size to micrometer size), requiring much less volume of sweat to provide a response to a specific analyte. Moreover, ISFETs provide an advantage over traditional electrochemical sensing electrodes as they are able to detect a single entity in an analyte (a single ion, molecule or protein), but also they can measure a large change in concentration, this will be explained in detail in Chapter 3. In addition, a microfluidic device fabricated on top of the ISFETs allows the control of the sweat flow with the possibility of manipulating volumes of liquid in a picoliter range as it will be demonstrated in Chapter 4.

Chapter 3 Sensing with computing technology

This chapter deals with the sensing technology used in the wearable system. Two state-of-the-art ISFET structures are described and their characterization as sensors is presented. These two ISFET architectures have proven to be excellent pH sensors with very high sensitivity. The importance of the sensing devices is paramount in a wearable system for different reasons: first, CMOS compatibility is desired as to offer the possibility to monolithically integrate in a single chip highly sensitive sensors with a readout system. Second, low power consumption is highly desired in order to avoid rapid battery exhaustion. These two requirements are satisfied by the ISFETs presented in this chapter. The enhancement of the sensors to be used for electrolyte sensing purposes is presented in chapter 5 of this Thesis.

3.1 The Ion Sensitive Field Effect Transistor

Ion sensing can be traced down to 100 years ago with the first Ion-Selective Electrodes (ISEs) [71] [72]. The most common devices ISEs are glass electrodes, which are still used for pH sensing in standard pH-meters [73]. Modification of the sensing interface allows sensing of other ions, such as sodium (Na^+) and potassium (K^+) [74]. With the development of metal oxide field-effect transistors (MOSFETs), studies of the interface between oxides, metals and semiconductors led to the development of Ion Sensitive FET (ISFET) [75]. The ISFET was introduced in the 1970's [76] as an alternative to the ISEs for pH and other ions' sensing with the perspective to miniaturize the system.

With ISEs, it is possible to quantify the concentration of a target molecule in a fluid by measuring the potential difference between the ISE and a reference electrode (typically and Ag/AgCl reference electrode), this type of measurement is a classic

electroanalytical method called potentiometry. The reference electrode is expected to be electrochemically stable via a well-defined redox reaction. This electrode is immersed in a solution of its own salt at high concentration, condition identified as a major drawback for making this electrodes smaller [77]. This thesis deals with the miniaturization of the reference electrode in section 5.2. In the ISE, the potential is directly proportional to the charge of the targeted analyte in a solution. Measurements of pH levels are the easiest experiments to carry on as any oxide in a surface attract naturally hydrogen ions [78] [79]. The pH is an indicator of the acidity or basicity of an aqueous solution and it is calculated with the following expression:

Equation 3.1

$$pH = log_{10}\left(\frac{1}{a_{H^+}}\right)$$

Where a_{H^+} refers to the concentration of Hydrogen ions. The change of pH is calculated with the Nernst equation:

Equation 3.2

$$|\Delta\Psi(pH)| = \frac{log_{10}kT}{q}\alpha \cdot \Delta pH_B \rightarrow \alpha \cdot 59.6\frac{mV}{pH}$$

With equation 3.2 it is possible to describe the proton concentration difference caused by the potential between the bulk solution of the oxide surface. The k constant refers to the Boltzmann Constant, T the absolute temperature, ΔpH_B is the pH variation in the bulk equation and α is a dimensionless sensitivity parameter which value is defined by the capacitive effect created with the ionic activity in a surface. The value of α varies between 0 and 1 and will be defined in section 3.1.1 of this text. By substituting the constant values in Equation 3.2 it is possible to calculate the ideal Nernstian response of a pH sensitive electrode which corresponds to 59.6 mV/pH.

ISFETs are also used for this kind of potentiometry measurements. As in ISEs, ionic activity is expected to create a change in potential in an oxide or metallic surface in the gate terminal of this type of devices. To understand this statement it is necessary to understand how a MOSFET an ISFET relate to each other.

The ISFET is similar to a planar metal oxide semiconductor field effect transistor (MOSFET) in many respects. The main difference being the gate electrode. The metallic gate of MOSFETs is absent in ISFETs, exposing directly the gate oxide to a liquid environment as can be seen in Figure 3.1. The gate electrode is therefore replaced with a reference electrode, thus, the potential at the silicon surface is a function of the reference electrode and the influence of the ions or charged molecules inside a solution. The electrostatic control of the source to drain current is then a direct consequence of ion sensing.
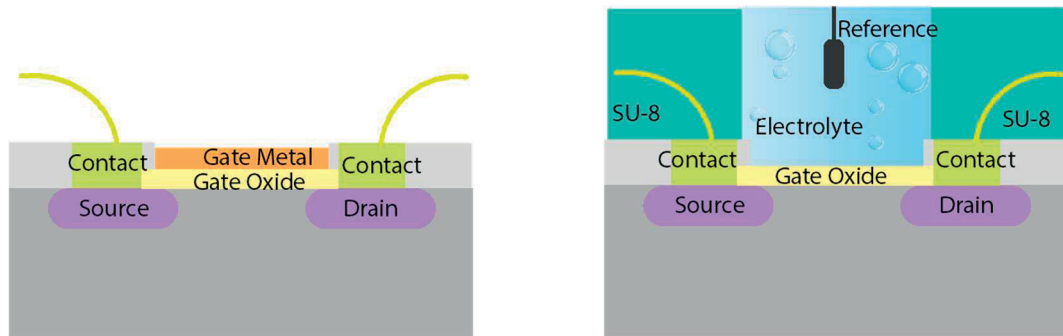
Figure 3.1 Diagrams showing the analogy between a planar MOSFET (left) and a planar ISFET (right).

In conventional MOSFETs, the gate voltage V_G can be described with the following equation:

Equation 3.3

$$V_G = \phi_{M-Si} + \Psi_{OX} + \Psi_{Si}$$

Where Ψ_{OX} is the potential drop across the gate oxide, Ψ_{Si} is an exponential potential drop occurring between the silicon oxide interface and the bulk

semiconductor, and ϕ_{M-Si} is a third potential drop that compensates for the different work functions of the metal and the semiconductor.

The threshold voltage V_{th}, in strong inversion, is given by equation:

$$V_{th} = \frac{\phi_M - \phi_{Si}}{q} - \frac{Q_{ox} + Q_{SS} + Q_B}{C_{ox}} + 2\phi_f$$

Where q is the elementary charge, Q_{ox} is the oxide charge, Q_{SS} is the interface charge, Q_B is the depletion layer charge in the silicon, C_{ox} is the gate oxide capacitance per unit area and ϕ_f is the Fermi potential.

A MOSFET works in three operation regimes, which are dependent on the applied V_G and V_{th}, these regimes are: accumulation $(V_G < 0)$, depletion $(0 < V_G < V_{th})$ and inversion $(V_{th} < V_G)$.

When the MOSFET operates in the linear region, the drain current I_d dependence with respect to V_G is given by the following expression:

$$I_d = C_{ox}\mu_e \frac{W}{L}[(V_G - V_{th})V_d - \frac{1}{2}V_d^2]$$

Where W is the width and L the length of the channel and μ_e is the electron mobility. V_d refers to the potential applied in drain terminal of the device.

In an ISFET, the contributions in potential of the reference electrode E_{Ref} and the chemical potential Ψ_0, which is related to ionic content of the analyte in contact with the gate dielectric have to be represented in the current-voltage equations.

These contributions replace the ones that the metallic gate cause and therefore Eq. 3.3 is modified and expressed with the following expression [75]:

Equation 3.6

$$V_g = E_{Ref} - \Psi_0 + \chi^{sol} - \frac{\phi_{Si}}{q} - \frac{Q_{ox} + Q_{SS} + Q_B}{C_{ox}} + 2\phi_S$$

With a threshold voltage in strong inversion [80]:

Equation 3.7

$$V_{th} = E_{Ref} - \Psi_0 + \chi^{sol} - \frac{\phi_{Si}}{q} - \frac{Q_{ox} + Q_{SS} + Q_B}{C_{ox}} + 2\phi_f$$

Where Ψ_0 relates to the surface potential due to the charged molecules absorbed and χ^{sol} is the surface dipole potential of the solvent (usually constant). ϕ_S refers to the surface potential at the Si-Oxide interface. In Equation 3.76, as there is no metallic gate, the contribution ϕ_M is not considered. For a fixed E_{Ref}, only the surface potential Ψ_0 varies as a function of the ionic content.

The Oxide-Electrolyte potential contributes linearly to the surface potential at the Si-Oxide interface, in other words, the electronic properties of the FET are not modulated by the Ψ_0 but rather shifted by it. It is important to remark as well that the Ψ_0 is also completely independent from the properties of the FET. Therefore, a change in Ψ_0 results in a change in V_{th}. This change in the threshold voltage can be then monitored by fixing the Reference Electrode Voltage and measuring the drain current.

In case of weak inversion operation, the surface potential of Field Effect Transistor (FET) varies between ΦF and $2\Phi F$ and the drain current depends exponentially on the gate to source bias. For instance, for pH sensing in weak inversion (at gate voltages smaller than the threshold voltage) operation [81], the following equation stands:

23

Equation 3.8

$$I_D = I_{D0}\exp\left[\frac{q}{nkT}\left(V_{GS} - \gamma - 2.3\alpha\frac{kT}{q}pH\right)\right]$$

Where I_D is the drain current of the ISFET, γ is a constant including the reference electrode potential, while the n-factor is the so-called slope factor of the ISFET including effects of the double layer and any other top passivation layer, if used. A functional operation of ISFETs in weak inversion operation offers ultra-low currents (below hundreds to tens of nA) and, therefore, guarantees low power per sensor [82] [83].

ISFETs share a similar condition to MOSFETs: in both, only with an ideal coupling between the oxide surface and the solution (or metal gate for MOSFETs), it is possible to allow the maximum change transduced by the device. The readout sensitivity S_{out} refers to the quality of the surface transduction and the electronic readout capability of the FET device [84]. The Readout Sensitivity is a quality factor representation as it can be described in terms of transconductance-to-current ratio, a very important parameter used in Integrated Circuit design [85]. The S_{out} is equal to the relative drain current variation before and after a change in a solution and it can be modeled with the following expression:

Equation 3.9

$$S_{out} = \frac{\delta I_d}{I_d} = \frac{\delta I_d}{\delta V_g} \cdot \frac{\delta V_g}{I_d}$$

$$= \frac{\delta I_d}{I_d \cdot \delta V_g} \cdot \delta V_g = \frac{\delta ln(I_d)}{\delta V_g} \cdot \delta V_g$$

$$= \frac{\delta V_g}{SS} = \frac{\Delta V_{th}}{SS}$$

$$= \frac{g_m}{I_d} \cdot \Delta V_{th} \cdot ln(10)$$

Where $\frac{g_m}{I_d}$ is the transconductance-to-current ratio. SS represents the subthreshold slope, which describes the variation of the drain current corresponding to a gate potential variation in the subthreshold region [86]:

Equation 3.10

$$SS = \frac{\delta V_g}{\delta(\log(I_d))}$$

$$= \left(\frac{kT}{q} \ln(10)\right) \cdot \left(1 + \frac{C_D + C_{it}}{C_{ox}}\right)$$

Where C_D is the capacitances in the depletion region and C_{it} correspond to the interface trap states region in the semiconductor/insulator interface.

The use ISFETs provide an advantage over traditional ISEs as they allow to work with non-linear output characteristics. This gives the possibility to detect a single ion or molecule but also allows measuring large changes in concentration of the analyte. Electrodes cannot handle the last condition as huge output signals cannot be handled by the electronics [77]. In addition, when miniaturizing ISEs, their resistance tends to increase and their capacitance to decrease, leading to poor potential stability [87]. A clear disadvantage when compared to ISFETs, which features can easily go below tenths of μm.

ISFET sensing devices have become promising candidates competing with other sensing technologies as they allow integration with various interfacing electronic readouts that are CMOS compatible. In addition, ISFETs provide the possibility of meeting the demand for multifunctional and scalable sensors with low fabrication costs [88] [89] [84].

Furthermore, ISFET technology is label-free, therefore there is no need to attach any label or probes to the analyte to improve the detection capabilities [90]. This characteristic provides the advantage of better real time detection with high specificity and detection sensitivity if compared to other label-free sensors. ISFETs also provide the cheapest manufacturing costs. Moreover, they provide

25

mechanical durability and resistance to the environment, making them reliable over time [88].

Other sensing counterparts to FET sensing include: gas sensors [91], optoelectronic devices [92] [93], mass spectroscopy [94] [95], microcantilevers [96] [97], quantum dots [98], Atomic Force Microscopy [99], carbon nanotubes [100] [101] and surface Plasmon resonance [102] [103]. However, these technologies require the use of complex instrumentation setups, making their integration in miniaturized systems complicated with respect to ISFETs.

3.1.1 The site-binding model

The gate oxides in the ISFETs are intrinsically responsive to inorganic salt ions. This mechanism is described with the site-binding model (SBM) proposed by Yates [104] and with the site-dissociation model proposed by Van der Berg [105]. The SBM explains the ISFET pH response as a purely capacitive effect (in the assumption that the interface is ideally polarized). The model describes the surface complexation in ions at oppositely charged oxide sites [106]. The adsorption of electrolytes on oxide surfaces has been extensively studied over the past decades [107] [108] [109] [110] [111] [112]. This research was essential for the development of glass electrodes, and afterwards other ion sensitive electrodes [113], including ISFETs [114] [115]. This research has allowed to model the Nernst equation (Equation 3.2) considering the influence of the gate oxide. To observe this, the parameter α is modified as follows:

Equation 3.11

$$\alpha = \frac{1}{2.3kT\frac{C_{diff}}{q^2\beta_{int}} + 1} \approx \frac{\beta}{\beta + 1}$$

Where β is the surface buffer capacitance of the dielectric of the gate terminal of the ISFETs. C_{diff} relates to the differential capacitance that depends on the ionic concentration in the solution. When α approaches unity, Ψ will reach the

maximum value of 59.6 mV/pH (Nernst limit). Equation 3.11 shows that besides the ionic concentration of the solution, and the temperature considered in the Nernst equation, it is important to consider the gate dielectric used for the gate terminal in the ISFET, which is typically an oxide in silicon substrate FETs.

Each oxide has on its surface a number of Hydroxyl groups (A-OH), described by the surface density N_S. These groups act as punctual sites and a chemical reaction occurs once there is a change in the concentration of H+ groups in the oxide-electrolyte interface. The hydroxyl groups could donate protons to the solution (acidic reaction), accept them (basic reaction) or they could be neutral, as can be observed in Figure 3.2. The balance mechanism between the surface potential and the H+ ion concentration in the bulk of the solution is described with the following equilibrations [116] [117]:

Equation 3.12

$$AOH \rightleftharpoons AO^- + H^+, K_a$$

$$AOH_2^+ \rightleftharpoons AOH + H^+, K_b$$
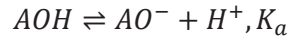
And:

Equation 3.13

$$K_a = \frac{v_{AO^-}.a_{H_S^+}}{v_{AOH}}$$

$$K_b = \frac{v_{AOH}.a_{H_S^+}}{v_{AOH_2^+}}$$

Every type of oxide has a specific number of sites N_S and a base or acid dissociation constant K_a & K_b. $a_{H_S^+}$ represents the activity of protons at the oxide/electrolyte interface and the number of sites per unit area m^{-2} of a particular surface group. The dissociation constants can be expressed in their logarithmic presentation:

Equation 3.14

$$pK_a = logK_a$$

$$pK_b = logK_b$$

Assuming that the total number of surface hydroxyl groups per unit are constant:

Equation 3.15

$$N_S = v_{AOH} + v_{AOH_2^+} + v_{AO^-}.$$

Equation 3.11 can be expressed in term of the dissociation constant and the differential double layer capacitance C_{DL} (determined by ion concentration of the bulk solution) [118], allowing to calculate the ΔV_{th} in terms of the oxide used in the ISFET:

Equation 3.16

$$\beta = \frac{2q^2 N_S (K_a K_b)^{\frac{1}{2}}}{kT C_{DL}}$$

Materials with a relatively high number of surface hydroxyl groups lead to a Nernstian response. In the case of this work, Hafnium dioxide is an important material as it has a high density of hydroxyl groups which translates to a higher pH sensitivity as will be shown in the next section of this thesis.
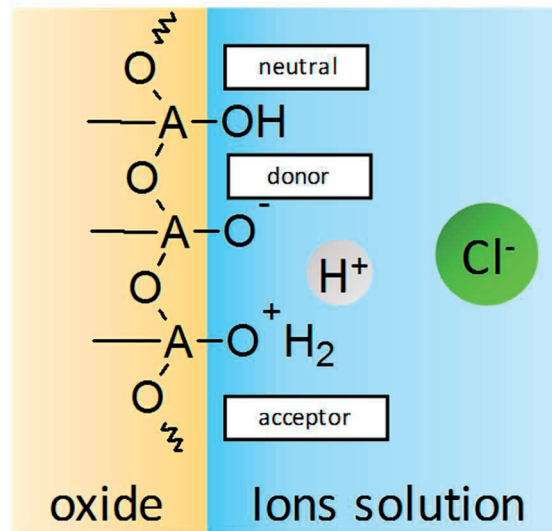
Figure 3.2 Site dissociation model with amphoteric sites.

Criticism has been raised against the assumption of a purely capacitive interface [74] [119] as it is stated that ideally polarized interfaces do not exist. This assumption raises questions on whether protons get adsorbed at the sensor surface or within the interface. However high-k dielectrics, such as hafnium, are excellent barriers against ionic diffusion and show negligible hydration [77].

3.1.2 Advantages of Hafnium-based dielectrics in ISFETs

Hafnium Oxide is part of a group of oxides called "high k", which include also ZrO_2, Ta_2O_5, La_2O_3, and TiO_2. The term high-k relates to a bulk property. With the scaling down of MOS transistors, the thickness of the normally used SiO_2 has decreased to a minimum of 1.2 nanometers, which account to an impressive number of only 5 atomic layers. This characteristic has brought undesired effects in the performance of transistors as high leakage currents have been observed, with a reduction of the breakdown voltage and also a reduction in the oxide reliability. High-k dielectrics offered an acceptable alternative to SiO_2 because of their higher permittivity [120] [121] [122] [123]. HfO_2 has been chosen in the CMOS

industry among other high-k dielectrics because of its large band offset with Silicon and its thermodynamic and kinetic stability [124].

Hafnium Dioxide offers advantages in terms of sensitivity too. HfO₂ offers a response to pH that is close to the Nernst limit (59 mV/pH at room conditions) [125] [126] [127] in comparison with SiO2, which reports less than ideal non-linear threshold voltage shifts per pH [128] [129] [130]. With an important ionic strength, the relationship described in equation 3.8 becomes exclusively dependent on the parameter β. A higher value of β translate into a higher change in the $\Delta\Psi(pH)$, which according to equation 3.5, will represent a higher change in the threshold voltage V_{th}. For thin and ultra-thin layers ($\leq 2nm$) of HfO2 the β value (~ 2) is equal or greater than the β value (1.3) that SiO₂ offers [131]. In chapter 6 of this thesis, the use of HfO₂ as a sensing material is justified, as the operation of the sensor is fully pH responsive and linear as is expected from HfO₂ devices. Using such thin layers of HfO₂ carry some tradeoffs, as the life time expectancy of the device is shortened as will also be discussed in chapter 6 of this thesis.

In this work, two types of ISFET architectures with HfO2 dielectrics were characterized in a miniaturized measurement setup environment. The first ISFET structure design (FinFETs as described in section 3.2) was fabricated by Dr. Sara Rigante [84] and the second one (Nanoribbon ISFETs as described in section 3.3) is being developed in by Doctoral Assistant Francesco Bellando [132], the two type of devices will be detailed in the following sections of this thesis.

3.2 FinFETs on Si-Bulk for sensing applications

The FinFETs with a liquid gate presented in this section have been developed by Dr. Sara Rigante [88]. The reason for the documentation of her works in this thesis is that the devices she developed are characterized in this work in a miniaturized experimental setup, as will be shown in <u>section 6.1</u> of this thesis.

FinFETs are recognized as one of the best performing nanoelectronic devices because of their excellent electrostatic control over the FET gate [88]. The FinFET is part of a group of transistors that are generally referred as multi-gate FET. One of the main advantages of these devices is that there is better control of the channel depletion with respect to a standard MOSFET while reducing the influence of the drain electric field on the channel.

A FinFET is a vertical transistor with lateral conductive channels as can be appreciated in Fig 3.5a. The gate generates an electrostatic potential surrounding the device almost in its totality providing excellent channel control. Thus, a steeper subthreshold slope can be achieved translating into higher readout sensitivity [133]. In literature, only one group has exploited a similar device for sensing applications, however only the top side of their FinFETs were used for sensing while the lateral sides were controlled by metallic gates [134]. In the case of this architecture, the whole vertical FinFET structure is fully immersed in the solution, giving total control of the channel to the potential in the analyte.

3.2.1 Technological development of FinISFETs

The FinFETs were fabricated by Dr. Sara Rigante in CMi, EPFL [88] [84]. The development was done according to a top-down approach on a silicon bulk substrate. The full process can be consulted in [88]. The whole fabrication process can be simplified as shown in Fig. 3.5.a. The final dimensions of the fabricated device are 16 nm < TFin < 40 nm, and 50nm < HFin < 120 nm, with HFin/TFin

always higher than 3. The quality of the device and the efficacy of the electrical insulation was first tested on the metal gate devices. All devices feature as HfO2 oxide with an HfO_2 thickness of 8 nm. The devices were passivated with an SU-8 layer exposing only the gate dielectric to the liquid.
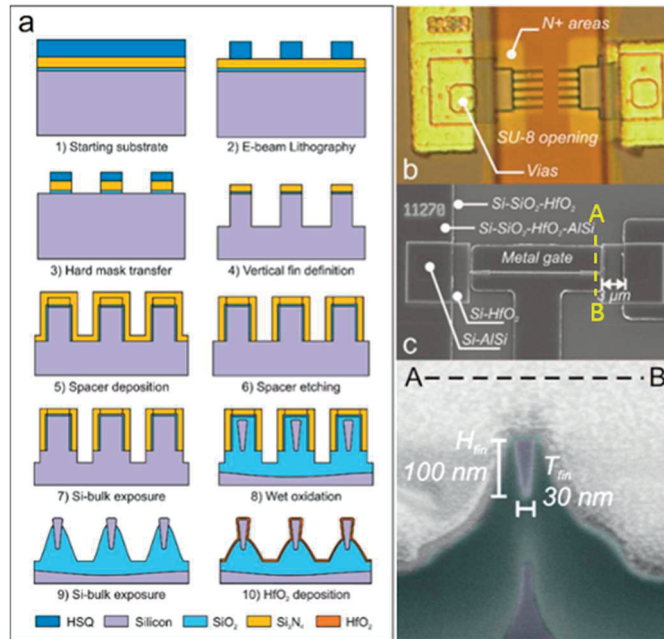
Figure 3.3 (a) Simplified process flow for two-dimensional FinFETs; (b) optical top image of a FinFET array for sensing applications with SU-8 next to the FET channels; (c) SEM top image of a single FinFET with metal gate; (d) SEM cross-sections obtained. Adapted from [84].

3.2.2 pH sensing with FinISFETs

Dr. Sara Rigante and the Nanoelectronics group of the University of Basel characterized the response of liquid gate FinISFETs. The pH sensing FinFETs achieved an almost full Nernstian response with $\Delta Vth = 57$ mV/pH between pH = 3 and pH = 10, as shown in Fig. 3.6. Moreover, the HfO2 FinFET exhibits excellent output sensitivity, as defined in Eq. 3.10. The drain current Id has been monitored in time, exchanging solution of different pH values from pH = 10 to pH = 3 and backward, as reported in Fig. 3.7. The FinFET has been biased at $V_{REF}= 1.5V$, $V_{DS} = 100mV$ at pH = 10. According to the $I_D(V_{REF})$ characteristics, such bias corresponds

to the subthreshold region of the FinFET where the subthreshold slope is steep and constant. Long-term stability measurements have been performed over 4.5 days. The liquid environment was kept at constant pH = 6. After a stabilization time of about two minutes the V_{TH} was extracted at I_{TH} = 2 nA. For a 3 wire FinFET with T_{Fin} = 20 nm the drift is 0.10 mV/h, while for a 5 wire FinFET with T_{Fin} = 30 nm is 0.12 mV/h.
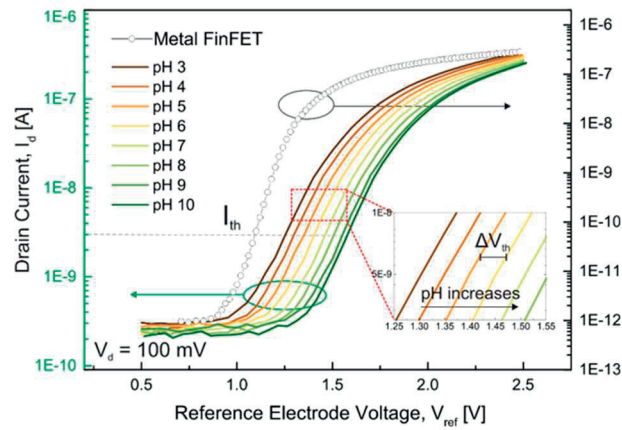
Figure 3.4 Transfer Characteristics from FinFET sensors. Extracted from [84].

Subthreshold slope values are in the range 70 mV/dec ≤ SS ≤ 79 mV/dec, while 10^5 ≤ I_{ON}/I_{OFF} ≤ 10^6 with the highest value I_{ON}/I_{OFF} = $2*10^6$ obtained. Such excellent results imply that there are no parasitic contributions through the Si-Bulk.

From figure 3.7, it is also possible to observe the reversibility of the current level for the same pH values. By calculating the mean I_D value for each population of data at a specific pH value the current hysteresis can be estimated. The higher current hysteresis is ΔI_H = 8.6 nA at pH = 7 and the average current hysteresis is ΔI_H = 5.6 nA.
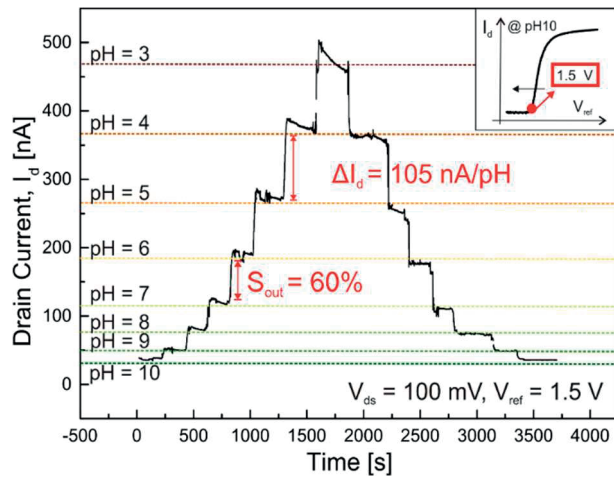
Figure 3.5 drain current I_D for a FinFET sensor during a time period of 1 hour from pH = 10 to pH = 3 and backward at V_{REF} = 1.5 V and V_{DS} = 100 mV. Extracted from [84].

3.3 Fully Depleted UTB SOI FETs for sensing applications

Due to the complexity and cost of fabricating FinFETs, a second architecture of ISFET is explored. This process has been developed by PhD candidate Francesco Bellando [132]. This thesis summarizes his work as the FD SOI ISFET sensors are characterized for electrolyte sensing in <u>section 6.2</u> of this thesis.

The devices are built on an ultra-thin SOI substrate (20nm Si on 145nm BOx), which allows us to achieve a good electrostatic control by eliminating the parasitic capacitances and reducing the OFF-state current by preventing the formation of parasitic current paths. Another of the main reasons to use an SOI substrate is to explore the possibility in the future to test the devices with a back gate. The interest in this research relies in the possibility of avoiding the use of a reference electrode in the sensing system, as reference electrodes are bulky components and hard to miniaturize, this will be discussed in chapter 5 of this thesis. Up until the time of publication of this Thesis, it has not been proven that ISFETs can be biased with a back gate.

Photolithography has been chosen over e-beam lithography for the definition of the FET shape as photolithography grants fast, cheap, parallel fabrication of chips, which is necessary for moving to industrial production. Furthermore, e-beam normally uses an HSQ-based negative resist for the definition of sparse structures, which after exposure becomes extremely similar to SiO2, making its removal dangerous for the exposed BOX.

3.3.1 Technological development

The main fabrications steps of the ISFETs in Ultra-Thin BOX chips are described in Fig. 3.6. The devices are built on Fully-Depleted (FD) SOI substrate, which allows to achieve excellent electrostatic control and low current leakage. The SOI FET

sensors have ribbon-like form factors, with a Si film thickness of 30nm and channel widths ranging from 0.8 to 4μm with lengths of 15μm. The 3nm HfO2 gate dielectric offers nearly ideal Nernstian sensitivity to pH and ultra-low gate leakage. The Atomic Layer Deposition (ALD) of HfO2 is performed on top of 3 nm of dry SiO2, resulting in a defect free interface with zero-hysteresis C_V characteristics. AlSi 1% metal lines are deposited by lift-off, followed by contact annealing. 100 nm layer of gold has been sputtered on top of the gate stacks for the ionic sensors that need integration of functionalization layers and for the control sensors. The pH sensors have no metallization on the high-k gate stack. Next, a 3 μm passivation layer of SU-8 photoepoxy is processed on top of the wafer to isolate FET sensor interconnects, with openings left only in the sensor channel regions (and for contact pads).
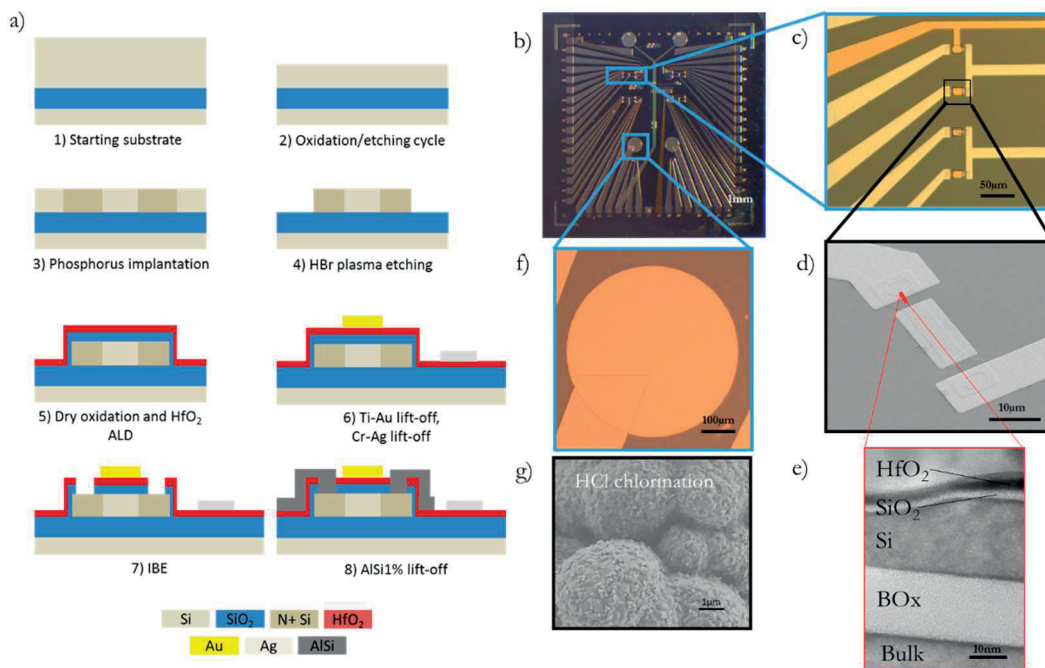
Figure 3.6 a) Simplified process flow for FD SOI ISFETs; (b) optical top image of fabricated chip with the ISFET arrays. C) ISFET array for sensing applications with SU-8 next to the FET channels; (d) SEM top image of a single ISFET with metal gate; (d) SEM cross-sections obtained showing the gate stack of the ISFET. (f) Miniaturized reference electrode optical image, (g) SEM of the Ag/AgCl layer of the Q.R.E.

3.3.2 Device Layout

The layout of the devices is shown in figure 3.7 below. It consists of a chip with an area of 82 mm², comprising 28 ISFETs and 2 MOSFETs (for characterization purposes). The chip has 4 arrays of 8 transistors each. Each array of transistors share a common source. The use of arrays in the design allows to functionalize each quadrant for a different analyte detection. The length of the channels of the ISFETs (as displayed in Fig 3.7) is of 15 µm, and the results presented in this thesis correspond to that gate length unless indicated differently.
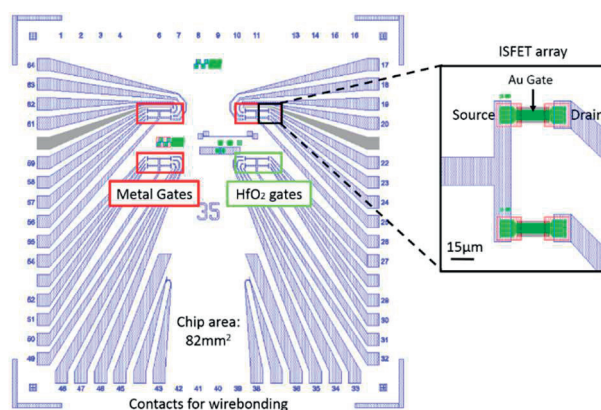
Figure 3.7 Sample layout. Blue areas are the AlSi lines for contacts. Green areas are the lithography design for the ion implantation. Grey areas are the gold lines for the metallic gate. Inset) Close up for the upper right array comprising an array of 8 FETs comprising ISFETs with a channel length of 15 µm and a width of 2 µm.

3.3.3 Characterization of ISFETs in a liquid environment

The sensor performance characterization experiments in a liquid environment shown in the following chapters were made using a shielded cascade manual probe station (Cascade Microtech Inc., Summit 1200) and a precision semiconductor analyzer Agilent 4156A. A PDMS stamp with patterned channels was mechanically fixed on top of the sensors as can be seen in figure 3.8. A syringe pump 11 Elite Harvard apparatus regulated the liquid flow rate in the system (typically up to 100µl/min), flushing the analyte through a PTFE tube connected to

37

the inlet of the system. An external reference electrode (MI-16-701, Microelectrodes Inc.) biased the system. Figure 3.8 shows this measurement setup.
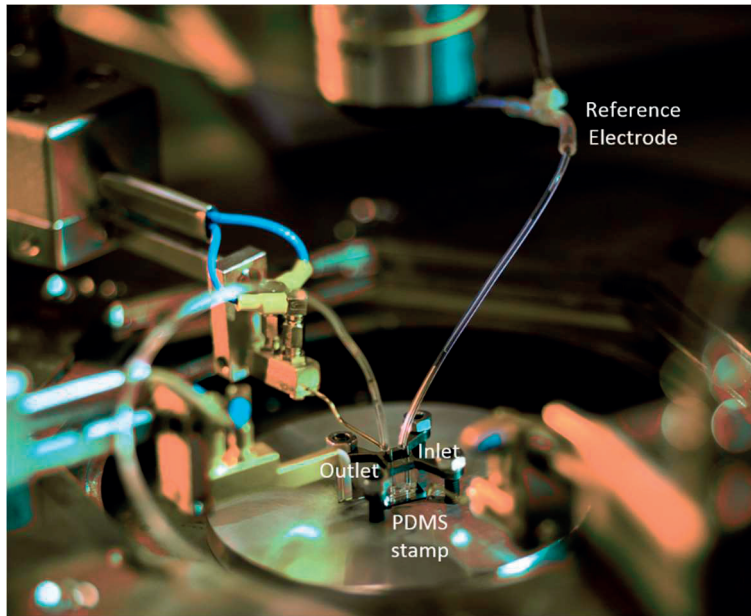
Figure 3.8 Measurement setup for ISFETs in liquid environment

3.3.4 pH sensing with FD SOI ISFETs

Two sets of experiments were performed with the sensors. The first steady-state measurements were performed to obtain the transfer characteristic of the devices with the reference electrode biasing the liquid gate exposed to different pH buffers (pH=3-9) and measuring the variations of the drain current (V_D was set at 200 mV while the V_{REF} potential was applied from -0.5 to 1V with steps every 10mV). The results are SS=210 mV/dec with a highest value $I_{ON}/I_{OFF} > 10^3$. The sensitivity for this sensor was 53.8 mV/pH as shown in figure 3.9. Sensitivities were extracted at different drain current levels to see the linearity of the response of the sensor in the weak inversion region as can be seen in the bottom of figure 3.9
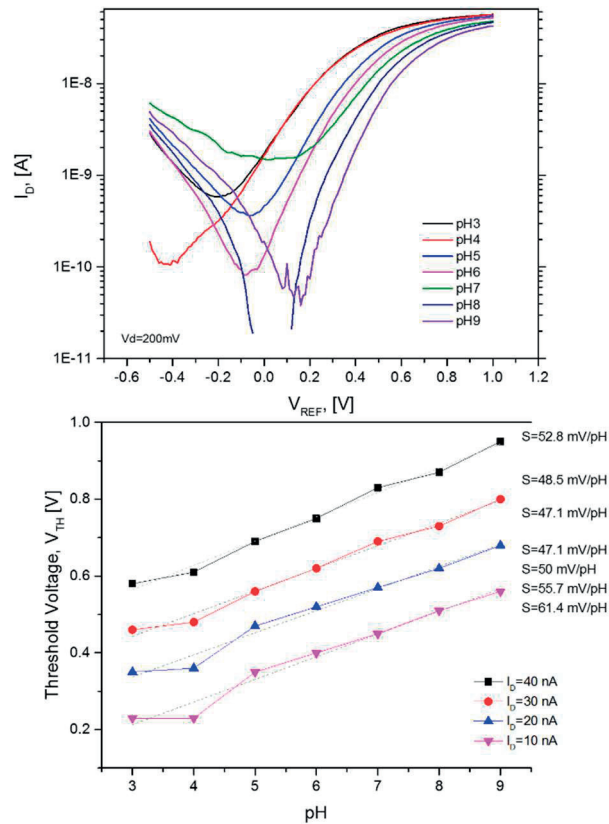
Figure 3.9 Top) Electrical characterization of ISFET devices for pH measurements with ISFETs on UTBSOI. Bottom) Sensitivity of the device extracted at different drain current.

The second round of measurements were performed at constant drain voltage and by fixing the voltage of the reference electrode. Due to the characteristic curve of our FinISFETs, a value of 620 mV at the reference electrode and a value of 200mV at the drain were fixed. If SNR is to be understood as the relation between the mean of the signal (σ) and 6 times the standard deviation of the same (6σ), we get a value of 18, which proves the distinction between pH levels with our system is very reliable. Working at these levels of voltage and current could enable our system to work at a nanoWatts range. The pH buffers were consecutively measured to evaluate the response in time of the device. Results showed an almost linear response of the sensor per pH value, estimating a variation of approximately 1 nA/pH. A very fast and clean response of the sensor (1.2 s from 90% to 10% of the

measured current) was appreciated with the variation of the pH buffers (figure 3.10).
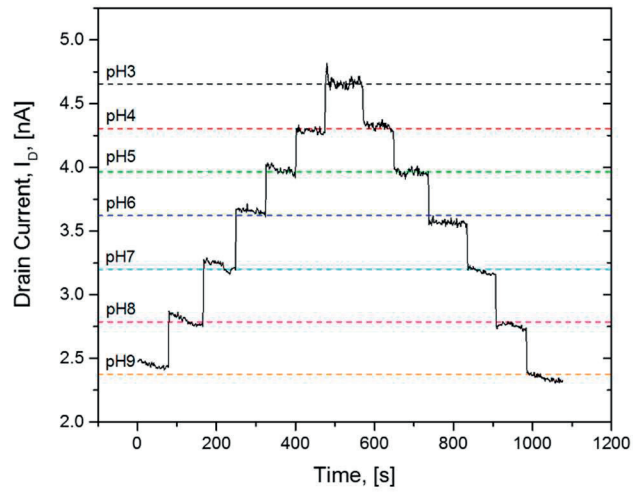
Figure 3.10 Time dependent measurements of the ISFET. ID measured while sampling pH buffers at a $V_{REF}=620mV$ and $V_D= 200mV$

3.4 Summary: high-k dielectric ISFETs for sweat analysis in wearable devices

This chapter has explained how an ISFET works and how it is intrinsically sensitive to pH due to the gate oxides. It has been explained how ISFETs are excellent sensors to replace ISEs for potentiometric measurements as they allow miniaturization and low power consumption. Moreover, this chapter has also shown the importance of the use of high-k materials as the gate dielectric in ISFET devices for pH sensing.

Two ISFET architectures have been described in this chapter. The first one, the FinFET structure for pH sensing has shown excellent results. However, the technological development of these devices is highly complex (over 80 steps) and can be difficult to industrialize. FinFETs with liquid gates are good chemical sensors, but their performance (in terms of sensitivity) is not expected to be better to other ISFET architectures [88]. Therefore, the nanoribbon ISFET (section 3.3) was developed, proposing a much simpler structure to fabricate and delivering similar sensitivities for measuring pH (57mV/pH and 53.8mv/pH respectively).

Both architectures have proven to be optimal pH sensors (with Nernstian response) that could be used as sensors in a wearable platform as they can work with ultra-low power consumption (in the nanoWatts range). As mentioned, another advantage is that the technology is CMOS compatible and therefore easy to integrate in more complex electronic systems including a read out system and a wireless communication system as will be discussed in the last chapter of this Thesis.

It has been observed that there is a weakening in the response of the sensors with time. This could be a direct consequence of a degradation of the ultra-thin layer of Hafnium Oxide. This has been reported before by Rigante [88]. Gentle cleaning procedures should be followed to avoid deterioration of the gate oxide. Avoiding

Hydrofluoric (HF) solutions and high power oxygen plasma steps should be a consideration while working with ISFET devices.

Electrostatic discharge is another important parameter to take care off. Extreme care has to be taken while testing the devices as they are very sensitive to discharges. As will be discussed in the next chapter, SU-8 photoresist provides a layer of protection aiding in this issue.

Yet another consideration has to be made while characterizing the ISFETs. The chemical composition contained in the pH buffers can directly influence the measurements. This has been reported by Tasarov [106]. This influence can be observed in the non-linearity of the V_{TH}.

This chapter has been focused only in pH sensing with ISFETs. The following sections of this thesis will discuss how to take advantage of this type of devices to obtain a wearable sweat sensor.

Chapter 4   Wearable passive microfluidics for sweat collection and analysis

This chapter explores the development of a passive microfluidic system that is able to successfully collect sweat from human skin and transport it to the sensing units of a wearable system (more specifically, the ISFETs presented in the previous chapter). The microfluidic platform proposed in this thesis aims to take advantage of the limited amounts of sweat that the human body produces. Together with the ISFETs, this biocompatible microfluidics could enable real time analysis of sweat.

As discussed in chapter 2, one of the main limitations of wearable sweat sensors is the absence of a system that is able to effectively manipulate the limited amount of available sweat coming out of the skin pores. As of today, all of the wearable sweat sensors have to be tested with subjects performing physical activities, limiting the applications of wearable sensing to the field of sports. The presented work aims to overcome that limitation with an innovative microfluidic system.

The design of the passive microfluidics presented in this chapter is strongly aligned with zero power consumption, therefore, this chapter explores the possibility of exploiting capillary forces in a portable microfluidic chip and specifically within full SU-8 devices. A brief introduction to the SU-8 material describes its composition and justifies its use in a wearable device as it has been demonstrated as a bio-compatible and resistant material [135]. Later, a detailed explanation on the design of the SU-8 microfluidics is given and its involvement with sweat acquisition and passive transportation from inlet to outlet of the microfluidics. This chapter concludes with the results of the validation experiments of the fabricated prototypes. The integration of the microfluidics with the ISFET devices described in the previous chapter of this thesis are presented in the chapter 5.

4.1 Capillary microfluidics

This microfluidic device presented in this work propose the use of capillary forces in the microfluidic chamber to transport the collected fluid through the system instead of using any sort of embedded micropump, a system that would be much more complex to fabricate and integrate within the system. Microfluidic capillary systems take advantage of the surface tension effect on a system to manipulate liquids [136]. Such systems have been successfully used in affinity assays experiments, supplying constant continuous flows over several minutes. Using capillary forces allows to obtain a system that is self-powered as no external power sources intervene in the system. In addition, capillary systems are self-regulated as liquid handling is structurally and chemically encoded in microscale conduits [137]. The inclusion of these two characteristics show an autonomous microfluidic capillary system as it requires no interaction from a user or external force. The next section briefly introduces the theory of capillary forces.

4.1.1 Capillary forces

The capillary effect is a driving force which allows for a pumpless drawing of a fluid in a small tube, thus, it becomes an ideal mean for achieving the initial filling of a channel in a wearable device. Its mechanism could be described as following: wall adhesion causes the water on the sides to creep along the boundaries until the correct Contact Angle (CA) is reached; this causes a deformation of the liquid surface (minimizing the surface energy) as can be observed in Figure 4.1. The contact angle, is the contact line between the solid walls of SU-8 and the liquid on the surface. Thus, the liquid at the center of the channel moves forward, causing the liquid on the border to lose again the correct CA and to creep along the boundaries again to recover it.

The process would stop when the fluid mass reaches the critical point at which the gravity force equals the capillary force; however, in a microenvironment that

would never occur. Therefore, the flow continues until it reaches the end of the channel or until all the available liquid has been pumped (whichever happens first). An absorbent material inserted at the outlet of the channel could act as another capillary pump in series, causing the liquid to continue flowing within the system.
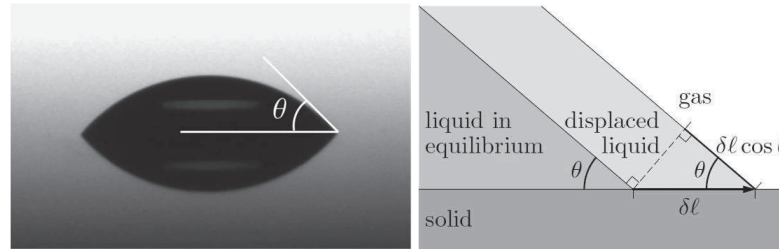
Figure 4.1. Left. The angle between the solid-liquid and the liquid-gas interface at the contact line. The picture is taken from a measurement of the contact angle of a water drop on SU-8 in air showing a C.A. θ = 64.1. Right Displacement δℓ of the contact line away from the equilibrium position. The change of the interface areas are proportional to +δℓ, δℓcos θ, and - δℓ for the solid-liquid, liquid-gas, and solid-gas interface, respectively. Reproduced from [138].

The capillary filling is a consequence of the interaction between the surface tension of sweat and the geometry of the surfaces of the system [138]. Fig. 4.2 illustrates the capillary filling in a channel. When the contact angle of a wall is θ<90° it is considered wettable or hydrophilic (high surface energy), if θ>90°, the wall is considered hydrophobic (low surface energy). The motion of a fluid inside a patterned surface is due to the interaction between the surface tension of the liquid and the chemistry and geometry of the solid-liquid interface [139] [140] [141]. The capillary filling has been extensively studied and it can be described with the following model.

The interfacial pressure P_C of a liquid that is front advancing into a rectangular channel is described by the following equation [142]:

Equation 4.1

$$P_C = -\Upsilon \left(\frac{cos\theta_B + cos\theta_T}{h} + \frac{cos\theta_L + cos\theta_R}{w} \right)$$

where Υ is the surface tension of the liquid, h and w are the height and width of the channel, respectively, and $cos\theta_{B,T,L,R}$ correspond to the contact angles of the liquid with the surface of the bottom, top, left, and right walls, respectively.

The volumetric flow rate Q is defined by:

Equation 4.2

$$Q = \left(\frac{\Delta P}{R} \right)$$

Subject to:

Equation 4.3

$$Q = \frac{dV}{dt} = wh\frac{dL}{dt}$$

Where $L(t)$ is the filling speed of a channel up to a distance by capillary action, $V(t)$ is the time-dependent volume filled, ΔP is the difference in pressure, and R is the hydrodynamic resistance of the channel, which for a rectangular microchannel is described by:

Equation 4.4

$$R \approx \frac{12\mu L}{wh^3} \left(1 - 0.63\frac{h}{w} \right)^{-1}$$

where μ is the fluid viscosity. By substituting Equation 4.4 in Equation 4.2, and equating Equations 4.3 and 4.2, the following expression is obtained [143]:

Equation 4.5

$$L \cdot dL = P_C \frac{h^2(w - 0.63h)}{12\mu w} \cdot dt$$

which by integrating leads to:

Equation 4.6

$$L(t) = \sqrt{P_C t \frac{h^2(w - 0.63h)}{6\mu w}}$$

which is also known as the Washburn equation [144]. This equation describes the progression of the advancing meniscus in the microchannel. When at least one wall is very hydrophilic, filling times are independent of the contact angle of the opposing substrate and are significantly faster than when both substrates have identical, moderate contact angles.
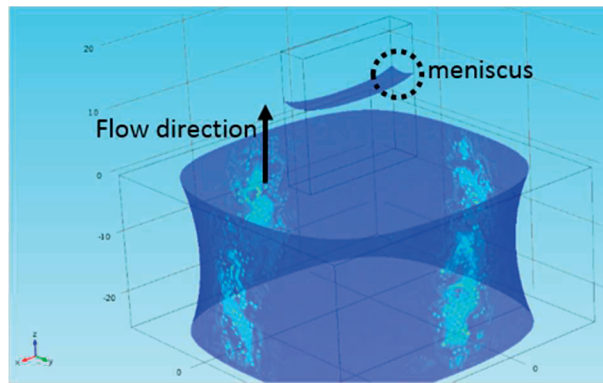
Figure 4.2 COMSOL simulation of capillary filling of a 3D single structure. Adapted from [145]

Each wall in the microfluidic system contributes to generate a negative pressure in front of the liquid, drawing the liquid into the channels. If the cross section of a channel is reduced, the capillary pressure will increase and vice versa. This gives to possibility to adjust the flow of the liquid through the channels by playing with

the geometry of the system, giving the ability to valve, guide, and displace liquids along surfaces as reported by [140] [142] [146].

The following sections of this chapter present three different methods of increasing complexity and efficiency for sweat collection on skin with capillary systems.

4.2 Microfluidics for collection and flow control of sweat

This section presents three methods for sweat collection on skin with flow control. The first method consists of using a hydrophobic cavity to accumulate sweat produced by human skin. This method is similar to what every previous work on wearable sweat sensing application utilize as reported in the state-of-the-art presented in Chapter 1. The second method explores the possibility of using a patterned SU-8 surface to reduce the high volume of sweat that the traditional methods require. This is a very important enhancement of the system that could provide sweat collection even when people are at rest. The third and last method described an improvement of the latest, achieving control of even lower volumes of sweat.

4.2.1 Sweat collection based on a sealed cavity.

Under exercise or high temperature conditions, the human body can produce up to **1.5 microliters of sweat per cm2 per minute** [19]. This simplifies the development of a microfluidic interface as a simple spatially delimited collection cavity containing the sweat sensors for biochemical analysis. In literature, all the wearables for sweat sensing rely on this principle. That is the main reason why other experiments have to be performed under physical activity. This section shows the development of a prototype designed to manipulate sweat in a high sweat rate regime adapted to our sensor system design. The research presented in

this section has been developed in collaboration with MSc. Clementine Lipp from XSensio.

Figure 4.3 shows the schematic of a cavity on top of a substrate. The cavity consists of a sealant ring and an absorbent material to expel the sweat once the collection area is filled. The cavity is delimited on the side by a frame (or ring) of medical adhesive attached under the chip (Trilaminate acrylic medical adhesive, Vancive MED6000), on the top and bottom by the chip and the skin surfaces. The adhesive ring fulfils three functions: fixation of the device on the skin, sealing the cavity, and acts a spacer material to avoid contact between the skin surface and the sensors.

The outlet of the system or drain, consists of a strip of textile-based wicking material (e.g. an absorbent material such as silk) that is attached to the chip by the adhesive, as shown in figure 4.4. The drain may be dimensioned as to provide a lower flow rate than the flow rate of the collected sweat, such as to keep the cavity filled (and the sensors wet). This method will guarantee a constant operation of the system as it is constantly acquiring fresh samples of the biofluid. All of the materials used in this prototype are biocompatible.
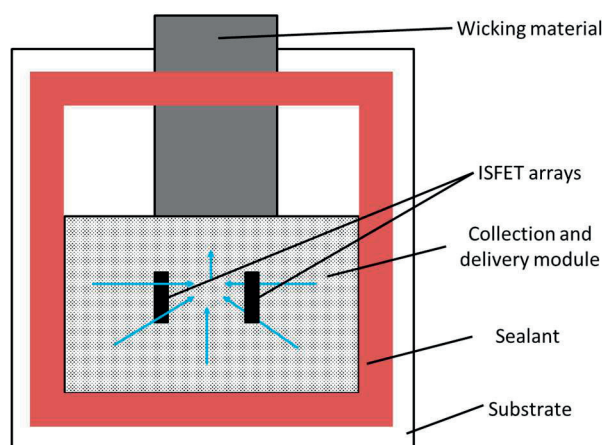
Figure 4.3 sealed cavity for sweat collection

The sealant material has an approximate thickness of 200µm and the inner dimensions of the frame is a square of 5mm side. Therefore the volume capacity of

sweat required to fill the space is 5mm^3 or 5µl. Considering, sweat collection on a person's arm, if the corresponding flow rate of the sweat is the theoretical maximum of 1.5µl/cm^2/min, it would take approximately 13 minutes for the sweat to fill up the cavity and reach the sensors, as illustrated in figure 4.4.
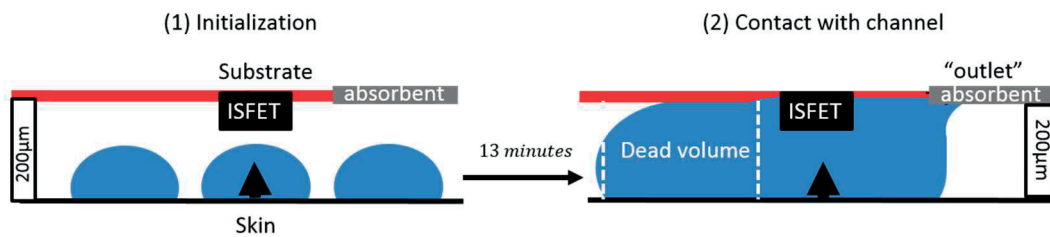
Figure 4.4 Filling of cavity

After assembling the microfluidics, the device was tested on skin to observe the filling of the cavity under exercise conditions. A food dye solution was applied on the skin and was allowed to dry before applying the device, in order to color in blue any sweat that would form on the skin, as can be observed in Figure 4.5. It was observed that after 15 minutes of exercise, sweat was successfully transported through the drain after filling the cavity. Afterwards, the absorbent material regulated the draining of the sweat.

Figure 4.5 Left. Microfluidic collection device for high sweat rates. Right. After 15 minutes of sport, sweat started to get drained by the absorbent material

As described above, a strip of absorbent material is placed in the outlet to drain the sweat out of the system. The method to regulating the flow of the microfluidic channels by an absorbent material for sweat analysis purposes has been exploited by previous reports [147]. For our application, it is important to guarantee that the channels are wet at all times, therefore a brief study was performed on absorbent materials to study the rate at which they drag liquid. A schematics of the experiment can be observed in figure 4.6. Water transport in textile material is regulated by capillary action as well. Four absorbent materials were tested to observe their performances as flow regulators, as shown in Figure 4.6.
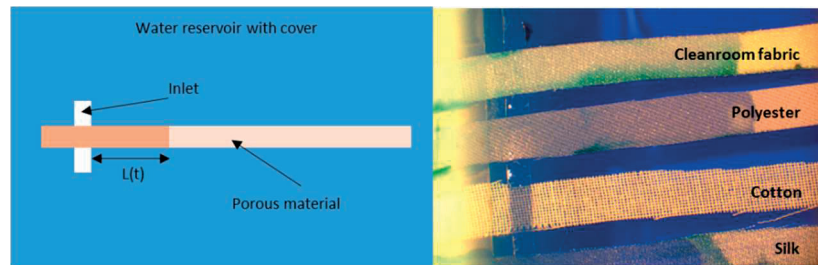
Figure 4.6 Left, Experiment setup to measure the sorptivity of different absorbent materials. Right, experimental setup to compare the volume of liquid filled in different absorbent materials.

The sorptivity of a porous material allows to calculate the speed in which the liquid is transported through the drain of the system. The sorptivity is the capacity of the medium to absorb the liquid [148] and is defined by the next equation:

Equation 4.7

$$V = AS\sqrt{t}$$

Where V is the volume intake of the porous material, A the cross-section area of the material, S: sorptivity [$\text{ms}^{-1/2}$] and t is time the porous material takes to be filled. The sorptivity of the different materials was obtained by measuring the water intake versus time in a determined length $L(t)$ along them from the following equation:

Equation 4.8

$$L(t) = S\sqrt{t}$$

To regulate the flow rate at which a liquid is expelled from the system, different porous materials can be used and their geometry can be tuned (thickness and cross-section). In this work, different kinds of fabrics were characterized to extract this quantity. Table 4.1 shows the different values of sorptivity for fabrics that were used as wicking materials.

Table 4.1 Absorption capabilities of different fabrics

Material	Thickness [μm]	Time at 10mm [s]
Cleanroom fabric	360	0,95
Polyester 94% Lycra 6%	125	1,48
Cotton	175	114,7
Silk	**60**	**5,37**

In order to find the most suitable drain for the application, it is important to consider the flow rate at which the liquid will be drained by the wicking material. A very fast draining flow rate like the one produced by cotton would empty the cavity of the system immediately and dry out the sensors. Another consideration to be made is the thickness of the material, as the thicker the material, the harder it is to integrate, and the bigger the volume required for the sweat to be in contact with the sensor (as it increases the distance between the skin surface and the chip surface). Considering this, the material that provides the best compromise between thickness and speed of absorption should be the best option for the system. As a result, silk can be considered as the optimal material as it provides with an

acceptable draining speed, a minimal material thickness, a good resistance and ability to keep its shape when wet.

4.2.1.1   Discussion on sealed cavity microfluidics

This section showed the performance of a sealed cavity employed as a sweat collector in wearable devices. As it has been shown, it takes a long time for sweat to arrive into the sensing area since the dead volume of the cavity has to be filled first. The main consequence of employing this type of microfluidics is that it limits the use of the sensor to high sweat rate conditions, limiting its use to the field of sports. This type of microfluidics exposes another problem: the high dead volume of the cavity would limit the time resolution of the measurement of any change of concentration in the sweat emerging on the skin surface, since the new sweat will be diluted with the old sweat already present of the cavity. The time resolution of the measurement of a change of concentration of an analyte in the sweat will hence be limited by the time to renew the liquid in the cavity, limiting the real-time measurement's performance of the system.

The following section proposes a solution that decreases the required volume of sweat needed to reach the sensing area.

4.3 Microfluidic devices for low sweat rates

As previously mentioned in chapter 2, when a person is at rest, human skin typically produces as little as **20 nanoliters per minute per cm²** [19]. Due to the limited amounts of sweat available there is a need to develop better microfluidic systems for sweat collection in this regime. The approach that this thesis proposes is the use of a patterned surface to enhance the collection of sweat and requiring lower volumes of liquid to fill the system.

One constraint that the microfluidic design tackled was the fabrication process' compatibility with a CMOS process line. This is important to facilitate industrial processes for mass production. The most feasible solution was to use a structural photoresist that could be used in contact with the skin. This thesis proposes the use of the SU-8 resist as it is a very suitable material for these purposes, as it is easy to integrate with sensing devices fabricated on silicon wafers. The SU-8 epoxy negative photoresist benefits from well-defined microfabrication processes and it has been proven to be a biocompatible material. The next subsection presents the properties of SU-8 photoepoxy.

4.3.1 SU-8 resist

SU-8 has been used as a material for microfabrication since 1997. SU-8 is a negative tone structural photoresist developed by IBM [149]. Due to its composition, SU-8 is a good material to fabricate 3D structures which require high resolution and high aspect ratio on thick layers. SU-8 is a multifunctional epoxy derivative of bisphenol-A novolak, which is a resist designed for spin coating of very thick films (>500 μm). With time, SU-8 became a good alternative to X-ray lithography, offering extreme aspect ratios and precision [150] [151].
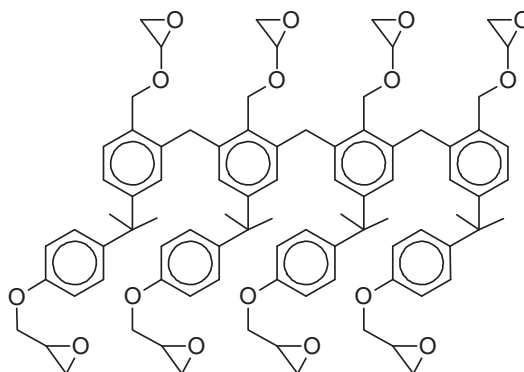
Figure 4.7 Structural formula of the SU-8 oligomer, featuring 8 epoxy functions. Upon photoactivation the epoxy rings open and bind with epoxy groups of other oligomers to form a highly crosslinked network.

SU-8 was developed by dissolving the EPON SU-8 epoxy resin in a solvent (*gamma-butyrilactone* or *cyclopentanone*) with a photoinitiator (*triaryl sulfonium salt*). SU-8 oligomers' structural formula features 8 epoxy-functions (thus, the name SU-8) [152]. Epoxy rings will open and bind with epoxy groups of other oligomers after photoactivation to form a highly crosslinked network. High crosslinking results in solvent-induced swelling of other negative resists. Another important property of SU-8 is its high epoxy content, as this enhances adhesion of SU-8 to other materials and makes it highly sensitive to UV exposure. Furthermore, an extra consequence of the highly cross-linked matrix is that the resist is chemically very inert and temperature stable, making it resistant to prolonged plasma etching, which makes it hard to strip a layer of SU-8.

As previously mentioned, this work aims to find a suitable interface that is compatible with human skin, therefore, biocompatibility of SU-8 becomes of the uttermost importance. Recent studies have proven SU-8 as a material that offers biocompatible conditions such as already FDA approved materials like silicone elastomer, Buna-S and medical steel. Sources have shown that implants with SU-8 inside of mice had no effect whatsoever on the animal's tissue. After 8 weeks of analysis, no degradation of the SU-8 surface was observed [135].

After 20 years of use, SU-8 has become one of the standard microfabrication materials. Nowadays, several processes have been optimized to make it easier to

use. In this work, the necessity for high aspect ratios (leading to the innovative design of passive microfluidics), low surface roughness (control of contact angle for microfluidics) [153] and relatively high dielectric strength (protection for electrostatic discharge of sensors) [154] make it ideal for use in this application.

To validate SU-8 as a suitable material for a capillary system, its contact angle was measured to determine its hydrophilicity. The CA was characterized with the machine Krüss DSA-30E. This tool allows to deposit a 3 µl droplet of water on a surface and to analyze its surface profile to automatically compute the CA with a precision of 0.1°. As seen in figure 4.8, the results were promising as the measured contact angle was of 64.1°, making it a suitable material for capillary microfluidics.
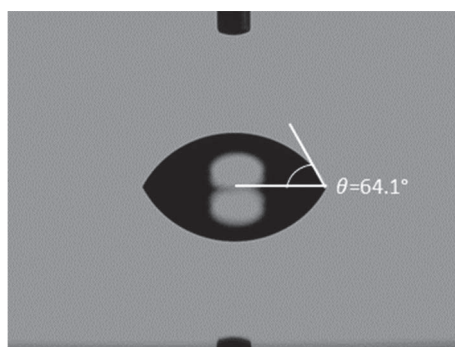
Figure 4.8 Contact angle measurement of a drop of liquid on top of a SU-8 surface after hard bake.

It is possible to decrease the contact angle of SU-8 by surface treatment. This was demonstrated by applying a short low power plasma treatment (1 minute, 100W). In figure 4.9, it can be observed that the surface treatment decreased the contact angle of SU-8 to zero. However, the plasma treatment will last for a limited time, and thus, SU-8's contact angle will stabilize again to its initial condition. Nevertheless, as the aim of this work is to guarantee the continuous operation of the microfluidic device for long periods of time, the plasma treatment was kept for prototyping purposes.
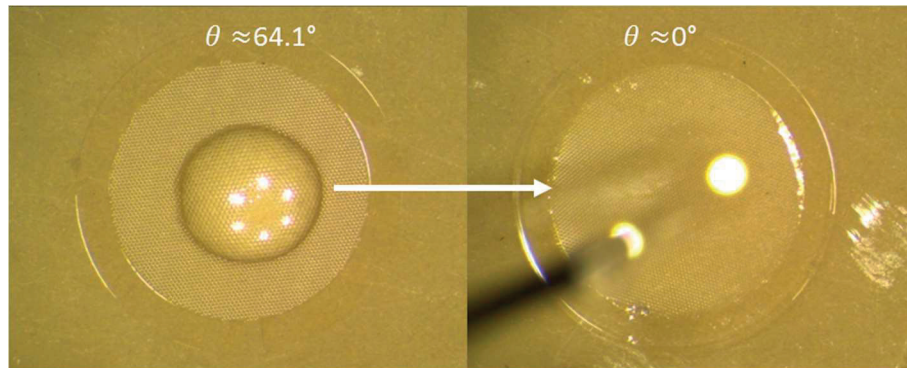
Figure 4.9 Plasma treatment effect in a SU-8 surface filled with micropillars. The contact angle decreases to zero degrees making SU-8 very hydrophilic.

This research validated the use of SU-8 as a feasible material for wearable sweat sensing devices as it is a material that is biocompatible and compatible with microfabrication techniques. The next section presents the development of a SU-8 microfluidic device to collect sweat on skin.

4.3.2 Open microfluidics for wearable sweat sensing

This section presents a microfluidic system that benefits from a complex design for sweat collection and transportation. The design includes an arborescent pattern with very thin channels enhancing capillary forces to act and drag the liquid droplets towards the sensors. Figure 4.10 shows the design of the proposed microfluidic structure. As can be observed, the arborescent structures are expanded as much as possible over the area of the chip. The objective is to try to collect sweat from as many pores as possible. The prototype presented in this section has been developed in collaboration with Dr. Fabien Wildhaber and Mr. Pietro Clement from XSensio.
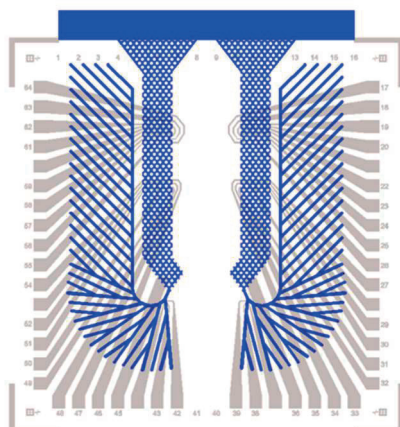
Figure 4.10 a) Arborescent design for open microfluidics.

Considering a thickness of the microfluidic layer of 25 µm, the fluidic capacity of the entire microfluidic structure is limited to 174 nanoliters, which accounts for 3.48% of the volume required by the sealed cavity microfluidic system presented in the past section. Once the channels are filled, the sensors will be in contact with the liquid allowing a constant analysis of the sweat ionic content. To avoid the channels emptying in a short time, a flow control structure (micropump) is embedded after the channel. The capillary pump has the largest capillary pressure on the chip and it determines the flow rate in the system. The microfluidic passive pump reduces drastically the speed of the fluid inside of the channels, allowing the liquid to remain for longer periods of time in contact with the sensor in the channel.

Flow rates are encoded in the design of the pump [155] [156]. The micropumps consists of an array of micropillars, these pillars are patterned as hexagons at regular intervals to achieve a relatively low flow resistance as shown by Gervais and Delamarche [157] [158]. It is important to mention as well that the direction of the flow can be controlled by using arrays of asymmetrical micropillars [159]. The distance between the pillars in the different designs are varied in order to vary

58

the pressure inside of the micropumps, and thus, the speed of the liquid displacement.

The micropump leads then to an absorbent material at its outlet to allow longer operation times and by evacuating the liquid and hence allowing fresh samples of sweat to arrive in the system. The next section details the fabrication process of the open SU-8 microfluidics.

4.3.2.1   Fabrication process for open SU-8 microfluidics

The fabrication process begins by preparing a Borofloat®/Burosilicate glass (float) wafer with a thickness of 550 μm (Low Resistivity of 9.7 [ohm.cm] at 100 Hz, at 25 °C). The wafer is exposed to a short plasma treatment for surface cleaning. The step is processed on a Tepla 300 machine, applying 400 ml/min of O2 for 7 minutes with a 500 Watt power.

After preparation of the substrate, a first spin coating of a 3 μm layer of SU-8 (Gersteltec GM1050) on the bottom wafer is done with a Sawatec LSM200 coater. This layer works as a passivation layer for the sensors in the system. When testing with float wafers though, it is critical to use this layer as it acts also as an adhesion layer for the microfluidic system that is placed on top. After spincoating, the wafer is placed on a Sawatec HP401Z for 30 minutes at 30°C to obtain a better uniformity of the surface. Subsequently, the temperature was increased to 120°C for 45 minutes with increasing and decreasing ramps of 4°C per minute. This softbake is a required step to evaporate the solvent in the SU-8 resist.

After the softbake of the first SU-8 layer, the substrate is exposed to UV light through a photolithographic mask with the Süss MA6 double-side mask aligner. An exposure dose of 100 mJ/cm2 for 4.8 seconds delivered the best results as seen in Figure 4.11. After exposure, the wafer was placed back in the Sawatec hotplate to perform the Post Exposure Bake treatment. The post exposure bake enhances the cross linking of the exposed patterns in the SU-8. The wafer is left for 20

minutes at 90°C while using a ramp of 2°C per minute to rise from and to fall back to room temperature. The wafer is then placed in a wafer box overnight for relaxation. The next step is the immersion of the wafers in PGMEA to develop the SU-8. Better results are achieved by using two Propylene Glycol Monomethyl Ether Acetate (PGMEA) baths, one of 40 seconds and a second of 20 seconds, followed by an IPA bath of 1 minute.
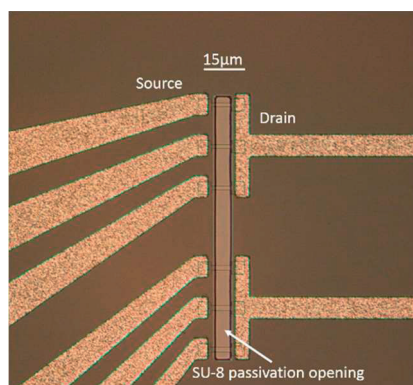
Figure 4.11 First layer for passivation with SU-8

After the first SU-8 layer is deposited on top of the wafer, a second layer of 30µm (Gersteltec GM1070) is spin coated on top. This layer corresponds to the channels and micropumps of our microfluidic layer. Exposition and baking times of the photoepoxy are crucial to achieve the aspect ratio and definition of our structures. After several exposure tests, a 5.6 seconds UV exposure was found to be optimal for both the channels and the hexagon shape of the pillars inside of the micropump. In the results section of this chapter the different considerations for the shape of the micropumps are presented. Experimentation to find ideal development times was also performed, concluding that the best results are obtained after a first bath of 60 seconds and a second one of 30 seconds in PGMEA development, followed by a rinse in IPA as can be seen in Figure 4.12. The fabrication concludes with a last step of baking of the SU-8 to eliminate any possible residues of solvent and to improve adhesion of the SU-8 to the substrate. The wafer is left for 1 hour at 180°C to achieve this. The ramp times have been

found to be critical for this process. Ramps have been programed with increases and decreases of minimum 2°C per minute.
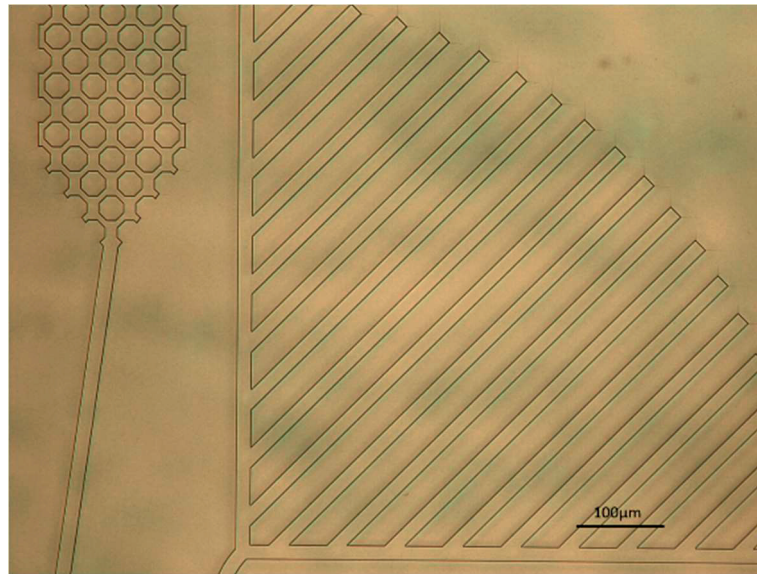
Figure 4.12 SU-8 development for micropumps

4.3.2.2   Microfluidic system characterization

In order to simulate the sweat flow through human skin and the filling of microfluidic channels in contact with it, an artificial skin setup was designed as observed in Figure 4.13. The idea of testing the system with an artificial skin comes from the need to observe whether the system is able to collect liquid in its inlet, fill the channel, and maintain a continuous and unilateral flow. The setup is made of an aluminum body containing a cavity filled with artificial sweat. A glass slide fits at the bottom of the cavity allowing for observation through the cavity (and the liquid it is filled with) with an inverted microscope, and the artificial skin (a molded lens of agarose hydrogel) is mounted on the top. The flow rate may be controlled via a syringe pump to simulate sudation of human body at various range of physical activity.
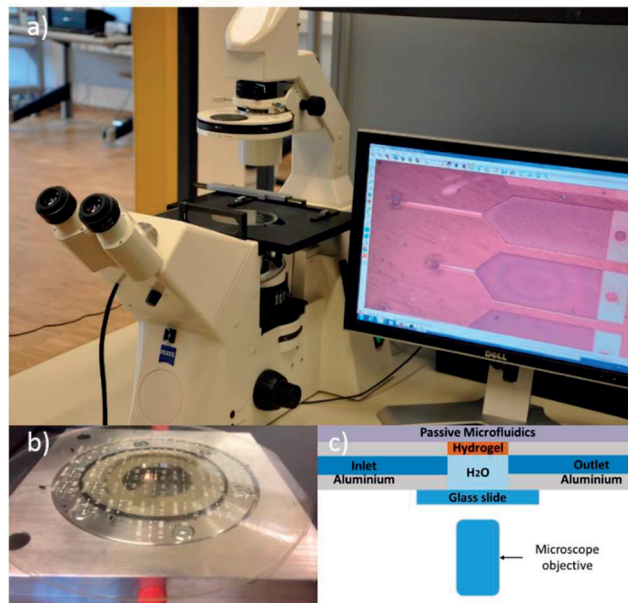
Figure 4.13 Experimental setup for characterization of passive microfluidics. a) Wafer set on an inverted Zeiss microscope. B) Wafer mounted on top the artificial skin setup. c) Schematics of the artificial skin setup (Cross section).

One way to improve the microfluidic characterization setup is to employ fluorescence techniques. Fluorescence facilitates the visualization of the flow of liquid inside of microfluidic channels. Figure 4.14 shows the artificial skin setup enhanced mounted with an opaque membrane (copper + polyimide laminate) with pores (perforated with a 250 μm drill) compatible with fluorescence microscopy. The liquid filling the cavity is a solution of fluorescent rhodamine dye and the microscope is equipped with the corresponding filter set. In this case the observation is done from the top of the membrane and not through the cavity.
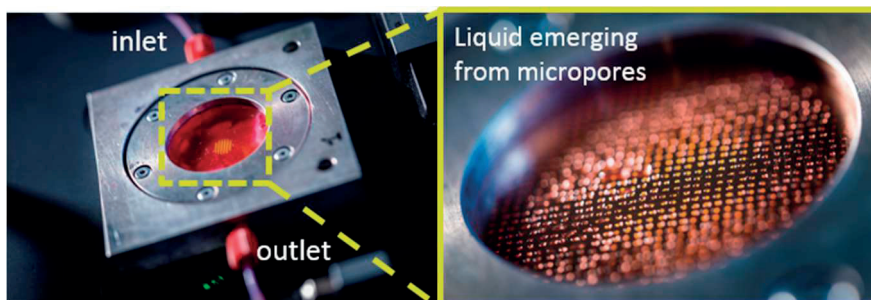
Figure 4.14 Artificial skin setup with fluorescence

4.3.2.3   Experimental results on open microfluidics

After fabrication the chip was placed on top of the artificial skin setup. Figure 4.15 shows how the liquid is successfully collected from a pore by the arborescent structure and then transported through capillary forces to the outlet area. Experimentation shows that it takes only 1.74 seconds for the liquid to arrive to the drain material in the outlet of the pump. It is important to highlight the action of the micropump, as it diminished the velocity of the liquid front compared to the microchannel. Figure 4.15 shows how the liquid takes less than a second to fill all the microchannels but it took approximately one more second to advance some 100 μm inside of the micropump. As mentioned before the microfluidic device requires only 174 nanoliters to be completely filled, therefore these results led us to the conclusion that it is possible to collect ultra-low volumes of sweat on SU-8 open microfluidics.
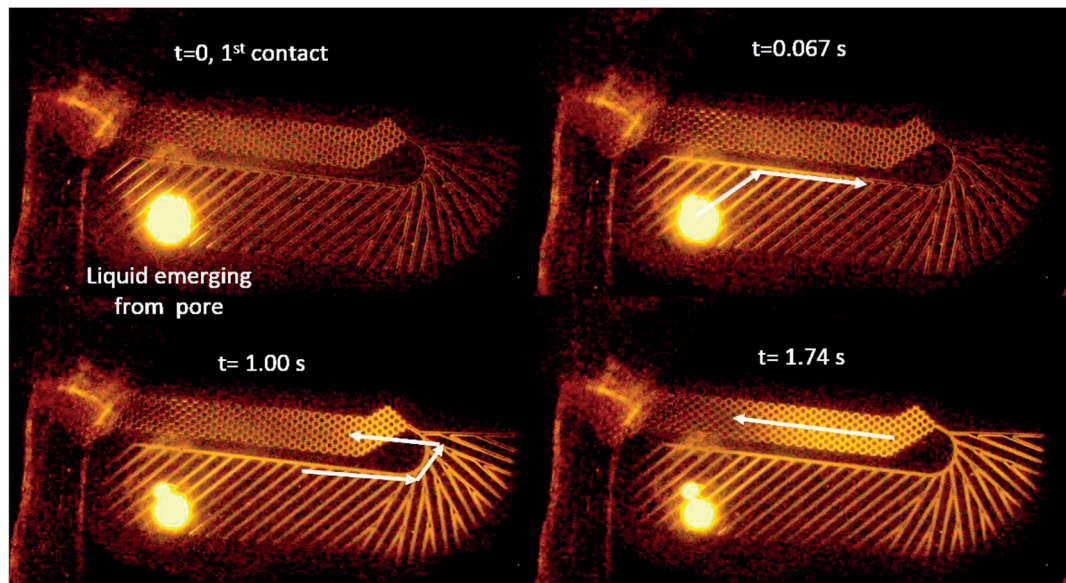
Figure 4.15 Sweat transport through SU-8 microfluidics

4.3.3 Closed microfluidics for wearable sweat sensing

An alternative to the previously proposed method is to close the channels with a second SU-8 layer. This encapsulation will allow the micropump to better control the flow as it will be enclosed in a sealed cavity. In addition, SU-8 could help to protect the ISFETs from any electrostatic discharge coming from the skin. Also, a second layer avoids contamination of the system with dead skin, lipids (such as sebum), bacteria, etc.

Nonetheless, the technological challenge is more complicated as creating full SU-8 devices relies on a highly complex microfabrication process. Figure 4.13 illustrates the concept of full SU-8 microfluidic devices and its interaction with an electronic system and human skin. As in the previous design, the microfluidics design includes an inlet with an arborescent design to absorb sweat from skin, a channel and a micropump. As previously mentioned, the micropump is added in order to control the speed in which the liquid is flowing through the microchannel.
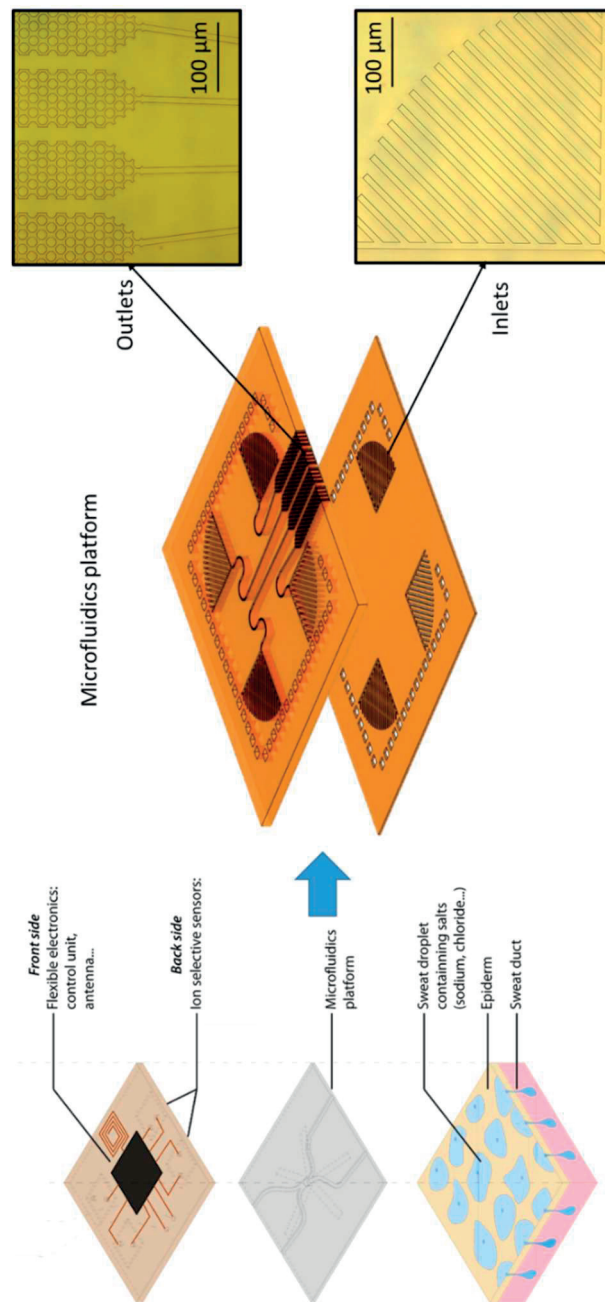
Figure 4.16 Sweat analysis patch concept. Left: concept for wearable device to enable sweat analysis in real time. Center, 3D model of the presented microfluidic chip. Right: zoom in constituent inlets and outlets of a 30 µm layer of SU-8 in a 4" Borofloat wafer.

4.3.3.1   Overview of the fabrication process flow

As mentioned before, one of the main challenges to obtain multilevel structures with SU-8 is to be able to close the channels after patterning them on a wafer. To do this, a two-wafer process was developed [160]. The main steps can be seen in Figure 4.17. The device fabrication was realized at the Center of MicroNanotechnology (EPFL-CMi). The key features of the process are:

- **Technology**: Silicon bulk and Borofloat glass
- **Total number of steps:** 34
- **Total number of masks:** 2 Chromium masks and 1 virtual mask
- **Critical steps:**
    1. Exposure times in order to achieve a good compromise between the correct development of the micropillars and the channels.
    2. Bonding process between two wafers with SU-8 layers.
    3. Anodic dissolution of Aluminium.
- **Main cleanroom techniques:**
    1. UV lithography
    2. Sputtering
    3. SEM, mechanical profilometers.

The fabrication process begins by preparing the substrates to be used. A bottom float wafer with a thickness of 550 μm, with a Low Resistivity of 9.7 [ohm.cm] at 100 Hz, at 25 °C and a top double side polished silicon wafer with a thickness of 380 μm, boron doped to a resistivity of 1-10 ohm.cm. Both wafers are exposed to a short plasma treatment for surface cleaning. The step is processed on a Tepla 300 machine, applying 400 ml/min of O_2 for 7 minutes with a 500 Watt power.
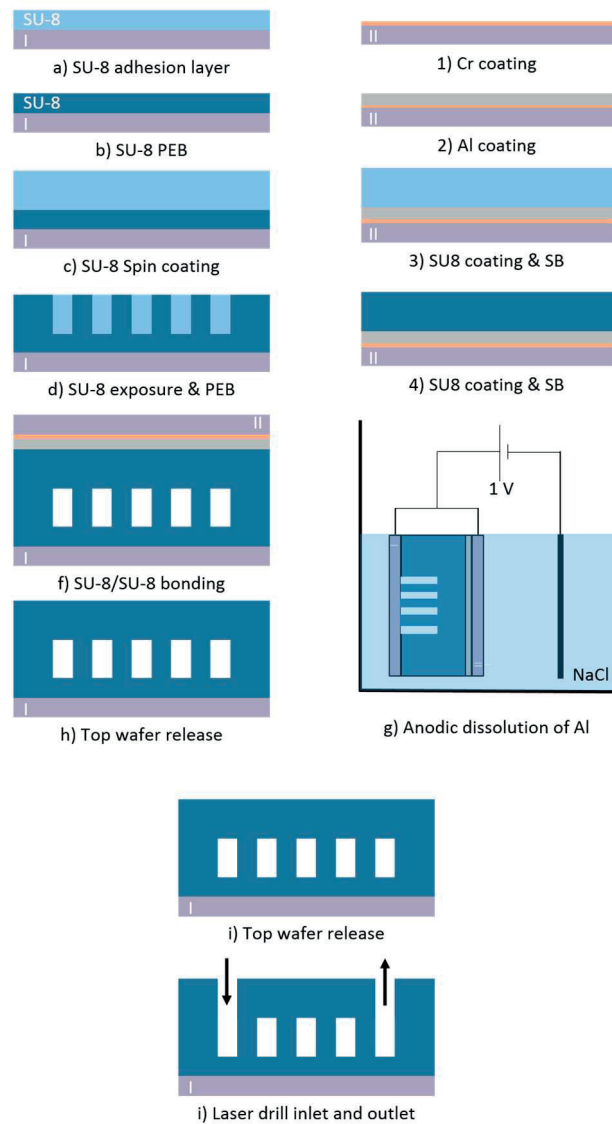
Figure 4.17 Process flow to fabricate full SU-8 devices

The bottom wafer process follows the same steps presented in the previous section (section 4.3.2.1). After development, the pillar structures were very well defined as can observed in figure 4.18. The array of pillars are used as micropumps as described in section 4.3.2. Arrays of pillars with different size and different space between each pillar were patterned in the SU-8 to obtain different flow rates. All

pillars are shaped as hexagons, but 2 diameter sizes were tested, 10 μm (Fig 4.18A & B) and 20 μm (Fig 4.18 C & D). The spacing between each pillar was also varied, with values of 10 μm in the x axis and 10 μm in the y axis (Fig 4.18A&C), an increase in the x axis to 20 μm can be observed in Fig 4.18B. Figure 4.18D shows a distance of 10 μm in both axes. The results of the flow rate dependence on the pillar array is discussed in the next section of this thesis.
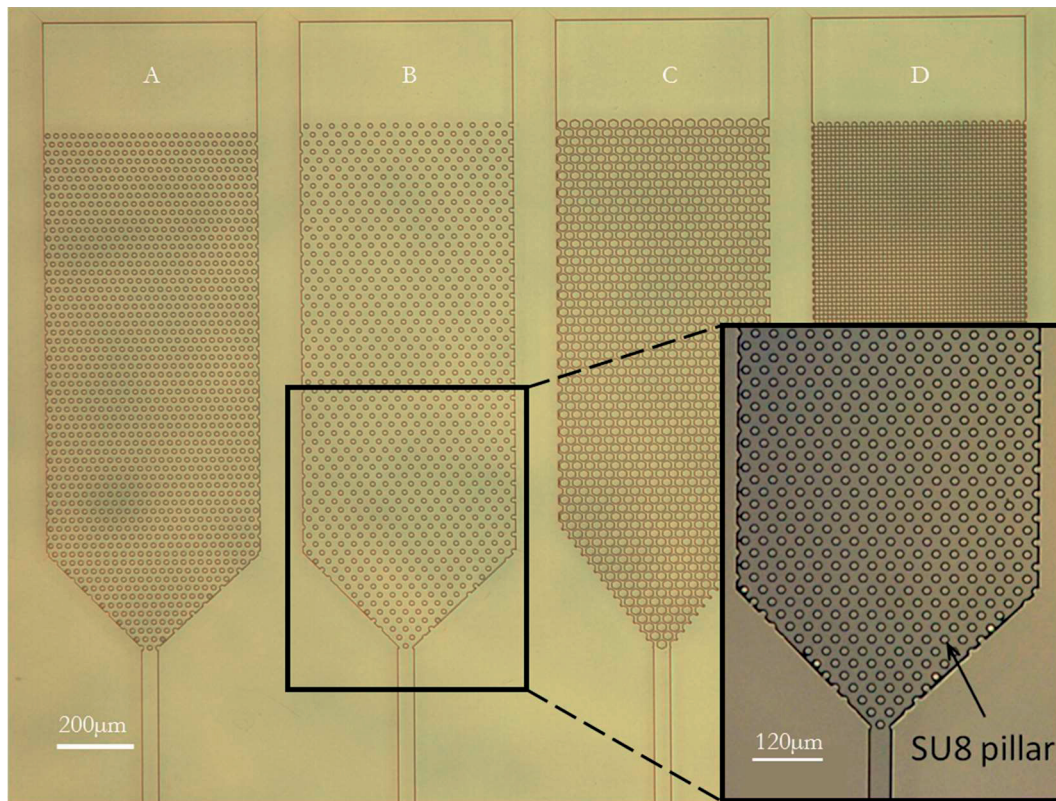
Figure 4.18 Micropumps patterned in SU-8.

To close the channels and the micropumps with a layer of SU-8, a second wafer is processed. On this double side polished silicon wafer, a 20 nm layer of Chromium is sputtered, followed by 100 nm layer of Aluminum sputtered deposition. Both thin film layers are deposited with the DP 650 Alliance-concept machine. The Aluminium layer will be dissolved later in the final steps of the process. Once the Aluminium is in place, a 30 μm layer of SU-8 is placed on top following the same

procedure mentioned before. Although, because of the reflectivity of the Aluminium layer below, the exposition time is decreased to 5 seconds. After the PEB, both wafers are put in contact while applying a 130°C temperature and a 4.5 bars pressure for 90 minutes with 4°C per minute ramp sequence. This is achieved by employing the Süss SB 6, vacuum anodic bonder. This step bonds the SU-8 layers. This phenomenon is a result of further cross linking of the SU-8 in the interface between both wafers.

After processing, channels are closed. In order to release the microfluidic structure, the wafer sandwich is put under a 1 Molar Sodium Chloride solution and a 5 Volt potential is applied to the backside of the wafer with a platinum counter electrode (connected to the negative terminal) to anodic dissolve the Aluminum.

The anodic dissolution of aluminium occurs as the material will react with the chloride ions in the solution once a potential is applied to it. The phenomenon is described by the following reaction:

$$Al + 3Cl^- \rightarrow AlCl3 + 3e^-$$
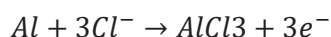
This step releases the top wafer leaving the full SU-8 structures. Finally, inlets and outlets are drilled with an excimer laser (OPTEC LSV3). After experimentation it was determined that a low frequency (150 Hz) with 100 shots was optimal to open the top SU-8 layer without damaging the layers below. The laser was set to work with 5mJ of power. Figure 4.19 shows the drilling of a 100 μm outlet in full SU-8 microfluidics.
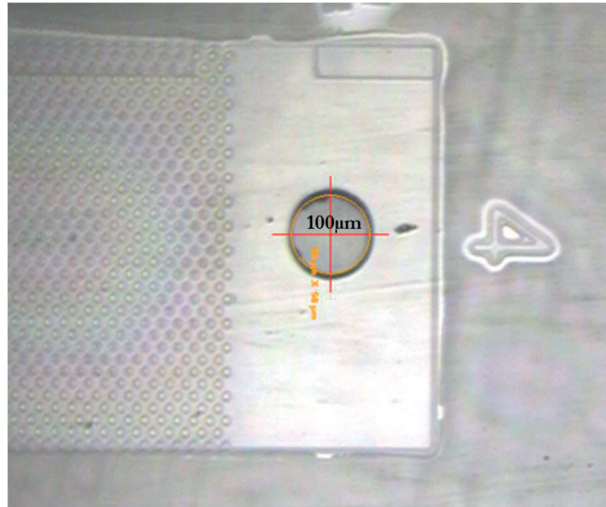
Figure 4.19 Outlet opening with Excimer Laser

4.3.3.2   Experimental results

After fabrication, the wafer was placed on top of the artificial skin setup described before in this chapter. The wafer was not treated prior to the experiments (no plasma activation). Once the liquid arrived from the artificial skin to the inlet, it was possible to observe the liquid flow through the system. The liquid then went to the first microfluidic structure, a channel with a 100 µm length, a 30 µm width and a depth of 30 µm (capacity of 90 picoliters of liquid). The channel filled in less than 1 second as observed in Figure 4.20.
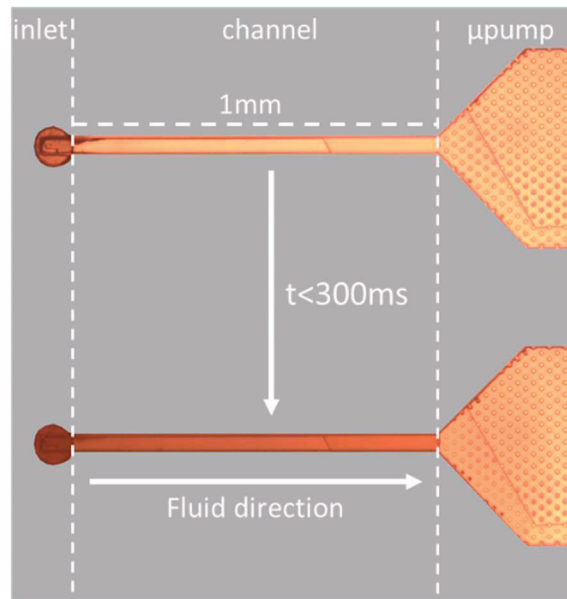
Figure 4.20 Filling of an SU-8 channel by capillary forces

The menisci of the filling fronts move from regions of high capillary pressure (the channels) into regions of reduced capillary pressure (the passive pumps) without generating air bubbles.

A first set of micropillars was tested, the diameter of the hexagons inside the micropumps was designed at 10 μm with spacings between each pillar of 20 μm in the x and 10 μm in the y axis (Fig 4.18B). The flow inside of the micropump was measured at **120 picoliters per minute**. With such a low speed of the volume, the liquid inside of the channels started evaporating before the liquid was reaching the outlet.

In order to increase the speed of the liquid inside of the system it is necessary to reduce the fluidic resistance. This is achieved by increasing the size of the pillars, to test this, a second set of micropillars were tested, the pillars have a 20 μm diameter, and the space between the pillars is reduced to 10 μm in the x axis and 0 μm in the y axis, as has been shown in Fig. 4.18C. The flow rate was increased to **4.2 nanoliters per minute**. The displacement of the liquid can be observed in figure 4.21. It is worth mentioning that a slight spread of liquid was observed along the

edge before the pump started filling. Nevertheless, the amount of liquid running through the edge is almost negligible. The increased size of the pillars seems to have reduced the pressure in the sidewall of the channels as the spreading effect over the edges was less noticeable with that configuration.
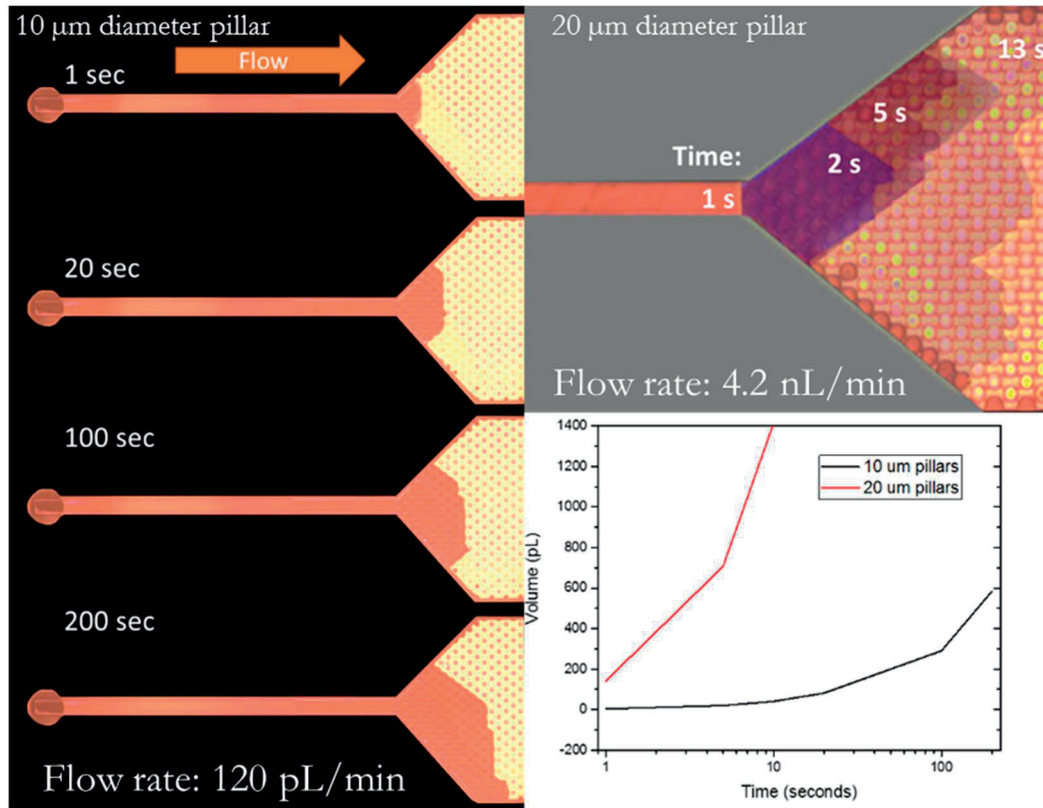
Figure 4.21 Left: Micrograph of a micropump with 10 μm-wide pillars showing unilateral flow of liquid from inlet to outlet. Top right: Micrograph of a micropump with 20 μm-wide pillars showing an increase in the speed of the flow. Bottom right: Variation of flow rates for different size of micropillars. [161]

4.4 Summary & discussion

This chapter has presented three methods to integrate a microfluidic interface that can provide sweat collection and flow control in wearable sweat sensing devices. The first presented method is important as its relative simplicity allows for fast testing of the devices. With this sealed cavity microfluidics we have successfully collected sweat from human skin while controlling the flow of the liquid inside. This is the only method that can be compared to what literature shows in state-of-the-art wearable sweat sensors. As it was mentioned, due to the high volume of sweat required to fill this sealed cavities, the use of this kind of microfluidic devices is limited to sweat analysis under physical activity.

The following two methods propose the use of a patterned microfluidic interface to guarantee the operation of the wearable device to operate even when people is at rest, assuring the acquisition of fresh sweat samples while avoiding sample evaporation and the dilution of biomarkers, and hence ensuring reliable quantification of the concentration of the molecules of interest with ISFETs. To our knowledge, this is an option that has not been explored or considered before in wearable sweat sensing systems, and poses therefore an essential impact in the field. The main contributions of this work can be summarized as follows:

- Through the careful design of the microfluidics, we have successfully developed a microfluidic interface capable of drawing volumes of liquid from an artificial skin setup. The approximate volume acquired in the open microfluidic device is in the order of 200 nanoliters. Reducing by a factor 10 the volume of liquid needed compared to a non-patterned microfluidic device. We have shown successful unidirectional flow of liquid through the microsystem.
- An improved version of the latest microfluidic system has successfully reduced the volume of sweat to fill the system by another factor of 10, allowing manipulation of volumes of liquid of the order of 20 nanoliters.

As has been demonstrated, the use of micropumps allowed to control the flow rate from 120 pl/min to 4.2 nl/min by adjusting the space between the pillars.

- The parameters for fabrication presented in this thesis allowed the fabrication of micropumps in full SU-8 devices, a process that is extremely complicated due to the fragility of the micropillars. Even if the fabrication of the devices was successful, the yield was low. Further optimization of the process can improve the results. Special attention has to be put in the anodic dissolution of the aluminium sacrificial layer, as the release of the top wafer is likely to damage the full microfluidic structure.

- The microfluidic interface proposed in this chapter is CMOS compatible and benefits from standard microfabrication procedures, making this process suitable for mass production once optimized. The integration of the microfluidic interface paves the way toward a better understanding of the biochemical dynamics of sweat.

Chapter 5 Heterogeneous Integration of functionalized ISFETs with embedded passive capillary microfluidics and miniaturized Ag/AgCl Q.R.E

This thesis has discussed in the previous chapters the utility of using ISFET sensors in wearable sensing systems as they are compact devices that operate with low power consumption. In addition, this thesis has discussed the importance to use a microfluidic interface between the sensors and human skin to take advantage of very low volumes of sweat. This chapter deals with the integration of the different technological modules, presented in the previous chapters, to develop one of the first low power electrolyte sensing microfluidic chips based on the heterogeneous integration of: (i) high-k *functionalized* ISFET sensors, (ii) passive microfluidics on SU-8, and (iii) a miniaturized *Ag/AgCl quasi-Reference Electrode*.

Functionalization of ISFET sensors is of the utmost important in sweat sensing systems as they allow quantification of other ions besides hydrogen. Therefore, this chapter describes three functionalization methods to achieve sodium and potassium sensing with ISFETs. These methods are 1) Self-Assembled Monolayers (SAMs) on HfO_2, 2) SAMs on Metal gate ISFETs and 3) Ion Sensing Membranes (ISM).

Later, a process for the miniaturization of an Ag/AgCl quasi Reference Electrode (QRE) on top of SU-8 surfaces is proposed. As discussed in chapter 3, the reference electrode is paramount in ISFET measurements as its stability determines an expected fixed potential E_{Ref}. This thesis provides a method to deposit a stable Miniaturized QRE, lasting for up to 24 hours of continuous measurements.

Finally, the heterogeneous integration of the three components is described, providing a fully integrated and compact platform that could be exploited for

electrolyte monitoring in biofluids for healthcare applications. We describe the full fabrication process for the microfluidic system with the embedded reference electrode.

5.1 Functionalization of ISFETs for electrolyte sensing

After the successful detection of pH with high-k dielectric ISFETs (described in Chapter 2), efforts were dedicated to adapt ISFET technology to provide Sodium and Potassium ion sensing in a biofluid such as sweat. To achieve this, the surface of the gate oxide has to be modified, or functionalized. The main objective of the functionalization is obtaining measurements that show high specificity between the different ions, while maintaining the ISFET optimal performance. In this section, three possible methods for functionalization of ISFETs are discussed. A brief introduction to each method is given in order to understand the main differences between each functionalization process and later discuss the results obtained with each method. The development of this work has been developed in collaboration with Dr. Negar Moridi, Dr. Johan Longo and Dr. Neil Ebejer from Xsensio.

5.1.1 Self-Assembled Monolayers of crown ethers on HfO$_2$

Self-Assembled Monolayers allow the interaction of molecules with a substrate in a densely packed arrangement. This influences the physical properties of the exposed surface [162] [163] [164]. The functionalization is based on host-guest inclusion interactions between the sensor surface and a target molecule. This requires covalent attachment of "host" molecules like crown ethers at the surface of the ISFET gate terminal [165]. The modification of the surface of the gate with crown ethers creates a screening effect that allows the quantification of the targeted ion.

This section provides the detailed procedure for covalent immobilization of crown ethers on the surface of hafnium oxide substrates. Crown ethers are cyclic chemical compounds that consist of a ring containing several ether groups. The denticity of the polyether influences the affinity of the crown ether for different cations (such as sodium and potassium) as figure 5.1 illustrates.

SAMs combine two properties, first the existence of a specific and reversible interaction between guest and the monolayer assures selective recognition, also, the binding of a guest has to be transduced into an electrical signal [166] [167] [168]. As seen in literature, most of the work regarding functionalization with SAMs has been performed on top of noble metals (especially gold) on electrodes. Nonetheless, before moving forward to a post-process to deposit a metal gate on top of the ISFET sensors, we decided to test the SAMs on top of HfO_2 directly. Research has been done to place SAMs on oxides, focusing mostly on electrodes [169] [170], although the works from Zhang proposes a method to deposit SAMs on top of SiO_2 Nanowires [171].
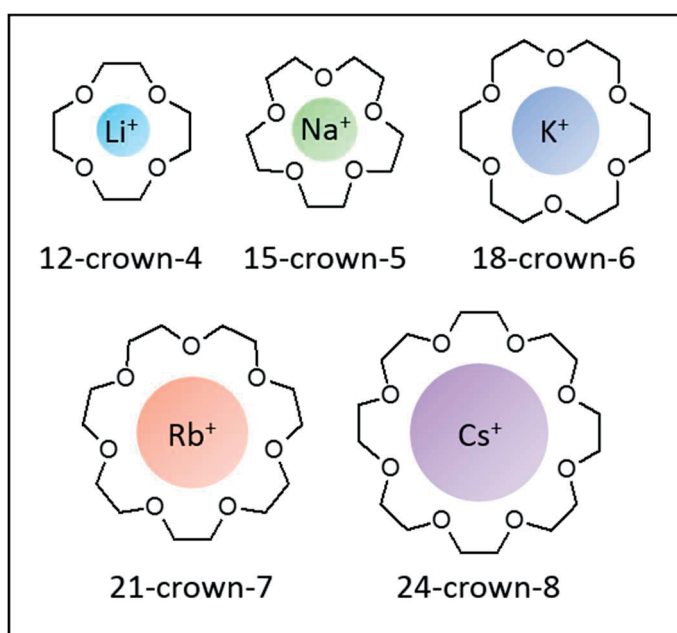
Figure 5.1 Crown ether composition to allow the detection of different molecules

A protocol has been developed for selective detection of sodium and potassium in sweat. This requires covalent immobilization of crown ethers as "host" molecules on the sensitive HfO_2 surface of the sensors. The functionalization protocol is developed here on a simple potentiometric (ISE) sensor formed of platinum electrodes covered by HfO_2 (and measured with a commercial Ag/AgCl reference electrode). This research has been developed in collaboration with Dr. Negar Moridi.

Immobilized SAMs of crown ethers on HfO2 substrates were used as "host surfaces" for the detection of alkali metal ions as guest molecules. This strategy was applied for a selective detection of sodium and potassium as target molecules. The binding of metal ion to polyether is strongly dependent on the size of the metal ion and the size of the cavity in the center of polyether. 15-crown-51 selectively forms complexes with Na^+ as its ionic diameter match perfectly with the cavity size. Similarly, 18-crown specifically binds to K^+ (Table 1). Therefore, 4'-aminobenzo-15-crown-5 was used for selective detection of sodium ions and 2-aminomethyl-18-crown-6 was used for selective detection of potassium ions.

Cation	Ionic diameter (Å)	Crown ether	Cavity size (Å)
Na^+	1.94	15-crown-5	1.7-2.2
K^+	2.66	18-crown-6	2.6-3.2

Table 1 Ionic diameters and cavity sizes.

5.1.1.1   Formation and characterization of a self-assembled monolayer

The simple potentiometric sensors, i.e. ion selective electrode (ISE) sensors (Fig. 5.2) were fabricated as follow: The starting substrate was a silicon wafer with a 1 µm thick layer of SiO_2. First 20 nm thick Cr adhesion layer and a 100 nm thick Pt

layer have been sputtered. The electrodes have been patterned with photolithography and plasma etching of the metals. After a short oxygen plasma to remove the remaining photoresist, 3 nm of HfO_2 have been deposited by ALD.
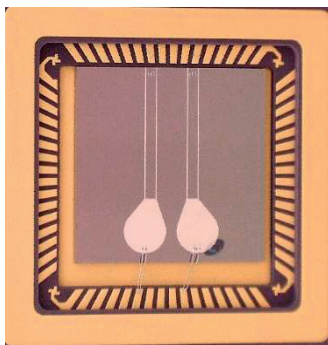
Figure 5.2 Picture of a die of "Pt/HfO₂ potentiometric sensors": here two Pt working electrodes are present on the die which is wire bonded to a chip carrier for subsequent electrical measurements.

The procedure to perform selective sensing of sodium ions with functionalized ISFETs with crown ethers was first reported by Wipf et al [172]. The same chemical process was followed to achieve selective sensing of Na^+ ions in ISEs that count with HfO_2 as a sensing layer as explained before. SAMs of crown ethers derivatives were prepared in three steps (Fig 5.3a). Cleaned hafnium oxide substrates were prepared by immersing in piranha solution (H_2SO_4:H_2O_2, 70:30, v/v) at 100°C for 20 min. The sensors were then thoroughly rinsed with deionized water and ethanol for 10 min respectively and dried under a nitrogen stream. Amino terminated SAMs were obtained by immersing the cleaned substrates in 10% v/v solution of (3-aminopropyl)triethoxysilane (APTES) in ethanol for 12 hours at room temperature. The substrates were then rinsed with ethanol and dried under N_2 stream. The formed APTES layer was cured at 100°C for 24 h. Subsequently, isothiocyanate functional groups were introduced on to the monolayer by exposure to a solution of 1,4-phenylene diisothiocyanate (0.1 M) in toluene at 50°C for 2 hours (Fig 5.3a step ii) followed by rinsing with toluene and drying in a stream of N_2. The self-assembled monolayer (SAM) layers formed were reacted with the 2-aminomethyl-15-crown-5 to allow its covalent immobilization. This was achieved by incubating the samples in a solution of **2-aminomethyl-15-crown-5** (5

mM) in borate buffer (50 mM, pH 8.5) at 50°C for 2 hour, after which the substrates were sonicated in deionized water in order to remove physisorbed molecules. After immobilization, the contact angle increased from 18° to 78°, suggesting the successful grafting of APTES. The presence of the isothiocyanate functional groups at the surface of the sensors was evidenced by XPS measurements taken on functionalized substrates. The results revealed that the atomic ratio of S/N increased from 0 to 0.34 for APTES and isothiocyanate functionalized substrates respectively. This proved the successful immobilization of isothiocyanate groups on the HfO$_2$ surface. Furthermore, an increase in atomic ratio of C/Si from 3.5 to 6 was measured for isothiocyanate and crown ether functionalized sensor respectively. That suggest the successful immobilization of crown ethers on hafnium oxide substrates. In order to detect Potassium ions, SAMs of 18-crown-6 on hafnium oxide was prepared following the same procedure described above, by using **4'-aminobenzo-18-crown-6 instead of 2-aminomethyl-15-crown-5.**
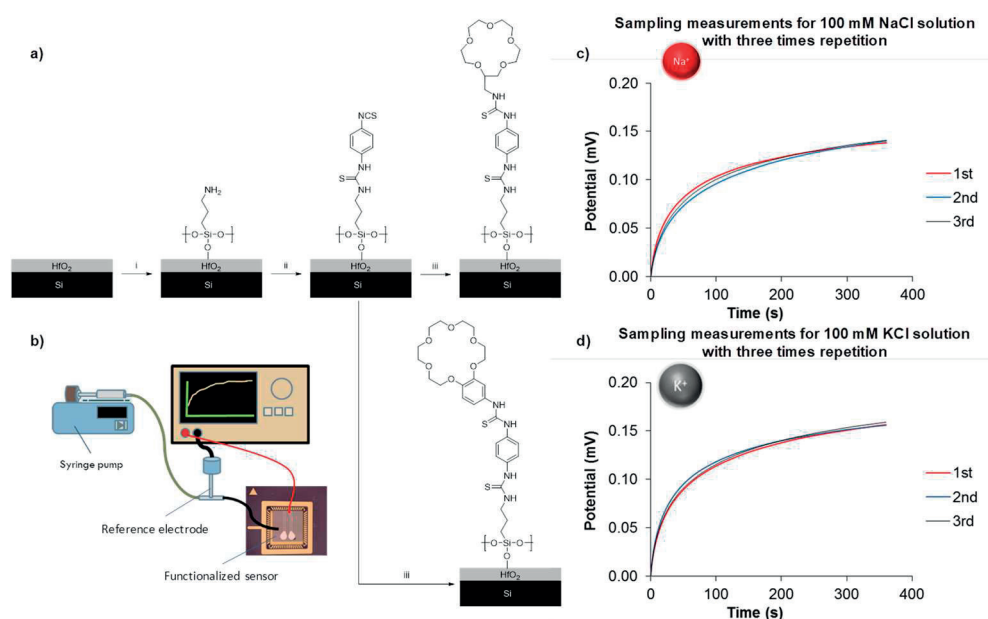
Figure 5.3 a) Formation of organized monolayers of amino derivatives of crown ether on hafnium oxide surfaces. i) (3-aminopropyl)triethoxysilane; ii) 1,4-phenylene diisothiocyanate; iii) 2-aminomethyl-15-crown-5 (Na+ sensors) or 4'-aminobenzo-18-crown-6 (K+ sensors) ; b) Schematic representation of experimental setup; c) Sampling measurements for 100mM NaCl of Na+ sensors with three times repetition; d) Sampling measurements for 100mM KCl of K+ sensors with three times repetition

5.1.1.2 Assessment of sensitivity and selectivity of sensors functionalized for Na$^+$ and K$^+$ ions

In order to test the fabricated ISE sensors, the open circuit potential was measured against a commercial Ag/AgCl reference electrode, Microelectrodes Inc. 16-702 Ag/AgCl reference electrode (Microelectrodes Inc., Bedford, USA). The ISE sensors dies were mounted and wire bonded in chip carriers using epoxy to passivate the wiring and form a small well. A syringe pump was used to fill the well with a given electrolyte solution (ions and concentration) maintaining the liquid contact between the ISE sensor and the flow-through electrode via the electrolyte-filled tubing, as shown in Fig 5.3.b. Measurements were performed on an HP 4156A parameter analyzer (Hewlett-Packard JP, Tokyo, Japan). In the open circuit potential measurements, no current is applied in the system, the reference electrode provides a stable reference potential for the measurement of the potential of the fabricated functionalized (working) electrodes. Thus, the reference electrode is connected to ground and zero current is applied on the fabricated ISE sensors, only measuring the potential over time.

The sensitivity of each (sodium and potassium respectively) functionalized test sensor was assessed separately using different buffer solutions of NaCl and KCl respectively with varying concentrations. OCP sampling measurements were performed for 6 minutes for each functionalized sensor with each analyte/concentration solution and repeated three times (Fig 5.3.c&d). Fig. 5.4 demonstrate the open circuit potential (OCP) measurements of sensors functionalized for sodium (Fig. 5.4a) and potassium (Fig. 5.4b) in the electrolyte solutions with concentration of 0.1-300 mM Na$^+$ and K$^+$ respectively. For both sensors a linear relationship with a regression coefficient of 22.3 mV/dec (sensor functionalized for sodium) and 26.1 mV/dec (sensor functionalized for potassium) between open circuit potential and Na$^+$/K$^+$ concentration in logarithmic scale was observed.

The selectivity of the sodium (respectively potassium) functionalized sensor was assessed by measuring the cross-sensitivity to the non-target ion: potassium (respectively sodium). This was achieved by using increasing concentration of KCl and NaCl (0.1-300 mM) for Na^+ and K^+ sensors respectively. It was observed that depending on non-target ion concentration the response was at least 50% lower for each sensor compared to the response for their target ions (Fig. 5.4a&b). For both sensors a linear relationship with a regression coefficient of 11.4 mV/dec (sensor functionalized for sodium, response to potassium) and 14.1mV/dec (sensor functionalized for potassium, response to sodium) between open circuit potential and Na^+/K^+ concentration in logarithmic scale was observed.

In parallel, an APTES modified sensor [172] as a reference sample, was studied following the same experimental procedure. Fig. 5.4a demonstrates the open circuit potential measurements of Ref sensors in the electrolyte solutions with concentration of 0.3-300 mM NaCl for sodium functionalized sensor. Fig. 5.4b demonstrates the open circuit potential measurements of Ref sensors in the electrolyte solutions with concentration of 0.3-300 mM KCl for potassium functionalized sensor. Regarding the values measured for the reference sensors, one hypothesis could be that the OCP measured for reference sample comes from a cross sensitivity with Cl^- and therefore these values were subtracted from values measured for sensors functionalized for sodium and potassium (Fig. 5.4c&d). For both sensors a linear relationship with a regression coefficient of 13.7mV/dec (sensor functionalized for sodium) and 15.2mV/dec (sensor functionalized for potassium) between open circuit potential and Na^+ /K^+ concentration in logarithmic scale was observed. Depending on non-target ion concentration, the response of the sensor was 91% to 100% lower, compared to the response for their target ions (Fig. 5.4c&d).
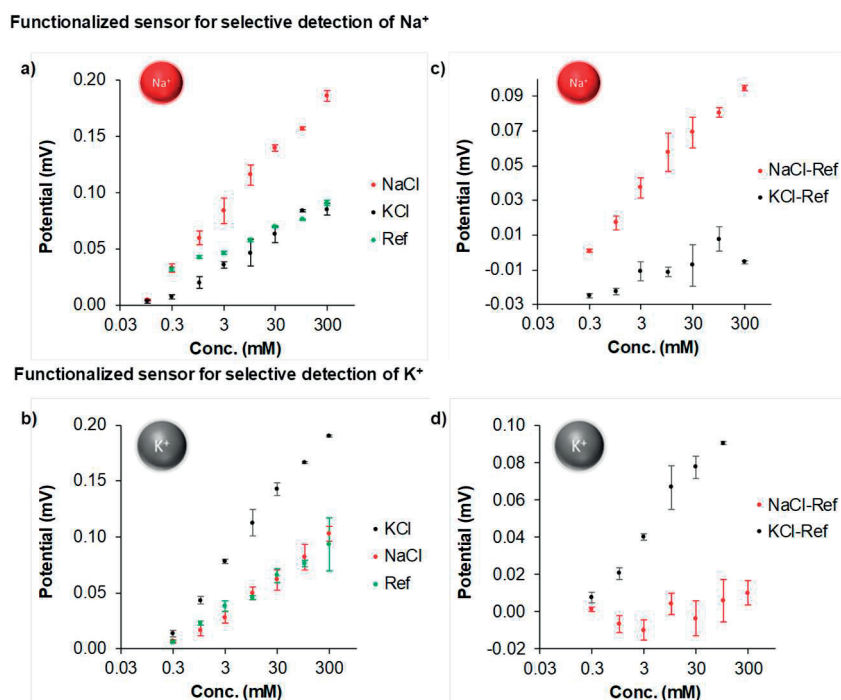
Figure 5.4a) Sensitivity and selectivity assessment of Na+ sensors; b) Sensitivity and selectivity assessment of K+ sensors; c) Sensitivity and selectivity assessment of Na+ sensors after Ref values were subtracted from values measured for sensors functionalized for sodium d) Sensitivity and selectivity assessment of K+ sensors after Ref values were subtracted from values measured for sensors functionalized for potassium.

5.1.1.3   Discussion: SAMs functionalization for ISFETs

After obtaining good results of selectivity and sensitivity with SAMs on ISEs with Hafnium dioxide as a sensing layer, the same process was replicated on top of the ISFET devices. Nonetheless, the sensors show no response with variations in the reference electrode voltages. The possible reason for this might be the use of the piranha solution used in the formation of the SAMs, it is possible that the SU-8 passivation layer gets degraded with the piranha and therefore creating a short circuit between the three terminals of the device. Due to the lack of results with ISFETs and the SAMs on HfO_2 FET gate, the presented process was modified and adapted to be deposited on gold gates on top of the gate oxide, as explained in the following section.

5.1.2 Self-Assembled Monolayers of crown ethers on a metal gate

The use of a metal gate (principally gold) in an ISFET has been exploited in literature to decrease the number of sites N_S in the gate terminal and thus, decrease the response the hydrogen activity in the surface of the gate terminal of the ISFET [172] [77]. A functionalization of the metal gate is then performed with crown ethers to improve the specificity of the system. The design of crown ethers that can form SAMs on noble metals typically requires the introduction of thiol functionalities in the crown ethers structure. It has been demonstrated that n-alkanethiols are also able to form self-assembled monolayers on gold substrates [173] [174]. In order to achieve this in our process, a 20 nm layer of gold was deposited on top of the gate dielectric as can be seen in figure 5.5. A 5 nm layer of titanium was sputtered as an adhesion layer.
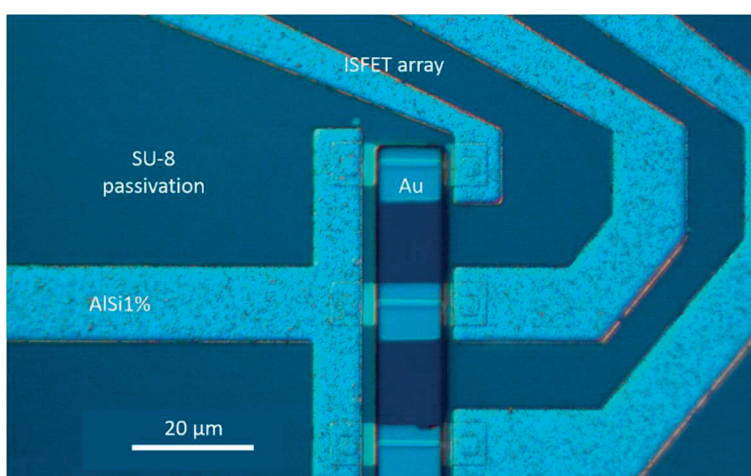
Figure 5.5 SEM picture of the deposition of a gold layer on top of a Nanoribbon ISFET.

The functionalization of the FET is based on a thiol-gold interaction between thiolate ion-sensitive crown ethers and the gold gate of the sensor. The first part of

the process is dedicated to the hydroxyl to thiol crown ether modification, Fig. 5.6a. The alcohol group of the crown ether is converted to a sulfonate (leaving group) using toluene sulfonyl chloride. A nucleophilic substitution using 2,2′.(ethylenedioxy)-diethanedithiol is then performed to obtain a thiol functionalized crown ether. The FET arrays are functionalized for K^+ and Na^+ sensing (Fig. 5.6b&c) by putting them 12 hours in contact with a solution of thiolated crown-ethers in methanol.
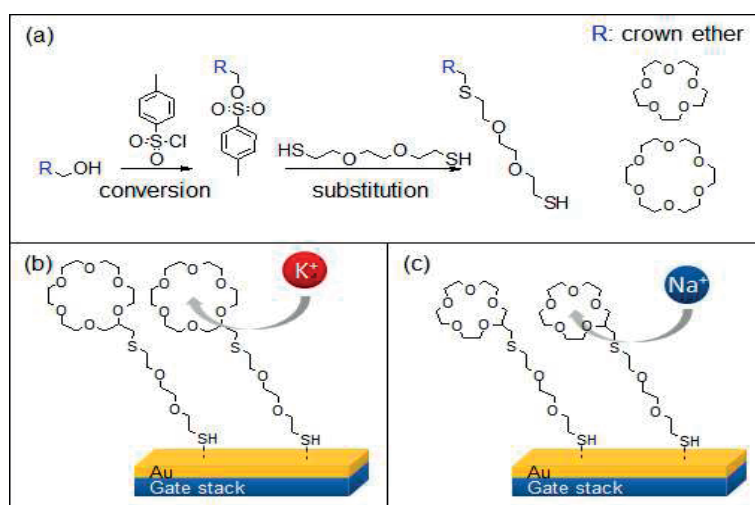
Figure 5.6 Functionalization chemistry of the Au gates for specific electrolyte sensors: a) hydroxy crown ethers modification, (b) and (c) FET gold gate functionalization for K+ and Na+ sensing, respectively.

The functionalization was tested directly on top of ISFETs, the results were positive for Sodium sensing, while the potassium functionalization was non-responsive. The characterization results are presented in the section 6.2.1 of this thesis.

5.1.3 Functionalization with ion sensitive polymeric membranes

Ion sensitive polymeric membranes (ISMs) deposited on electrodes can offer an alternative to SAM functionalization. This is one of the most used technologies when using chemical sensors [175]. ISMs are formed by a mixture of a PVC membrane with an ionophore. Ionophores are molecules that interact with a specific ion. The chemical composition of the ionophore is what defines its specificity [176] [177].

The challenge resides then in the proper integration of polymeric membranes on top of ISFET devices. This section shows the process to fabricate and deposit sensitive membranes for sodium and potassium on ISFET sensors with a gold gate. This is an adaptation of the process that Javey's group presented to deposit sensitive membranes on ISEs in [24].
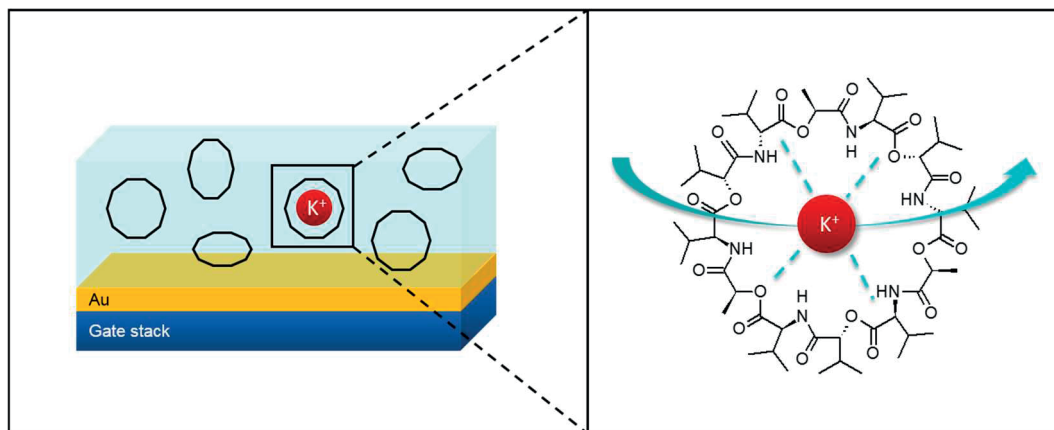
Figure 5.7 Functionalization chemistry of Au gates with a polymeric membrane for potassium sensing

The Sodium selective membrane was prepared by mixing Na ionophore X (1% weight, w/w), Sodium tetrakis[3,5-bis(trifluoromethyl)phenyl]borate Na-TFPB (0.55% w/w), Poly(vinil) chloride PVC (33% w/w), and dioctyl sebacate DOS (65.45% w/w). 100 mg of the membrane cocktail was dissolved in 660 μl of

tetrahydrofuran. The Potassium selective membrane cocktail was composed of valinomycin (2% w/w), Sodium tetraphenylborate NaTPB (0.5%), PVC (32.7% w/w), and DOS (64.7% w/w). 100 mg of the membrane cocktail was dissolved in 350 µl of cyclohexanone [59]. Ion-selective membranes were then prepared by drop-casting, respectively, 10 µl of the Na+- selective membrane cocktail and 4 µl of the K+-selective membrane cocktail onto electrodes. Figure 5.8 shows the drop-casting method of the membrane on top of electrodes with a 2 mm diameter.
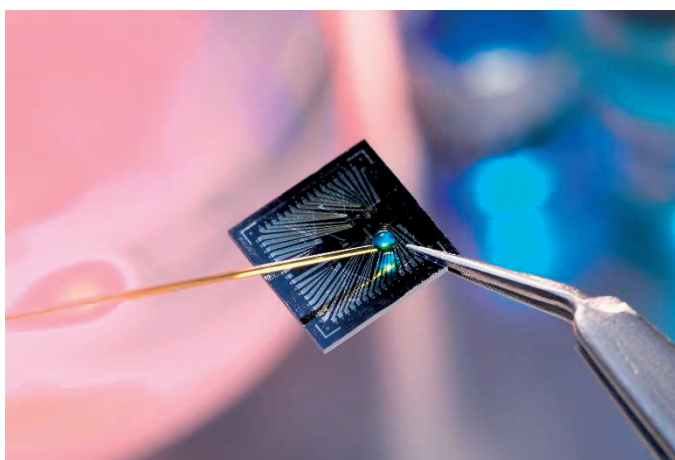
Figure 5.8 Dropcasting of ISM for sodium sensing

5.1.3.1   Sodium sensing with ISE's and a polymeric membrane

Prepared devices, were hydrated and equilibrated with the test solution (50mM NaCl and 20mM KCl for Na+ ISM and K+ ISM functionalized sensors respectively) before use for about 30 minutes. Measurements were ran until a stable value potential was reached. When going from a higher concentration to a lower one the devices were washed with deionized water to avoid contamination. All measurements were performed in a 2-electrodes arrangement using a commercial Ag/AgCl reference electrode.

The response for a sodium selective membrane is reported in Figure 5.9, showing a fast response to changes in the concentration of the analyte.
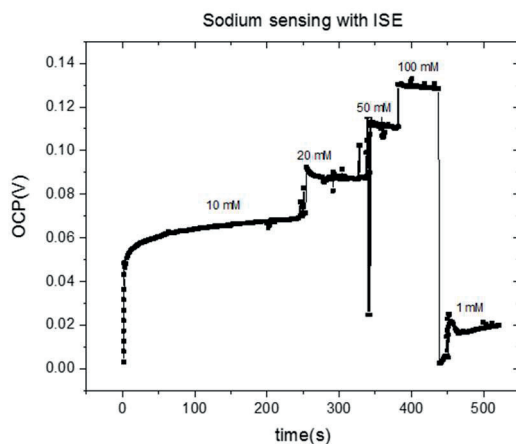
Figure 5.9 Sodium sensing with ISE functionalized with a polymeric membrane

The linearity of the system and the high selectivity of ionophore chemistry is shown in Figure 5.10, with a Near Nernstian behavior of 56.1 mV / decade. To evaluate the cross-sensitivity of the ISM, the sensor was alternatively put in contact with a solution of KCl (100mM) and NaCl (1mM) (see figure 5.10b). Experimental results highlighted a high selectivity of the Na^+ ISM against K^+ ions. Indeed, the response of the ISM for 100mM KCl is reported to be lower than its response to 1mM NaCl, leading to a negligible K^+ sensitivity of the sensor.
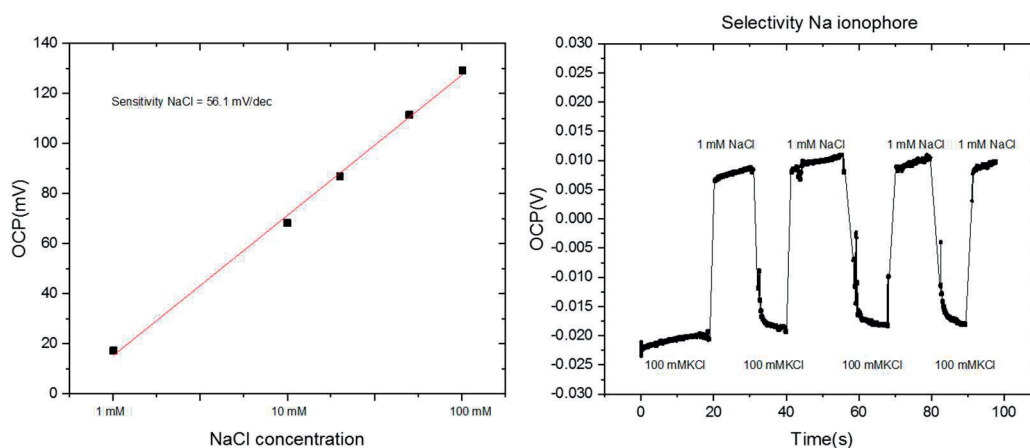
Figure 5.10 Left) Sensitivity of ISE to Na concentration, Right) Selectivity of Na membrane

5.1.3.2   Potassium sensing with ISE's and a polymeric membrane

The ISE with a potassium selective membrane below shows similar behavior to that for the sodium selective membrane as Figure 5.11 displays.
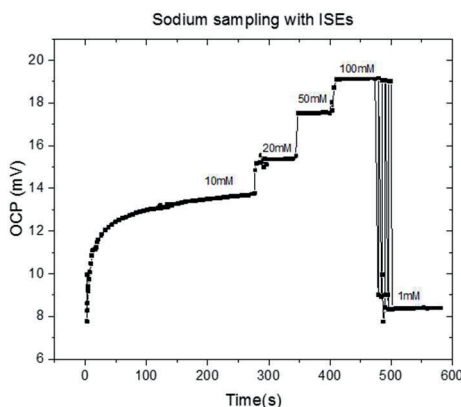
Figure 5.11 Sampling concentrations of KCl with ISEs and a potassium selective membrane.

Similar to the response of the membrane for sodium, the membrane for potassium showed a linear response with a 53.9 mV/dec sensitivity towards KCl concentration solutions as can be observed in figure 5.12. The ISE with a membrane for potassium sensing also showed a negligible cross sensitivity with Sodium when put in contact with a 100mM NaCl solution, as can be observed in figure below:
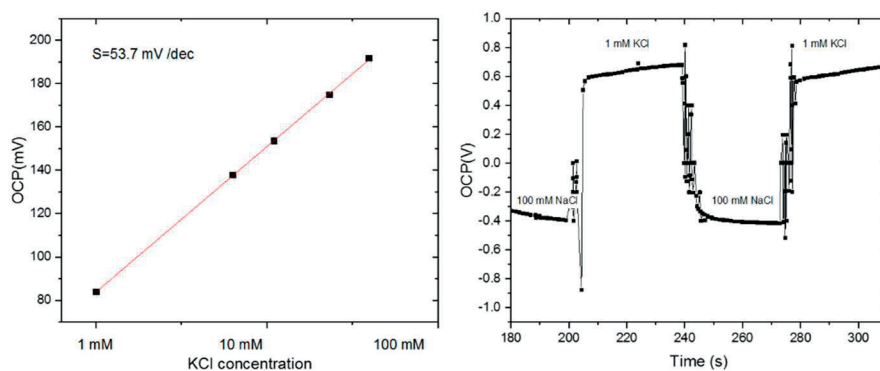
Figure 5.12 Left) Sensitivity of ISE to K concentrations Right) Selectivity of K membrane

5.1.4 Discussion: ISFET functionalization

This research focused on developing an optimal functionalization process for the gate dielectric of the ISFET devices. SAMs of crown ethers deposited on an electrode with an HfO_2 interface provided sensitivities of 22.3mV/dec and 26.1mV/dec for sodium and potassium respectively. No cross-sensitivity has been observed. Nevertheless, the values of sensitivity are below what we were expecting. On the other hand, the ion sensitive polymeric membranes on top of electrodes delivered quasi-Nernstian responses, with sensitivities of 56.1mV/dec and 53.9mV/dec for sodium and potassium respectively. This is a good indicator that functionalization of ISFETs with ISMs might offer better results, as will be shown in the next chapter of this thesis.

The main reason to use ion sensitive membranes over SAMs for functionalization of ISFETs is because the deposition of ISMs involves no aggressive chemical process that compromise the integrity of the chip. On the other hand, the creation of SAMs on top of the ISFETs requires a first step of a piranha bath at a 100°C which compromises the SU-8 passivation layer, a risk that could result in eventual short circuits as liquid could create an electric path between the source and drain terminals of the FET.

5.2 Development of a miniaturized quasi Ag/AgCl Reference Electrode on SU-8 substrates

Chapter 3 of this thesis has described how potentiometry measurements work and how there is a need to have a potential reference electrode in the system. Since ISFETs work with a potentiometry principle, the reference electrode is a key component in ISFET operation. Originally, the ISFET concept was believed to abandon the need of an external reference electrode, but this assumption has been proven wrong and it is largely accepted that the reference electrode is necessary [75] [77] [178]. Therefore, efforts in miniaturization have been undertaken to develop miniaturized reference electrodes. Miniature reference electrodes have been the subject of many studies with different applications, but there is still big room for improvement concerning overall performance, and materials and methods for fabrication. This section presents the development of a process to integrate a miniaturized Ag/AgCl quasi reference electrode in a SU-8 environment. This work has been developed with MSc. Amira Muhech, Dr. Raffaele Cossimati, and Dr. Fabien Wildhaber from XSensio.

5.2.1 The reference electrode

In electrochemical studies, a reliable reference electrode is needed to provide a stable potential for measurement execution. The measurement of potential of an oxidation-reduction reaction with a working electrode requires a stable reference point, which is why an electrode with fixed potential is placed. This is called a reference electrode, and no current should pass through it [179]. In the case of an ISFET, the gate terminal is replaced by a reference electrode immersed in an aqueous solution. The potential at the surface of the gate oxide is related to the amount of charges present in the solution, which are contributions of both the reference electrode and the ionic charges in the liquid environment [180].

For our application, ideally, the reference electrode has to be stable over a defined range of pH (from 3-8), a defined range of NaCl and KCl concentration (1-100 mM). Additionally it has to be compatible with the SU-8 polymeric substrate with a long term stability (potential drift should be minimized during a long operation time). Moreover, it should not introduce toxic or hazardous materials. Additional advantageous characteristics would be resistance to corrosion (which would affect the reactions in the test solution), insensibility to interference species, and low noise [181] [182].

Electrode potentials are generally expressed with respect to the standard hydrogen electrode (SHE). The SHE is a reference electrode that has a defined potential of 0V at standard conditions (25 ºC, 1 bar pressure). This electrode is used as the standard reference for measuring cell potentials. However, given that it needs a constant flow of hydrogen gas, it is difficult to fabricate, if not miniaturize [183].

Most experiments in aqueous solutions use a saturated calomel electrode, or a silver-silver chloride electrode (Ag/AgCl). The calomel electrode, commonly used in the laboratory, has great potential stability, however, it requires a large amount of mercury for its fabrication, controlled H_2 pressure, and it cannot be used above 80 ºC. It is generally avoided in microchip applications [184]. The Ag/AgCl electrode is therefore the best choice for miniaturization, for its simplicity of use and compatibility with microfabrication techniques, plus its electrochemical characteristics. However, the integration of an Ag/AgCl reference electrode is not possible in a microsystem due to its size. Therefore, the use of a quasi-reference electrode has to be considered.

5.2.2 Ag/AgCl Quasi Reference Electrode on SU-8

A quasi-reference electrode typically consists of a metal wire that is inserted directly into the analyte. An important difference between a reference electrode and a QRE is the lack of thermodynamic equilibrium in the later [185]. The advantages they offer are a small impedance effect (which, nevertheless, could

make the system susceptible to environmental noise), no liquid junction potential (potential that develops when two solutions are in contact), and no contamination of the analyte due to electrolyte leakage. This makes the design much simpler.

However, the drawbacks are: slight potential shift during the measurements (because of formation of surface oxides) [186], and often, operation performance varies depending on pH or temperature [185]. Moreover, it is susceptible to changes in the activity of its primary ion (Cl⁻) [187].

An important issue to overcome when designing and fabricating a quasi-reference electrode is the lack of stability when used in different conditions. Instability is often attributed to the dissolution of the salt layer, and the development of mixed potentials at the electrode/solution interface. The solubility constant for AgCl is $1.8x10^{10}$ so approximately 1.9 mg of AgCl will dissolve in a liter of water at room temperature [188]. It is then easy to suppose that in a miniaturized version, with a considerably smaller AgCl volume, the layer will dissolve more easily, giving place to unwanted perturbance. According to a previous study by Polk and colleagues [188], a good solution would be to increase the quantity of available AgCl on the electrode. To achieve this, a thicker layer of silver is needed, naturally.

A solution to the previously mentioned issues would be to use a reference electrode with a solidified electrolyte, which could also function as salt bridge. Some authors have coated the Ag/AgCl electrode with polymeric materials saturated with KCl such as agarose [189], porous silicon [184], glass fiber filters [190], and hydrophilic polyurethane [191], to cite a few. These coatings provide a constant concentration of chloride ions [192], and make the reference electrode insensitive to changes in pH and Cl⁻ ion concentration. An outer polymer layer, such as Nafion, perfluorocarbon polymer (PFCP), cellulose acetate or polyurethane, is often used to help against degradation, and discriminate against organic species [184] [181] [192]. This work proposes coating the Ag/AgCl QRE with a polymer layer to stabilize the electrode as will be detailed in the next section.

5.2.2.1 Technological development

The process to obtain a miniaturized quasi reference electrode on a SU-8 substrate is described next. SU-8 (Gersteltec Sarl, Switzerland) was processed on a 4-inch Si wafer. The wafer is cleaned with oxygen plasma for 7 minutes at 500 W before the SU-8 procedure. A 5 μm layer of SU-8 was spin-coated using a Sawatec LSM200 (Sawatec AG, Sax, Switzerland). Then, the photo resist was baked for 25 min at 130°C. To evaporate the solvent and to smooth the surface, the wafers were then exposed to UV light on a Karl Suss MA6 back-side mask aligner (Karl Suss, Garching, Germany) for 6 seconds at an intensity 10 mW/cm2. Afterwards, the wafers were baked at 90 ºC for 90 minutes to achieve cross-linking of the resist. Finally, the processed SU-8 wafers were left to rest overnight.

A short surface treatment (30s at 200 W) of oxygen plasma was used on the SU-8 wafers prior to metal deposition (no other type of surface treatment was performed). Afterwards an adhesion layer of 40 nm of Chromium was deposited prior to the silver electrode (900 nm) deposition, Chromium was chosen as an adhesion metal due to its optimal performance in adhesion with SU-8 substrates. Metals were deposited by sputtering on a DP 650 (Alliance-Concept, Cran-Gevrier, France). Sputtering was selected as deposition method because it provides a more uniform layer, and stronger adhesion between metals. 3 μm of silver were then electroplated to obtain a more robust reference electrode. The electrode was then chlorinated as explained in the following section.

5.2.2.2 Chlorination

The typical methods for AgCl formation from silver include anodization in chlorinated solutions, and chemical chlorination [181] [188]. Anodization consists of the formation of a surface oxide in a chemical solution. Current is passed from the anode (material to oxidize) to the cathode (inert material) through an electrolyte.

In chemical oxidation, the electrode is immersed in an aqueous solution of $FeCl_3$. The reaction that takes place proceeds as:

Equation 5.1

$$FeCl_3 + e^- \leftrightarrow FeCl_2 + Cl^-$$

$$Ag^+ + Cl^- \leftrightarrow AgCl$$
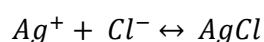
$FeCl_3$ is reduced to $FeCl_2$, and the silver cation combines with the chlorine anion to generate AgCl in the silver electrode's surface [193]. To chlorinate the electrode, $FeCl_3$ is pipetted on top of the silver electrode, letting the silver chlorinate for 75 seconds. Afterwards, the chip is rinsed in deionized water. SEM was used to characterize the electrodes; the results are shown in Figure 5.13.
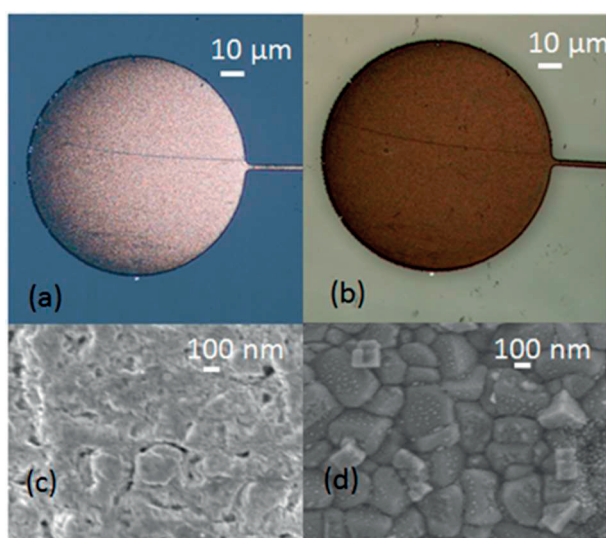
Figure 5.13 Top optical views, (a) and (b), and SEM magnifications, (c) and (d), of the fabricated Ag/AgCl Quasi-Reference Electrode, before and after the Chlorination.

After chlorination, the electrode was coated with a Butvon®, a polyvinyl butymal (PVB) polymer solution filled with NaCl. 5 µl of this PVB membrane were drop casted on top of the electrodes as described in [3].

5.2.3 Electrical characterization of the reference electrode

For assessing electrical performance, the fabricated electrodes were tested by measuring open-circuit potential (OCP) against a commercially available Ag/AgCl reference electrode (16-702 Microelectrodes Inc., Bedford, USA). All measurements were performed on an HP 4156A parameter analyzer (Hewlett-Packard JP, Tokyo, Japan). A diagram of the setup is provided in figure 5.14.
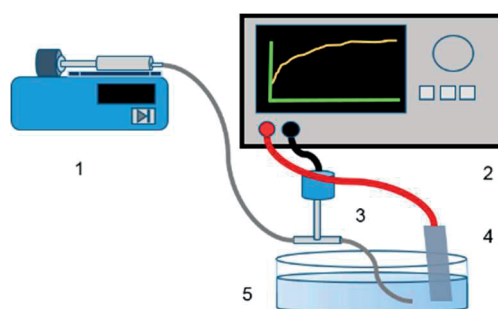
Figure 5.14 Setup for measuring open-circuit potentials. 1. Syringe pump to deliver a constant flow of 3 M KCl into the commercial reference electrode 2. Parameter analyzer 3. Commercial reference electrode 4. Fabricated reference electrode 5. Beaker with 3 M KCl. Note: The liquid contained in the pump is the same as the one in the beaker.

The miniaturized Ag/AgCl QRE was tested in a 23 mM NaCl environment under a continuous flow of 25 nl/min. The potential of the miniaturized QRE is fully stable, ensuring stable operation for 14 hours as can be observed in figure 5.15.
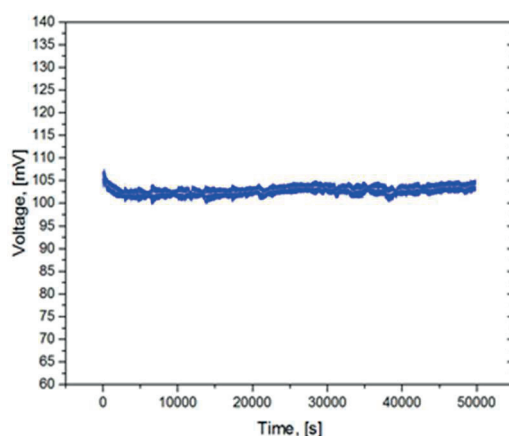
Figure 5.15 Stability plot of open circuit potential of the reference microelectrode while perfusing 23 mM NaCl at 25 nl/min through the channel (vs. a commercial flow-through AgCl ref. electrode).

96

5.3 Integration process for technological modules

This section presents a method to integrate all the different technology modules presented in this thesis to deliver the first "Lab-on-skin" system. The highest achievement of this work, is the successful combination of very different technologies in a single chip.

A first prototype to validate the functionality of the FinISFETs in a miniaturized characterization environment for pH sensing is presented. With this prototype, we evaluated the performance of the first architecture of ISFET sensors presented in chapter 3 with a Pressure Sensitive Adhesive (PSA) microfluidics and a miniaturized quasi reference electrode. Afterwards, this section shows the development of the SU-8 microfluidics (presented in chapter 4) with an embedded reference electrode over the nanoribbon ISFETs (presented in chapter 3).

5.3.1 Post processing of PSA microfluidics for FinISFET characterization

In this work, it was important to validate the operation of ISFETs in a miniaturized microfluidic environment. Pressure Sensitive Adhesives provides a good option for rapid prototyping of a system as it is easily manually manufactured [93]. Figure 5.16b shows the main fabrication steps to post process microfluidics and a miniaturized Ag/AgCl quasi reference electrode on top of the liquid gate FinFETs described in the third chapter of this thesis.
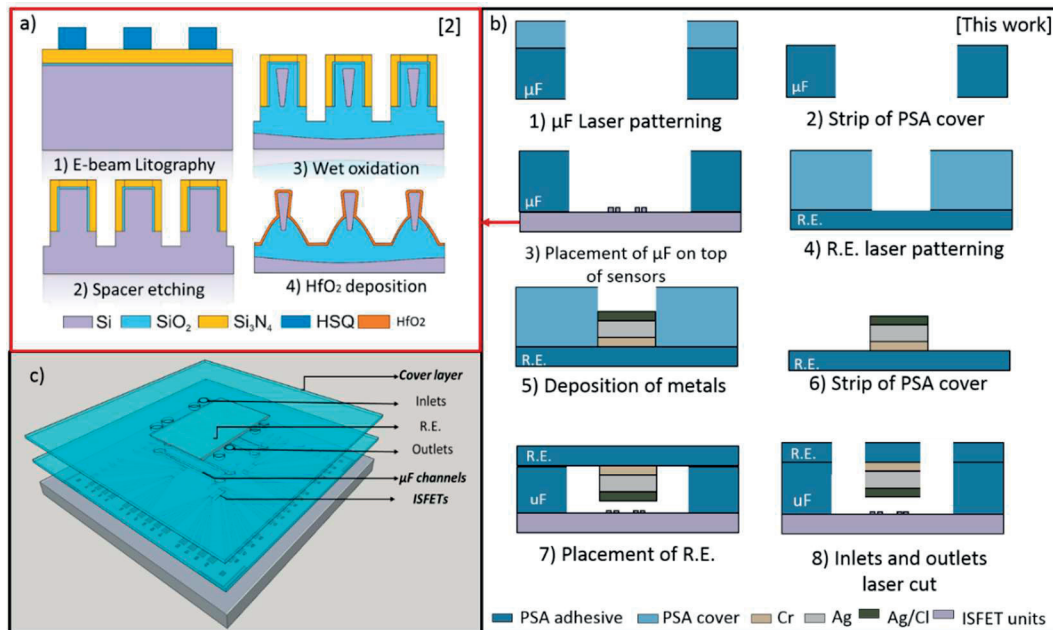
Figure 5.16 Integration of a miniaturized R.E. embedded in a microfluidic channel and a chip with ISFET pH sensors a) Critical steps for the fabrication of the ISFET devices. Description of process flow in [88] , b) Process flow to achieve the integration of the sensing unit, the microfluidic channels and the miniaturized reference electrode with the ISFET sensor chip. c) 3D model of the integrated system. Reproduced from [194].

The fabricated FinISFET devices have a maximum length of 15 μm, with this condition it was possible to design a very simple microfluidic system that could be filled with as little as 25 nL. The system consists of an array of single channels that are patterned in the PSA. When a drop of liquid was placed on top of the inlets, the liquid immediately filled the channels, as can be seen in figure 5.17. Nonetheless, there was no control of the speed or direction of the liquid inside the channel, condition that becomes a disadvantage when the amount of sweat to analyze is limited.

Figure 5.17. PSA passive microfluidics showing the transport of liquid from inlet to outlet by capillary forces.

Samples were prepared over 100 micron-thick PSA 93049 (Adhesives Research, Limmerick, Ireland). The OPTEC LSV3 Excimer Laser was used to pattern the reference electrodes in a single layer PSA sheet. The detailed workflow for the fabrication of this Reference Electrode is shown on Figure 5-15.b (Steps 4-6). The Reference Electrode pattern is a rectangle with a 50 mm² area. The microfluidic device was fabricated using a single layer Pressure-sensitive-adhesive (Adhesives Research, Ireland). The channels in the PSA were patterned with the OPTEC LSV3 Excimer Laser.

5.3.1.1   *Fabrication methods for PSA microfluidics on FinISFETs with integrated QRE*

Once the channels were patterned on the PSA, the adhesive foil was removed and then manually aligned to be placed on top of the FinFET sensors as described in Figure 5.16b (steps 1-3) and as it can be appreciated in Figure 5.16a. The closing lid for the microfluidic chamber is the PSA layer with the Reference Electrode. The protective lid of this PSA layer was removed and then manually aligned on top of the microfluidic channels to proceed with its placement. Once positioned, the inlets and outlets were opened with the OPTEC LSV3 Excimer Laser to get access to the microfluidic channels. Once the inlets and outlets were ready the integration of the system was achieved. As soon as a liquid reaches the inlets, the channels are automatically filled by action of the capillary forces. The continuous flow of the liquid through the channels is ensured by placing an adsorbent material in the outlets. Once the flow of the liquid has been established and stabilized, we have carried out the electrical characterization of the FinFET sensors.

After patterning, silver was deposited, nevertheless, silver metal requires an adhesion layer to avoid its detachment from the substrate. Different metal combinations were tried as adhesion layers. No reported adhesion layers for PSA were found in the literature, therefore we tried different adhesive layers that are commonly used for silver with other polymers. The metals chosen for adhesion

promoters were Cr based on [195], a Cr/Ti combination based on [196] and Al based on the experiment performed by [197].
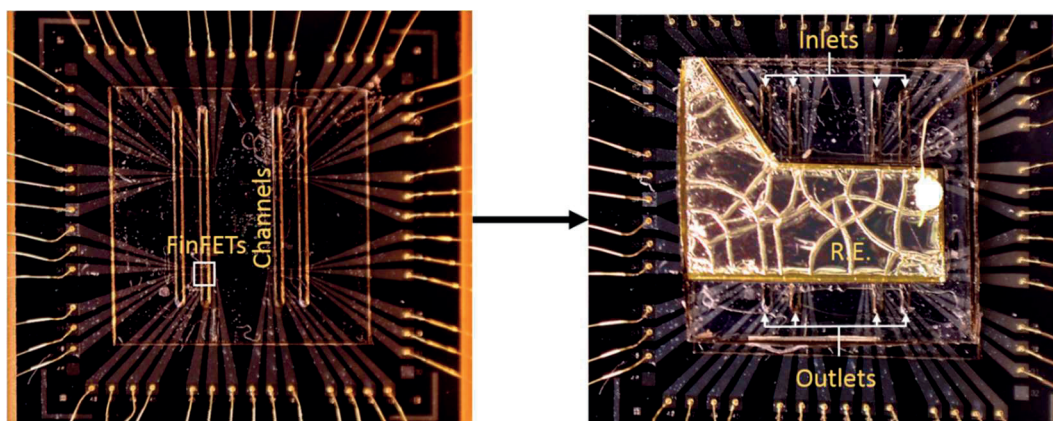
Figure 5.18 Top optical picture of the passive microfluidic layer integrated on top of the FinFET sensor chip. Left) PSA channels placed on top of the ISFET sensing unit. Right) Closing lid of the microfluidic channel with the integrated Reference Electrode.

To evaluate the adhesion of metals to the PSA, the tape test method, based on ASTM standard D3359 (ASTM International, 1996) was used. Scotch tape (3M, Maplewood, USA) was pressed carefully on top of the metal layer. A finger was run over it to enhance contact, and afterwards, the tape was pulled quickly. The best results we obtained by placing Chromium as the adhesive enhancer between the silver and PSA. The metals were deposited by sputtering on a DP 650 (Alliance-Concept, Cran-Gevrier, France). First, 46 nm of Chromium were deposited as an adhesive layer and then 900 nm of Silver were deposited. Although in previous studies thin-films had been deposited by evaporation, sputtering was selected as deposition method because it provides a more uniform layer, and stronger adhesion between metals. Additionally, it allows to deposit thicker layers in less time and it has a lower operational cost.

In this work, anodization was selected as the method for AgCl formation for its simplicity and safety. Surface cleaning to remove possible impurities was performed prior to chlorination. Samples were dipped in a solution of 0.3 M HNO3

for three minutes and rinsed with deionized water two times. The silver electrode sample was used as the anode, and a platinum thin-film counter electrode was used as a cathode. Both electrodes were dipped in a 3M KCl solution. Afterwards an electrical current was allowed to pass in the interface. A current density of 2 mA/cm2 was applied for 37 seconds, to achieve 200 nm of silver chloride. An SEM picture of the Ag/AgCl reference electrode on top of the PSA layer can be seen in figure 5.18. The characterization results of the system are presented in the next chapter of this thesis.
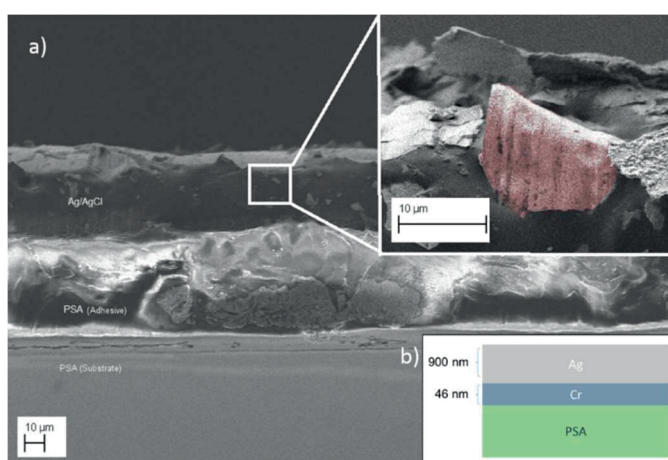
Figure 5.19 Fabrication of miniaturized Q. R.E. a) SEM images of the miniaturized reference electrode showing the Ag/AgCl formation, AgCl salts can be appreciated in red b) detailed cross section of the deposition of the silver on top the PSA layer, adapted from [198]

5.3.2 Lab-on-skin devices

This section reports the wafer-level 3D heterogeneous integration of the FD UTB SOI nanoribbon ISFETs, presented in chapter 3.3, and SU8 micro/nanofluidics, presented in chapter 4, to obtain wearable multi-sensing system, called Lab-on-skin™ [199].

The Lab-On-Skin concept is depicted in the 3D embodiment showed in Fig. 5.20. The reported design includes different sensor arrays based on ionic-sensitive FD SOI sensors with high-k dielectric gate stack: (1) bare HfO_2 gate stack sensors array

for pH sensing, (2) functionalized gold gate stacks arrays with specific functionalization for Na$^+$, (3) functionalized gold gate stacks arrays with specific functionalization K$^+$ detection.
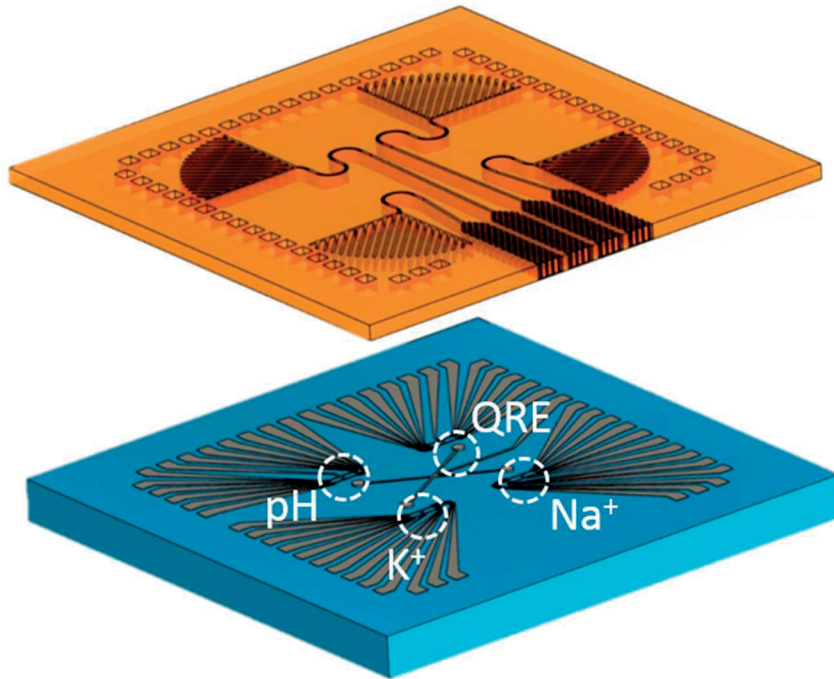
Figure 5.20 Top: Lab-on-skin™ concept, depicting the design of the sensing and microfluidics layers, with a 3D perspective of the various layers.

The SOI FET sensors have been fabricated with the process reported in Chapter 3. Next, a 3 μm passivation layer of SU-8 photoepoxy is processed on top of the wafer to isolate FET sensor interconnects, with openings left only in the sensor channel regions (and for contact pads).

Once the passivation layer is placed, the second layer of SU-8 is processed with the parameters described in Section 4.3.2.1 to create the microfluidic structures on top. Next, the reference electrode is chlorinated with the process described in Section 5.2.2.3. The chip was then wirebonded to a flexible PCB with the ball bonding technique using gold wires (25 μm). Epoxy is then deposited on top of the wires to passivate them. Figure 5.21 depicts the final assembly of the first Lab-on-skin

device. The remaining process is the functionalization of the ISFET devices. To achieve this, ion selective membranes for sodium and potassium are drop casted on top of the ISFETs as described in Section 5.1.3. The next chapter presents the electrical characterization results of the Lab-on-skin system.
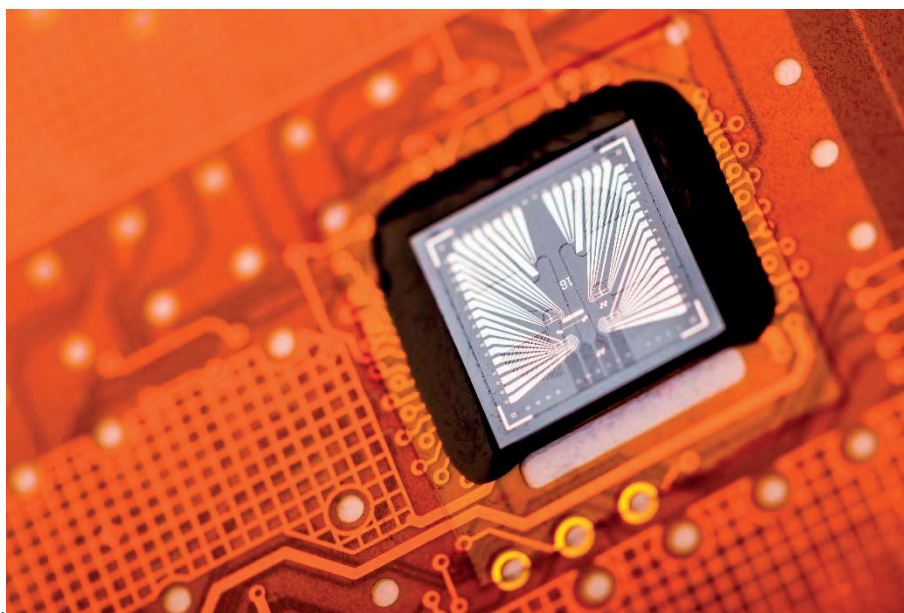
Figure 5.21 Lab-on-skin chip after integration with a flexible Printed Circuit Board

5.3.2.1 Discussion: Heterogeneous Integration of Lab-on-skin system

This section has presented a method that allows the successful integration of functionalized ISFETs with a microfluidic interface and a miniaturized Ag/AgCl quasi-reference electrode. It is important to remark that there were a lot of constraints towards the full integration of the system, due to incompatibility of the different technologies in the assembly. The first consideration to be made is the functionalization method chosen. We have decided to use the ISM (as described in 5.1.3) for functionalization of ISFETS because it shows a better Nernstian response for sensing. In addition, when testing, the deposition of SAMs damaged the ISFET devices. This was a consequence of the aggressiveness of the solvents required to perform this functionalization process. Additionally, concerning the integration is

the use of the open microfluidics (as proposed in Section 4.3.2.1). Even if the integration of full SU-8 microfluidics is desired, its fabrication process is not compatible with the ISMs, as the bonding process requires relatively high temperatures (which would also damage the QRE's PVB membrane). Nonetheless, as concluded in chapter 4 of this work, one layer of SU-8 allows the operation of the system with volumes of sweat in the nanoliter range, triggering sweat analysis even in low sweat rate conditions.

The next chapter presents the characterization results for these devices.

5.4 Summary & discussion

This chapter has shown the development of a process to allow the detection of hydrogen, sodium and potassium electrolytes with the nanoribbon ISFETs described in section 3.5 of this thesis. Two methods to achieve this functionalization were discussed. First, functionalization with Self Assembled Monolayers was tested. The SAM functionalization was first tested with ion selective electrodes, which showed high specificity for sodium and potassium ions. Nonetheless, the functionalization required the use of a piranha bath that damaged the passivation layer of our ISFET devices. The functionalization of ISFETs with SAMs was successful for sodium sensing, delivering good sensitivities and no cross sensitivity with pH. On the other hand, the functionalization with ion sensitive membranes requires no aggressive chemical treatment and therefore, a better alternative for electrolyte sensing with wearable sweat sensors.

The integration of a miniaturized Ag/AgCl quasi reference electrode on chip is also proposed in this chapter, the critical points for a successful integration of a reference electrode was the use of a chromium layer as an adhesion layer to improve the mechanical stability of a silver layer on top of SU-8 surfaces. Another key point is the spontaneous chlorination of the silver with $FeCl_3$ to obtain the

AgCl layer of the reference electrode. We propose the use of this chlorination method as it avoids any risk of cross contamination with the $FeCl_3$ as it is directly dropcasted on top of the silver. The use of a PVC membrane protecting the reference electrode has been used as a way to extend the lifetime of the reference electrode, which is shown by the 14 hours of constant potential that the reference electrode has kept under constant operation. The lifetime of the reference electrode could be extended if a thicker layer of silver is deposited on top of the SU-8 substrate, however, this step would require a step of electroplating that could pose a risk of contamination to the ISFET gate terminal. This is a parameter that should be considered, but nevertheless, future work should consider tests with thicker layers of silver.

The successful development of a Lab-on-skin wearable sweat sensing system has been achieved by the on chip heterogeneous integration of functionalized nanoribbon ISFET devices with a miniaturized reference electrode and a microfluidic interface for skin. The next chapter of this thesis will show the electrical characterization of the system to show its high specificity to pH, sodium and potassium.

The most important achievements of the system integration development are summarized below:

Technical outcomes:

- Functionalization for sodium and potassium sensing
  - Self-Assembled Monolayers of crown ethers on ISEs with HfO_2
    - Sensitivity $[Na^+]$ =22.3mV/dec
    - Sensitivity $[K^+]$ =26.1mV/dec
    - No Cross-sensitivity, the response of the sensor to non-target ion concentration was 91%-100% lower compared to the response of the sensor to the target ion.
    - Not compatible for ISFET functionalization
  - Self-Assembled Monolayers of crown ethers on Gold gates

- Successful functionalization of ISFETs for sodium sensing
- ISFET Sensitivity [Na$^+$] =-37.5mV/dec (presented in next chapter)
- Functionalization for K$^+$ was not responsive to variations in potassium concentration.
- o Functionalization with ion sensitive polymeric membranes on ISEs
  - Nernstian response to variations of NaCl and KCl
  - Sensitivity [Na$^+$] =56.1mV/dec
  - Sensitivity [K$^+$] =53.9mV/dec
  - Negligible Cross-sensitivity measured
- Miniaturized Ag/AgCl quasi reference electrode
  - o Fabrication of Ag/AgCl QRE on SU-8 substrates
    - Use of Chromium as an adhesion layer showed optimal results
    - Simple chlorination with FeCl$_3$
  - o Performance
    - 14 hours of stable operation in a saturated NaCl environment
- System integration
  - o The proposed process allows the successful integration of the different modules in the system, while avoiding any risk of damage within the polymeric membranes or the ISFET devices.

Main contributions to the field:

- Two functionalization processes for ISFET functionalization for sodium and potassium sensing
- Development of a stable Ag/AgCl reference electrode on SU-8 substrates
- Successful integration of functionalized ISFETs for sodium and potassium sensing with an embedded miniaturized quasi-reference electrode and a microfluidic interface for sweat collection on skin.

Chapter 6   Experimental results: Electrolyte sensing in a wearable system

This chapter collects all the electrical characterization measurements performed with the ISFET devices described in Chapter 3. The first section provides the electrical characterization of the FinISFETs in a miniaturized environment with PSA microfluidics and a miniaturized quasi-reference electrode. The second section provides the characterization results of the functionalized FD SOI ISFETs for sodium and potassium detection. Afterwards, the sodium sensitivity of the ISFET with a miniaturized QRE is reported.

6.1 pH-responsive FinFETs with PSA microfluidics and miniaturized QRE

In this section, the characterization of the FinISFET sensors (described in section 3.4) in a miniaturized characterization environment are presented. The miniaturized system includes a microfluidic system with an embedded miniaturized quasi-reference electrode embedded in a microfluidic channel. Biasing the reference electrode at different potentials allows to exploit the different operational regions of the transistor. Measurements were performed with a precision semiconductor analyzer (Agilent, 4156 A) connected to a low-leakage switching matrix (Agilent B2200A).

 Two sets of experiments were done with the sensors and the integrated reference electrode. The first steady-state measurements were performed to obtain the transfer characteristic of the devices with the miniaturized quasi reference electrode biasing the liquid gate exposed to a liquid to pH=7 at different potentials and measuring the variations of the drain current (V_D was set at 100 mV while the V_{REF} potential was applied from -1 to 3V with steps every 100 mV). I_DV_G

measurements were performed every 5 minutes and as it can be appreciated in figure 6.1.

Surprisingly, the subthreshold slope SS=141 mV/dec was steeper with the miniaturized reference electrode than with the external one (SS=180mV/dec). The I_{ON}/I_{OFF} kept a similar range between 10^4–10^5. A small drift in the reference electrode (tenths of millivolts) causing a variation in the response of the device was observed. However, this drift was almost irrelevant when the sensor was used to measure different pH buffers as seen in Figure 6.2.
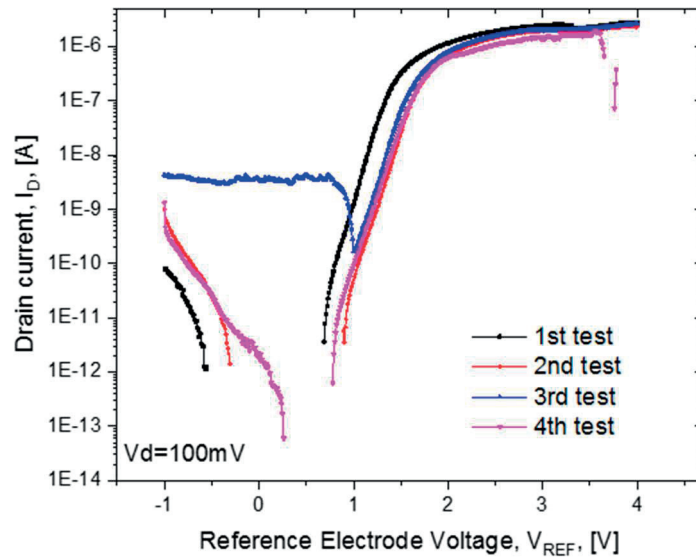
Figure 6.1 Id-Vg transfer characteristics of liquid gate FinFETs operated in pH=7 with integrated miniaturized Reference Electrode.

The time dependent measurements were performed at a constant drain current by fixing the voltage of the reference electrode. Due to the characteristic curve of our FinFETs a value of 1.55 V at the reference electrode and a value of 500 pA at the drain were chosen (Figure 6). Three pH buffers with a value of 4, 7 & 10 were consecutively measured to asses the response in time of the device. Results showed an almost linear response of the sensor per pH value, estimating a variation of 6mV/pH. A very fast and clean response of the sensor (3.1 s from 90% to 10% of

108

the measured voltage) was appreciated with the variation of the pH buffers (figure 6). An almost linear response was obtained from the measurement of the devices, delivering at the output a drain voltage sensitivity of 8 mV/pH. This level of voltage obtained from the measurements from our system are designed to be integrated with an ADC converter from a commercial microcontroller with 10 bits ADC to achieve mV resolution, making our device an option to be integrated in a wearable system.
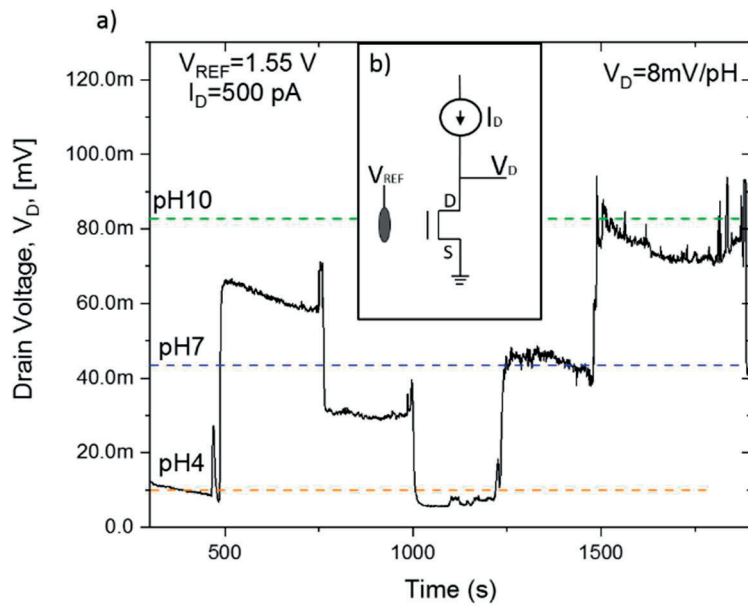
Figure 6.2 Time dependent measurements of the ISFET. a) VD measured while sampling pH buffers at a VREF=1.55 and ID=500 pA b) set up schematics for VD measurements with an ISFET.

The proposed microfluidic pH sensing microsystem-on-chip with the PSA microfluidics and the liquid gate FinFETs is suitable to be integrated into a wearable system since it takes into account essential requirements such as low cost, long term stability, biocompatibility and low power consumption. We have proposed and demonstrated a full process flow design that is compatible with standard semiconductor devices such as FinFETs and which includes a miniaturized reference electrode inside a passive microfluidic chip placed on top

of the sensing devices. We have reported fully functional sensors and reported their electrical characteristics and sensitivity. The small site and low power consumption of our sensing microsystem-on-chip makes it a credible candidate as a wearable device aimed for pH measurements and other types of ions in sweat.

6.2 FD UTB SOI nanorribon ISFET characterization for sodium and potassium sensing

This section presents the electrical characterization of the ISFETs presented in section 3.5 of this thesis. The characterization methods have been performed as shown in section 3.3. The experiments aimed at sodium and potassium sensitivity, with the evaluation of important parameters for a sensor, like sensitivity and stability.

The characterization results of two functionalization methods are reported in this section. First, the sodium sensing characterization results of the FD SOI ISFET sensors with a SAM functionalization on metal gates is presented. Finally, the sodium and potassium sensing characterization results of the ISFETs functionalized with ISMs is reported.

6.2.1 Sodium sensing with metal gates ISFETs functionalized with SAMs

This subsection presents the sodium characterization results of the metal gate ISFETs functionalized with a self-assembled monolayer. As reported by [172], in SAMs, any charged ion have an influence in the gate dielectric, creating a cross sensitivity effect. Therefore, the electrical signal generated by the ions on a functionalized sensor, will be the superimposition of those generated by both selective and non-selective sensing. Gold, has the property of keeping its non-selective ion sensitivity completely unchanged after thiol functionalization. This

allows us to use a second device, the control, in order to subtract the non-selective response from the measurement. The differential measurement is the subtraction of the response of a functionalized ISFET minus the response of a non-functionalized ISFET. Figure 6.3 shows a graphical explanation of the concept described before.
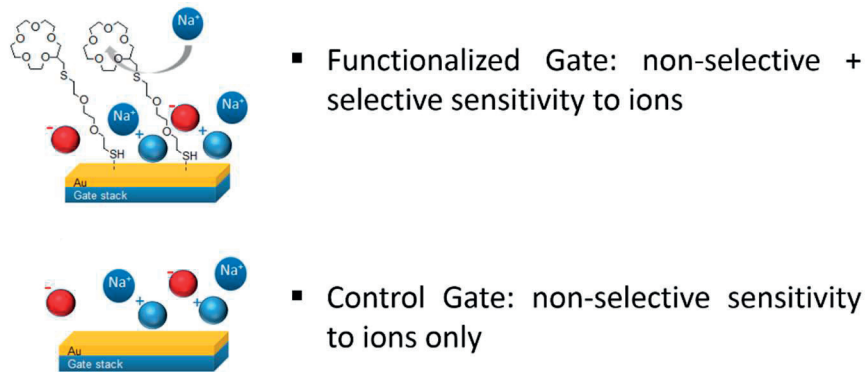
Figure 6.3 Differential measurements are performed with a functionalized gate and a control gate

The threshold voltage of the functionalized gate and control devices react differently to variation in Sodium concentration. This can be observed in Figure 6.4. The present difference indicates that the differential sensitivity will not be zero.
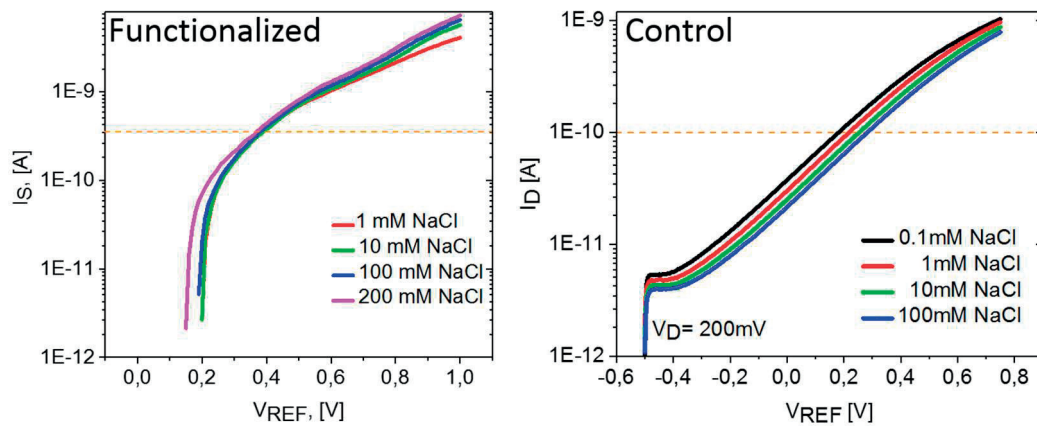
Figure 6.4 Response of functionalized and control ISFET to variations in the concentration of NaCl

111

In contrast, it is expected that the threshold voltage of the functionalized and control sensors react similarly to variations in the concentration of another ion, like Hydrogen. If this conclusion is satisfied, it can be concluded that the sensor avoids cross sensitivity. (SS=210mV/dec for functionalized sensor and SS=230mV/dec in non-functionalized). This is illustrated in Figure 6.5
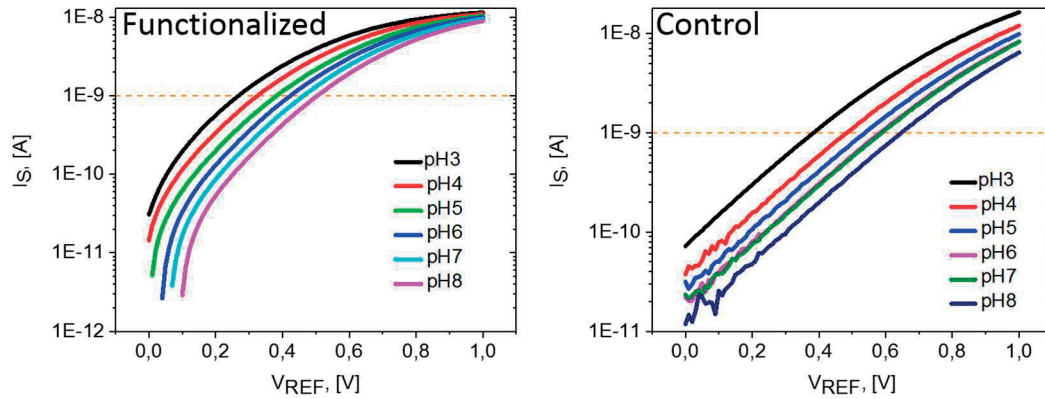
Figure 6.5 Functionalized and control sensors respond similarly to variation in pH values

Figure 6.6 shows the extracted sensitivities for both active and control sensors in full inversion at a constant current of 1 nA. With a differential measurement it is possible to obtain the value of the sodium sensitivity of the sensor, that is finally $S_{[NA]}$=-37.5mV/dec.
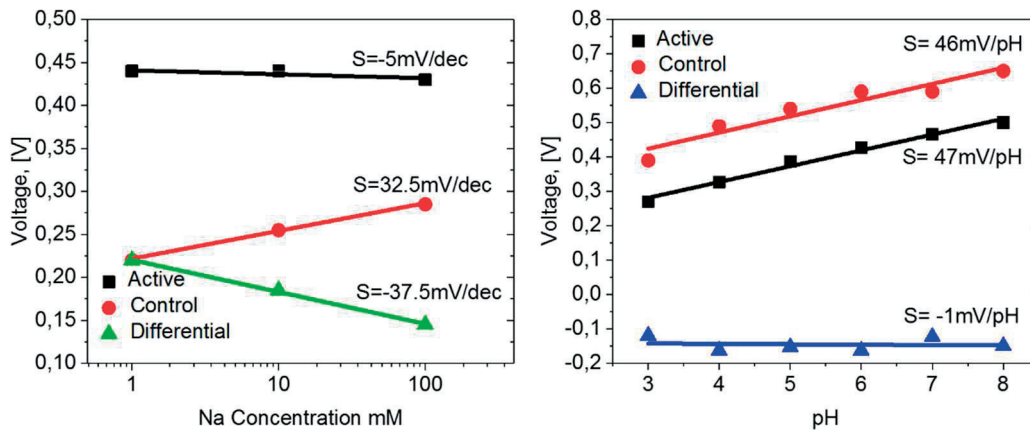
Figure 6.6 Sensitivity of ISFET functionalized with SAMs, showing no cross sensitivity with pH detection

Next, dynamic measurements of the sodium concentrations were performed. To do this a fixed potential of 200mV was fixed in the reference electrode and a fixed potential of 400mV was applied in the drain. Figure 6.7 shows the response of the sensor, that shows high stability and fast reaction times to variations in the concentration of NaCl.
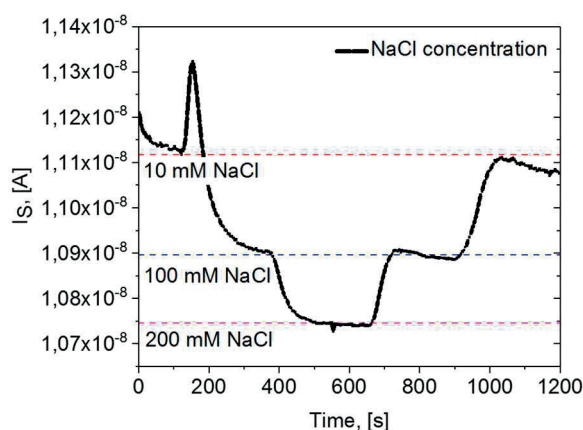
Figure 6.7 Dynamic detection of sodium with a functionalized ISFET

SAM functionalization proved to be effective for sodium detection. The same procedure was performed for Potassium sensing but the sensors were not responsive to the variations in the concentrations of KCl. This could be a consequence of the degradation of the HfO_2 layer or the SU-8 passivation layer. After several tests to functionalize for potassium, we decided to test the Ion Sensitive Membranes on ISFETs. The results with ISMs is presented in the following section.

6.2.2 Sodium and potassium sensing with functionalized ISFETs with ISMs.

This section reports the sodium and potassium sensitivity and cross sensitivity of functionalized ISFETs with ISMs. The process to functionalize ISFETs with membranes is described in section 5.1.3.

The sensitivities of the Sodium and Potassium-functionalized sensors to their respective ions have been evaluated extracting their transfer characteristics at different molar concentration of salts (NaCl and KCl respectively). The results can be observed in figure 6.8. For both sensors, a SS=140mV/dec was extracted. A negative shift in the transfer characteristic curves can be induced by increasing the concentration of the specific salt. In order to show the selectivity of the functional membranes for their specific ion (i.e. NaCl), an $I_D V_{REF}$ curve is extracted employing an analyte with high concentration of non-specific ions (i.e. KCl); for both sensors, it can be observed that the negative shift of the curves is negligible, even when compared with the minimal specific salt concentration studied.
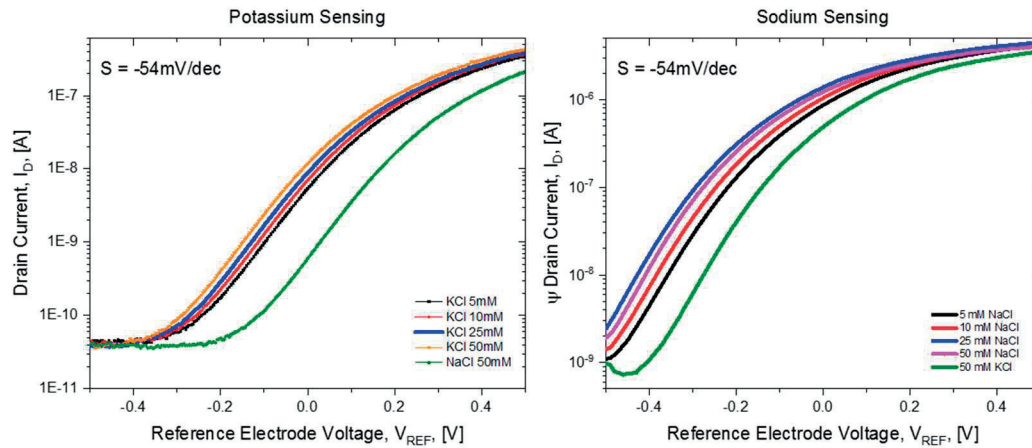
Figure 6.8 ID-VG characteristics of two different ISFETs functionalized for sodium and potassium respectively.

The sensitivity values were obtained by extracting the V_{TH} values in weak inversion corresponding to an I_D level of 100 nA. Both Sodium and Potassium

114

sensors show a strong, linear response to increases in their specific ions concentration. Excellent sensitivities have been obtained reaching the nearly Nernstian value of -54mV/dec as can be seen in figure 6.9.
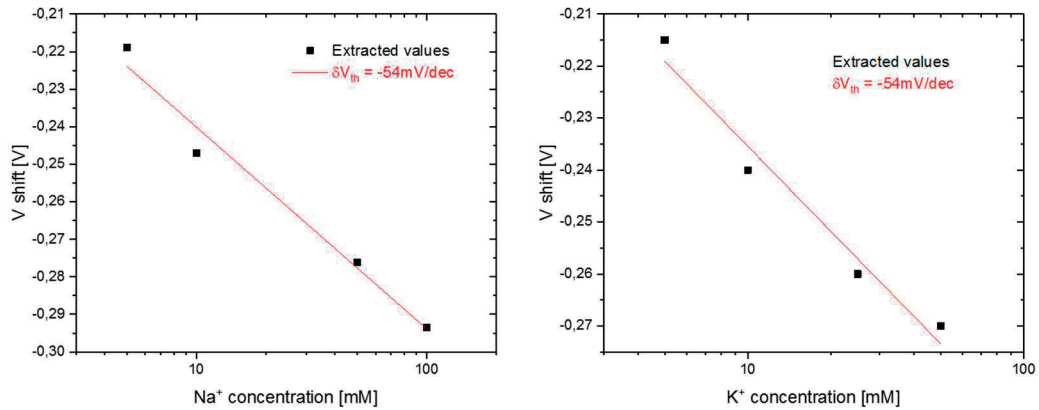
Figure 6.9 Sensitivity of ISFETs with ISMs

The dynamic measurements were performed by measuring the I_D while fixing V_{REF}=100mV and a V_D=200mV. As presented before, for increasing molarity values, the V_{TH} value is expected to be smaller, meaning that for the same V_{REF}, I_D will be bigger. This can be observed in Figure 6.10. It is possible to observe the low noise with $\sigma \approx$100pA and resulting averaged SNR$\approx$90. Figure 6.10 also demonstrates repeatability when the molarity concentration is exchanged in the opposite direction.
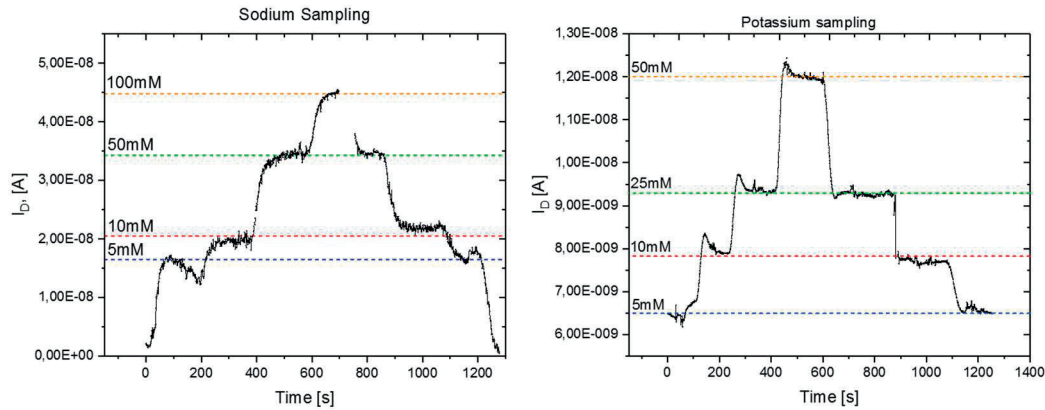
Figure 6.10 Dynamic response of ISFETs to variations in concentration of NaCl or KCl

6.2.3 Performance of the system with an Ag/AgCl miniaturized quasi-reference electrode

Once the sensors were characterized with an external reference electrode, their performance was evaluated with the miniaturized reference electrode embedded in the chip. This test is used to observe if there is any significant degradation in the response of the ISFETs in a miniaturized system environment. An ISFET with an ISM membrane for potassium was characterized. The transfer characteristic of the devices are extracted at different KCl buffer concentrations to extract the sensitivity of the device to concentrations of K^+ (Fig.1 inset f). The results and the extracted sensitivity, extracted at 100nA, are shown in Fig. 6.11.
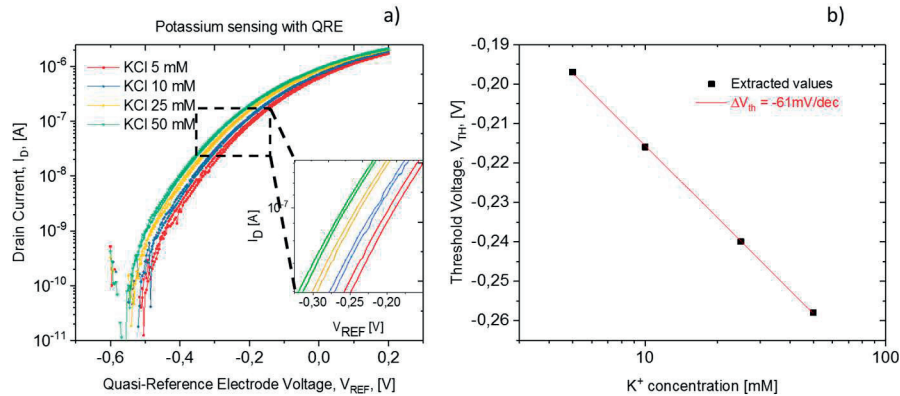
Figure 6.11 Characterization of functionalized ISFET with a miniaturized QRE a) $I_D V_{REF}$ for different [K^+] values, inset shows a zoom in constituent demonstrating the low hysteresis in the response of the sensor. B) V_{REF} extracted at 100nA for [K^+]

The transfer characteristics show a very low hysteresis (1-10mV) in the response of the sensor with excellent linearity and fully-Nernstian with a sensitivity S=61mV/dec for changes in the potassium concentration, demonstrating the efficacy of our miniaturized QRE and the possibility of acquiring clean data from our fully integrated system. A real-time measurement employing the QRE has also been performed, with 0V bias applied on the QRE, obtaining the graph shown in Fig. 6.12. We can highlight that even with the miniaturized reference electrode, we were able to operate the sensors with low power consumption, as 200mV were used to bias them.
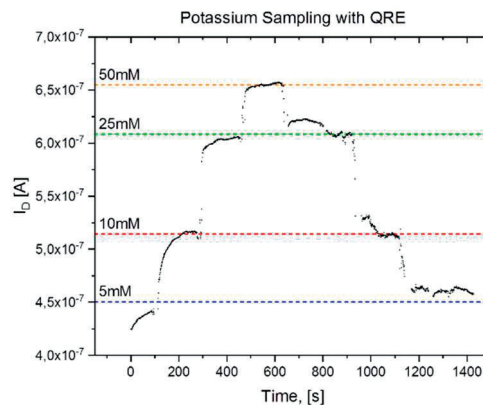
Figure 6.12 Real-time measurement of the potassium concentration in a liquid with an embedded Quasi-Reference Electrode

It can be observed that, thanks to the low hysteresis of the devices (observed in fig 11a), equal levels of current are obtained for equal molar concentrations of salts, independently from the values of the previous measurements. The response time, up to 30s, is clearly not due to the electronic properties of the sensor. We attributed it to the gradient-driven salt diffusion taking place inside the microfluidic channels and assumed it to be, in any case, absolutely compatible with the physiological variation rate of ion concentration in sweat.

The functionalization of ISFETs with ion sensitive membranes has been proven to be effective for sodium and potassium detection. The sensitivity of the devices is close to Nernstian values and it shows good selectivity. Thanks to the low hysteresis of the devices, equal levels of current are obtained for equal molar concentration of salts, independently from the values of the previous measurements. The response time, up to 20s, is clearly not due to the electronic properties of the sensor. We attributed it to the gradient-driven salt diffusion taking place inside the microfluidic channels and assumed it to be, in any case, absolutely compatible with the physiological variation rate of ion concentration in sweat.

6.3 Summary

This chapter has presented the characterization results for the wearable sweat sensing systems presented in chapter 5 of this thesis. First, the electrical performance of a FinISFET in a miniaturized characterization environment was presented. This system design included a 20 nL volume capacity in the PSA microfluidics and a miniaturized Ag/AgCl quasi reference electrode. The transfer characteristics of the liquid gate FinFETs showed an important drift in V_{TH}, most certainly, the reason could have been that the miniaturized reference electrode was not able to keep a stable potential for extended periods of operation.

Afterwards, the electrical characterization of functionalized nanoribbon ISFETs was presented. This results allowed to evaluate the performance of the ISFET with a thiol based functionalization and also with a PVC membrane functionalization. The thiol based functionalization on a metal gate nanoribbon ISFET a sensitivity of 37 mV/dec to variations in sodium concentration of an analyte, a number that could be considered low compared to the Nernst limit. The functionalization with a PVC membrane with an ionophore proved to increase this sensitivity value to close to Nernstian response of 54 mV/dec to variations in concentration of sodium and potassium.

The last electrical characterization results were obtained by operating the nanoribbon ISFETs with a miniaturized reference electrode. The sensors showed a Nernstian and linear response to variations in sodium concentration in an analyte. The dynamic characterization of this system show stable and repeatable response of the sensor to the variations of [Na^+]. These results show the high potential of the heterogeneous device integration we presented, marking a further step forward towards commercial sweat-based wearable diagnostic systems. The characterization of this devices with samples of sweat is still pending.

This last section summarizes the results achieved by the electrical characterization of functionalized ISFETs for sodium and potassium detection.

Technical outcomes:

- *Liquid gate FinFETs in miniaturized system:*
    - Subthreshold slope, SS = 141mV/dec
    - Ratio between I_{ON} and I_{OFF}, I_{ON}/O_{FF}=10^4
    - Sensitivity, S = 8mV/pH
- *FD SOI ISFETs functionalized with SAMs for Na^+ sensing:*
    - Subthreshold slope in functionalized device, SS = 210mV/dec
    - Subthreshold slope in non-functionalized device, SS = 230/dec
    - Ratio between I_{ON} and I_{OFF}, I_{ON}/O_{FF}=10^4
    - Sensitivity to [Na^+], S = -37.5mV/dec

- o No cross-sensitivity with pH variations
- *FD SOI ISFETs functionalized with ISMs for Na⁺ sensing:*
  - o Subthreshold slope, SS = 140mV/dec
  - o Sensitivity to [Na⁺], S = -54mV/dec
  - o Ratio between I_{ON} and I_{OFF}, $I_{ON}/_{OFF}=10^4$
- *FD SOI ISFETs functionalized with ISMs for K⁺ sensing:*
  - o Subthreshold slope, SS = 140mV/dec
  - o Sensitivity to [Na⁺], S = -54mV/dec
  - o Ratio between I_{ON} and I_{OFF}, $I_{ON}/_{OFF}=10^4$
  - o No cross sensitivity with [Na⁺] variations
- *FD SOI ISFET functionalized for K⁺ sensing, characterized with miniaturized QRE:*
  - o Subthreshold slope, SS = 100mV/dec
  - o Sensitivity to [Na⁺], S = -61mV/dec
  - o Ratio between I_{ON} and I_{OFF}, $I_{ON}/_{OFF}=10^5$
  - o No cross sensitivity with [K⁺] variations

Main contributions to the field:

- Demonstration of a well-known electronic unit, the ISFET, as a reliable sodium and potassium sensor.
- Demonstration of successful functionalization of ISFETs with Ion Sensitive Membranes
- Demonstration of the operation of the system with an "in-situ" miniaturized Ag/AgCl quasi-reference electrode

Chapter 7 Conclusions

This thesis has presented an innovative wearable sweat sensing system with unique figures of merit regarding low power consumption, Nernstian and selective response of sensors to variations in concentrations of electrolytes in a solution and offering the possibility to work with ultra-low volumes of sweat. In this chapter, the main achievements of this thesis are summarized. Then, an overview to compare our technology with State-of-the-art wearable sweat sensors is presented in order to highlight the contributions of this thesis to the field. Finally, prospects for further functionalization methods are discussed.

7.1 Main achievements

The main achievements of this thesis can be summarized as follows:

1. **Microfluidic interface for low sweat rates**

The realization of a patterned SU-8 microfluidic layer brings many advantages to traditional sweat collection methods used in literature. The microfluidic interface proposed in this work is able to collect volumes of sweat in the nanoliter range, bringing the opportunity to perform sweat analysis even when a person is at rest. This characteristic also allows to reduce the amount of dead volume of sweat in the interface. The flow control that the interface provides, avoids dilution of the sweat sample, making sweat analysis more accurate. In addition, the fabrication method for the microfluidics is compatible with microfabrication techniques, making its industrialization possible.

2. **Successful functionalization of ISFETs for electrolyte sensing**

This work has proved that nanoribbon ISFETs are compatible with Ion Sensitive Membranes. The sensors provide a Nernstian response for both sodium and

potassium sensing ($S_{[Na,K]}$=54mv/dec). Compared to SAM's, ISMs provide the advantage of being specific to only one ion, avoiding the need to perform differential measurements (that would translate in computational power consumption).

3. Integration of a miniaturized Ag/AgCl quasi reference electrode

We have demonstrated the performance of a miniaturized quasi-reference electrode capable of operating for 14 hours in continuous operation. Such an stable QRE allow to keep a very stable potential in the liquid environment of the system, reducing a possible source of noise while characterizing ISFET devices. The operation of the ISFET with the proposed miniaturized reference electrode delivered an impressive value for sensitivity to variations in concentration of sodium in an analyte (S [Na^+] =61mV/dec).

4. Heterogeneous integration of technological modules

This thesis has successfully integrated a functionalized sensing layer, a microfluidic layer and a reference electrode in a process that is fully compatible with the requirements of each technology. The final module is therefore ready for industrialization.

7.2 Comparison with other sweat sensing systems

Herein, the experimental results are presented in comparison with other State-of-the-art sweat sensing systems. The comparison is organized in four fields:

1. Sensing technology: It reports the technology used for sensing of biomarkers and functionalization methods (if applicable).
2. Power consumption per sensor: It reports the power consumption of a single sensor in the system
3. Biomarker sensitivity: It describes the sensing unit outputs in terms of the Nernstian response of the sensors to different analytes in a solution

4. Microfluidic interface to the skin: It reports the employment of a microfluidic interface to achieve controlled collection of sweat on human skin.

Table 7.1 summarizes the data of all the fields. All data presented in this table are reported as maximum achieved values.

As can be observed in field 1, sweat sensing systems normally employ either ISEs [3] [51] [52] or ISFETs [56] [57] [58] as sensing technologies. Field 1 also shows that with the exception of the works from Cazale et al [57], the standard functionalization method for electrolyte sensing in sweat is the use of ISM membranes based on a PVC mixture. The work presented in this thesis offers an important advantage considering the miniaturization of the system. Our nanoribbon ISFET devices are only 15 µm long, the closest one is presented in the works from Sommer, with a 500 µm device length. The size of all other sensors used in wearable sweat sensing systems is longer than 2 mm.

Field 2 of table 7.1 reveals that in most of wearable sweat sensing systems, power consumption per sensor is not being considered. As mentioned before in this thesis a key limitation of modern wearables is their dependency on batteries as a power supply. Using low power consumption sensors can enable longer autonomous operation times. The work of Cazale et al [57] is the only that report any values of power consumption, they reported 313 nWatts consumed per sensor, which is at least 10 times higher than the value reported in this thesis (20 nWatts). With the data provided by Nakata [56] it is possible to approximate the power consumption of its sensors which would account to values close to 900 nWatts of power consumption. The power consumption of ISEs is not reported in the publications of Gao [3], Rose [51], Sonner [52], or Choi [53]. Nonetheless, in literature is widely accepted that ISFETs provide a clear advantage over ISEs regarding power consumption [180].

Table 7.1 Comparison of the Lab-on-skin wearable sweat sensing system with SOA

Reference	Mode	Field 1			Field 2	Field 3				Field 4		
		Technology	Length of sensor	Functionalization	Energy consumption per sensor	K+ S[mV/dec]	Na+ S[mV/dec]	pH S[mV/pH]	Other biomarkers	µfluidic interface	Volume capacity of µfluidic interface	Flow rate in system
This work	Potentiometric	ISFETs	0.015 mm	ISM PVC	~20 nW	55	62	36	-	Yes	174 nl	252 nl/hour
Nakata et al. [56]		ISFETs	~2.7 mm	-	~900 nW	-	-	51.2	-	-	-	-
Cazale et al. [57]		ISFETs	2.1 mm	Fluoropolysiloxane	Not reported	-	57.1	-	-	-	-	-
Douthwaite et al. [58]		ISFETs	Not reported	-	313 nW	-	-	~50	-	-	-	-
Gao et al. [3]		ISEs	~3.4 mm	ISM PVC	Not reported	61.3	64.2	-	Glucose, lactate	-	-	-
Rose et al. [51]		ISEs	~3 mm	ISM PVC	Not reported	-	57	-	-	Yes	-	-
Sonner et al. [52]		ISEs	0.5 mm	ISM PVC	Not reported	-	~49	-	Chloride	Yes	-	-
Choi et al. [53]		Ag/AgCl	Not reported	-	Not reported	-	-	-	Chloride	-	-	-
Kim et al. [54]	Amperometric	Iontophoretic sensing electrodes	3 mm	Enzymatic layer	Not reported	-	-	-	Alcohol	-	-	-
Koh et al. [55]	Colorimetric	Colorimetric dye	~3 mm	Not applicable	Not applicable	-	-	Not applicable	Lactate, chloride, glucose, creatinine, chloride	Yes	50 µl	680 nl/hour

124

Field 3 summarizes the sensitivity values to different ions that are targeted in sweat. As discussed in chapter 5 of this thesis, the sensitivity values of electrochemical sensors are expected to show a Nernstian response. Field 3 shows that all wearable sweat sensing systems achieve values higher than 50 mV/dec for different ions. As potentiometric measurements are limited by the Nernst limit, it is not expected to have more sensitive chemical sensors, however, for small biological entities which are not uniformly distributed in the solution, the geometry and the dimension of an ISFET can provide a higher response than other devices in case of a very localized change of surface potential [88]. This leads to the conclusion that eventually ISFETs will replace ISEs for any potentiometric sensing applications. The one remark to be made is that fabrication costs for ISEs are very low when compared to the fabrication costs for ISFETs.

Field 4 exemplifies another of the main advantages of our sweat sensing system, which is the microfluidic layer for ultra-low volumes of sweat. In literature, only the work from Koh [55] has considered the use of a similar microfluidic device to collect sweat and passively displace it with capillary forces. This wearable system still had to be tested with a person subject to physical activity (as in all other wearable sweat sensing systems in the State-of-the-art). The main reason could be that their system requires at least 50 μL of sweat to be filled, this volume can be considered is still high for a person at rest (average sweat flow rate at rest: 20 nL/min/cm^2). Our microfluidic device requires almost 200 times less that amount, an achievement that could trigger sweat collection at low sweat rates. The works developed by Rose et al. [51] consider the use of paper microfluidics to provide a control over sweat with a patch, however they do not report any quantification to evaluate the performance of their microfluidic system. More recently, Sonner et al. [52] has proposed the use of chemical stimulants to trigger sweat analysis with individuals at rest and claim no cross sensitivity risk for measurements. This is a very relevant study towards continuous sweat analysis. In this work, however, one of the main goals was to avoid any kind of external stimuli for sweat acquisition.

7.3 Outlook

In order to improve the platform developed in this thesis, there are some technological improvements that should be performed in the short and long term.

7.3.1 Technology

- Further work should consider adding a temperature sensor and a flow rate measurement tool as certain biomarker concentration in sweat are dependent on the sweat rate [19].

- There are commercial ionophores for calcium and ammonia that can be easily used in our system to increase the catalog of cations to be detected in sweat with ISM.

- For the time being, the membranes have to be drop casted on top of the ISFETs directly. Therefore, there is no option but to keep the microfluidics open. This would carry the consequence of needing higher volumes of liquid to be able to perform measurements. One way to get around the problem would be to close the microfluidic channels by other means. PSA would be a natural candidate but considerations towards industrial processes to pattern it would have to be considered.

- Research has to be performed to improve the metallic contact pads on the chip. It is possible that a thick layer of an oxide has to be deposited below the AlSi as it has been observed that wirebonding is piercing the metal creating a current leakage to the bulk.

7.3.2 Perspectives for biomarker detection with ISFETs

Future research should consider alternative functionalization methods for ISFET technology to enable biomarker analysis. This section discusses briefly three possible alternatives to ISMs.

7.3.2.1   Molecularly Imprinted Polymer Membranes for detection of proteins or glycoproteins with ISFETs

Molecularly imprinted polymer (MIP)-based field-effect transistor (MIP-gate FET) could be a good solution to detect selectively a targeted analyte as proteins or glycoproteins (for example cytokines in aqueous media such as biofluids). The Molecularly imprinted polymer membranes are synthesized on the gate surface of the FET device through the polymerization of a specific mixture made of monomers and chemicals if required in presence of the molecules of interest (Fig. 7.1).

The procedure for molecular imprinting involves complexation of functional monomers and target molecules of interest sites (Fig 7.1.b), followed by cross-linking of the monomers (Fig 7.1.c) and subsequent removal of the templates to create adsorption sites that are complementary in size and shape to the molecule of interest (Fig 7.1.d). The resulting templated polymer matrix is called molecularly imprinted polymer membrane and is suitable to selectively adsorb targeted molecules. Indeed, when the polymer matrix is put in contact with a solution containing the targeted molecules, they adsorb within the imprinted site of the template polymer matrix.
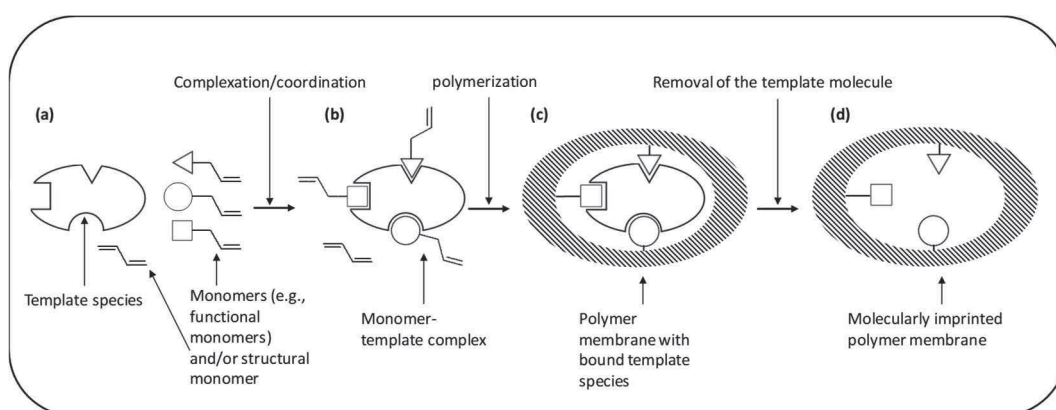
Figure 7.1 Schematic principle of molecularly imprinted polymer synthesis with (a) solution made of functional monomers, template molecules and monomers used to structure the MIP (if needed) (b) complexation of the template with one or several functional monomer(s) (c) polymerization of the solution to create a polymer matrix (d) removal of the template molecule

127

The molecules of interest adsorption rate and concentration change the physico-chemical properties of the MIP and can be deduced by monitoring these physico-chemical properties. For instance, the concentration of the target molecule in the liquid medium in contact with the MIP (e.g. on top of the gate of a FET) may modify the electrical potential of the MIP (but also the impedance, etc.) at the interface with the metal gate and in turn the FET gate potential. Ensuing from the working principle of a FET, the modification of the gate potential may change the electrical conduction of the FET channel that can be read out, for instance, as a variation of drain current or drain voltage. The characteristics of this electrical signal are correlated to the concentration of the targeted molecule in the liquid medium. Thus, the MIP-gate FET may be used as a biochemical sensor.

In all embodiments, the transduction surface in contact with the solution containing molecules of interest can be:

·   The FET gate dielectric fully or partially with a MIP
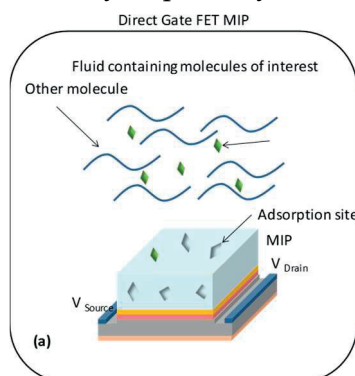
Figure 7.2 Schematic representation of direct gate FET MIP functionalization

·   An extended FET metallic gate covered fully or partially with a MIP
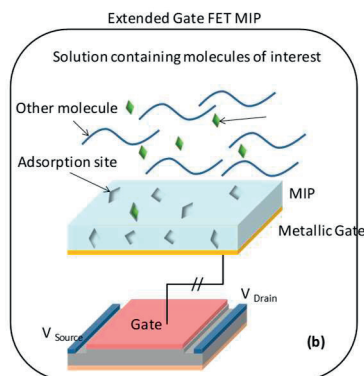
Figure 7.3 Schematic representation of an extended gate FET MIP functionalization

Molecular imprinted polymer membrane usually show less degradation, more stability over time, capability to operate in extended medium conditions (e.g. variation of pH, temperature, ionic strength) than biological compounds such as aptamers and antibodies typically used in the detection of proteins, peptides, nucleic acids, etc.

Additionally, the reversibility of MIP can be controlled through its oxidation by passing a current through the gate surface, leading to an easy and accurate way of recalibration and resetting of the biosensor. The use of MIP would permit the development of miniaturized and re-usable biosensors efficiently operating over various conditions.

7.3.2.2   *Protein receptor functionalization for cholesterol sensing*

In biochemistry, a receptor is a protein molecule from the cellular membrane, the cytoplasm or the cell nucleus that recognize and bind a specific ligand inducing physiological modifications. Ligands can be proteins or peptides, or another small molecule such as example hormone, toxin, neurotransmitters, etc. For example the receptor (LDL-R) is a cell surface receptor that recognizes the apoprotein B100 present in the outer phospholipid layer of LDL particles that could be used to detect cholesterol, which has a high concentration of LFL particles.

The functionalization of the FET gate can be done through the coupling of low density lipoprotein receptors or mimicking sequences of its recognition site or binding site made of proteins or amino acids to complex/bind/coordinate specifically the apoprotein B100 and/or the complex apoprotein B100/cholesterol and thus to determine the concentration of LDL in biofluids.

7.3.2.3   Sensor functionalization with Aptamers for cholesterol sensing

Aptamer are oligonucleotide or peptide molecules with an engineered sequence (such as DNA or RNA nucleotide sequence) that can be used as a probe to bind (reversibly and) selectively with a specific target molecule -usually complementary to the aptamer probe- typically through hybridization, thus enabling label-free detection. Aptamers can be an alternative process to sense the LDL receptors that can be found in cholesterol.

The aptamer is usually immobilized on the surface of the FET gate with a given concentration via the concentration of aptamers added to a functionalization solution with which the sensor is contacted and the amount of time this contact occurs. In order to immobilize the aptamer on the metal gate of a FET sensor made with gold (or other noble metals such as platinum), the aptamer sequence may be terminated (at the extremities) with thiol groups that will bind with the gold gate of each FET sensor via gold-thiol interactions/binding [200].

In order to immobilize the aptamer on the gate dielectric of a FET sensor (without metal gate) made with an oxide (e.g. silicon dioxide, hafnium dioxide), the aptamer sequence may be terminated (at the extremities) with silane groups that will bind with the gate oxide of each FET sensor via silane – hydroxyl group interactions.

The aptamer-target binding is usually not electrochemically active. In order to make the aptamer-target binding electrochemically active, the aptamer sequence may include an electrochemical redox reporter (e.g. methylene blue). Such electrochemical redox reporter is usually not necessary when using a FET sensor.

The principle of sensing is an indirect detection: the electrochemical activity (by extension the measured current) of the reporter varies as a function of the aptamer-target binding rate.

Once the aptamer is coupled to the gate electrode surface of the ISFET, it becomes sensitive to the presence of LDL. Indeed, the coordination or complexation of the aptamer with the targeted ligand (LDL) leads to changes in the electronic environment of the sensor surface which can be monitored through for example open circuit potential or impedance measurements. The changes are proportional of the LDL concentration.

7.4 Concluding remarks

With the results presented in Section 7.1, we can conclude that the integrated system is suitable for wearable sweat sensing applications. The sensing units provide high sensitivity and specificity for sensing, sodium and potassium sensing while assuring a small form factor. While the sensitivity that traditional ion sensing electrodes is similar to the sensitivity of ISFETs, in terms of miniaturization ISFETs have a clear advantage. Moreover using ISFETs provide a clear advantage over traditional ISEs as they allow to work with non-linear output characteristics. This gives the possibility to detect a single ion or molecule but also allowing to measure large changes in concentration of the analyte. A condition that cannot be satisfied by Ion Sensing Electrodes.

Traditional wearable sweat sensing systems rely on high sweat rate conditions, limiting the applications to the field of sports. Here, the integration in the wearable system of a patterned microfluidic interface for sweat collection is another important contribution to the field. This incorporation allows to collect as little as 200 nL of sweat, a condition that could enable sweat analysis when a person is at rest.

The thesis has presented the needed technological processes and optimizations, together with their characterization, to achieve the first of its kind Lab-On-Skin system.

References

[1]   S. Lueck, "Healthcare spending rises 8.7%, Fastest expansion in 10 years," *The Wall Street Journal,* p. D2, 8 January 2008.

[2]   J. Heikenfeld, "Bioanalytical devices: Technological leap for sweat sensing.," *Nature,* vol. 529, no. 7587, p. 475, 2016.

[3]   W. Gao, S. Emaminejad, H. Y. Y. Nyein, S. Challa, K. Chen, A. Peck, D. H. Lien and A. Javey, "Fully integrated wearable sensor arrays for multiplexed in situ perspiration analysis.," *Nature,* vol. 529, no. 7587, p. 509, 2016.

[4]   J. Andreu-Perez, C. C. Poon, R. D. Merrifield, S. T. Wong and G. Z. Yang, "Big data for health.," *IEEE journal of biomedical and health informatics,* vol. 19, no. 4, pp. 1193-1208., 2015.

[5]   X. Li, J. Dunn, D. Salins, G. Zhou, W. Zhou, S. M. S. F. Rose and R. Sonecha, "Digital health: tracking physiomes and activity using wearable biosensors reveals useful health-related information.," *PLoS biology,* vol. 15, no. 1, p. e2001402., 2017.

[6]   K. Bottles and E. Begoli, "Understanding the pros and cons of big data analytics.," *Physician executive,* vol. 40, no. 4, p. 6, 2014.

[7]   Y. L. Zheng, X. R. Ding, C. C. Y. Poon, B. P. L. Lo, H. Zhang, X. L. Zhou and Y. T. Zhang, "Unobtrusive sensing and wearable devices for health informatics.," *IEEE Transactions on Biomedical Engineering,* vol. 61, no. 5, pp. 1538-1554., 2014.

[8]   S. Pilehvar, A. Wilhelm, W. A., K. King and S. Emaminejad, "Emerging wearable technologies for personalized health and performance

monitoring.," in *Micro-and Nanotechnology Sensors, Systems, and Applications*, Orlando, Florida, May, 2018.

[9]   S. Emaminejad, W. Gao, E. Wu, Z. A. Davies, H. Y. Y. Nyein, S. Challa, S. Talebi, A. Jabey and R. Davis, "Autonomous sweat extraction and analysis applied to cystic fibrosis and glucose monitoring using a fully integrated wearable platform.," *Proceedings of the National Academy of sciences* , vol. 114, pp. 4625-4630, 2017.

[10] M. J. Buono, K. D. Ball and F. W. Kolkhorst, "Sodium ion concentration vs. sweat rate relationship in humans.," *Journal of Applied Physiology,* vol. 103, no. 3, pp. 990-994., 2007.

[11] D. Wendt, L. J. Van Loon and W. D. M. Lichtenbelt, "Thermoregulation during exercise in the heat.," *Sports Medicine,* vol. 37, no. 8, pp. 669-682., 2007.

[12] A. Takamata, T. Yoshida, N. Nishida and T. Morimoto, "Relationship of osmotic inhibition in thermoregulatory responses and sweat sodium concentration in humans. American," *Journal of Physiology-Regulatory, Integrative and Comparative Physiology,,* vol. 3, pp. 623-629, 2001.

[13] R. M. P. M. J. Morgan and M. A. Nimmo, "Acute effects of dehydration on sweat composition in men during prolonged exercise in the heat.," *Acta Physiologica,* vol. 182, no. 1, pp. 37-43., 2004.

[14] J. Weber, A. Kumar, A. Kumar and S. Bhansali, "Novel lactate and pH biosensor for skin and sweat analysis based on single walled carbon nanotubes.," *Sensors and Actuators B: Chemical,* vol. 117, no. 1, pp. 308-313., 2006.

[15] A. Mena-Bravo and M. Luque de Castro, "Sweat: A sample with limited present applications and promising future in metabolomics," *J. Pharm. Biomed. Anal.* , vol. 90, pp. 139-147, 2014.

[16] K. Sato, "The physiology, pharmacology, and biochemistry of the eccrine sweat gland.," *In Reviews of Physiology, Biochemistry and Pharmacology*, vol. 79, pp. 51-131, 1977.

[17] R. W. Bullard, M. R. Banerjee and B. A. Mac Intyre, "The role of the skin in negative feedback regulation of eccrine sweating.," *International journal of biometeorology*, vol. 11, pp. 93-104., 1967.

[18] M. Gleeson, "Temperature regulation during exercise.," *International Journal of Sports Medicine*, vol. 19, no. S 2, pp. S96-S99., 1998.

[19] Z. Sonner, E. Wilder, J. Heikenfeld, G. Kasting, F. Beyette, D. Swaile and R. Naik, "The microfluidics of the eccrine sweat gland, including biomarker partitioning, transport, and biosensing implications.," *Biomicrofluidics*, vol. 9, no. 3, p. 031301., 2015.

[20] L. B. Baker, "Sweating rate and sweat sodium concentration in athletes: a review of methodology and intra/Interindividual variability.," *Sports Medicine*, vol. 47, no. 1, pp. 111-128., 2017.

[21] L. B. Baker, K. A. Barnes, M. L. Anderson, D. H. Passe and J. R. Stofan, "Normative data for regional sweat sodium concentration and whole-body sweating rate in athletes.," *Journal of sports sciences*, vol. 34, no. 4, pp. 358-368., 2016.

[22] K. Wilke, A. Martin, L. Terstegen and S. S. Biel, "A short history of sweat gland biology.," *International journal of cosmetic science*, vol. 29, no. 3, pp. 169-179., 2007.

[23] J. L. Matousek and K. L. Campbell, "A comparative review of cutaneous pH.," *Veterinary dermatology*, vol. 13, no. 6, pp. 293-300., 2002.

[24] M. Bariya, H. Y. Y. Nyein and A. Javey, "Wearable sweat sensors.," *Nature Electronics,* vol. 1, no. 3, pp. 160-171, 2018.

[25] H. Sharlit and M. Scheer, "The hydrogen-ion concentration of the surface of the healthy intact skin.," *Archives of Dermatology and Syphilology,* vol. 7, no. 5, pp. 592-598., 1923.

[26] H. Öhman and A. Vahlquist., "The pH gradient over the stratum corneum differs in X-linked recessive and autosomal dominant ichthyosis: a clue to the molecular origin of the "acid skin mantle"," *Journal of investigative dermatology ,* vol. 111, no. 4 , pp. 674-677, 1998.

[27] P. M. Krien and M. Kermici, "Evidence for the existence of a self-regulated enzymatic process within the human stratum corneum–an unexpected role for urocanic acid.," *Journal of investigative dermatology,* vol. 115, no. 3, pp. 414-420., 2000.

[28] P. Thune, T. Nilsen, I. K. Hanstad, T. Gustavsen and H. D. Lövig, "The water barrier function of the skin in relation to the water content of stratum corneum, pH and skin lipids. The effect of alkaline soap and syndet on dry skin in elderly, non-atopic patients," *Acta dermato-venereologica ,* vol. 68, no. 4, pp. 277-283, 1988.

[29] D. S. Anderson, "THE ACID-BASE BALANCE OF THE SKIN.," *British Journal of Dermatology,* vol. 63, no. 8, pp. 283-295., 1951.

[30] K. Sato, W. H. Kang, K. Saga and K. T. Sato, "Biology of sweat glands and their disorders. I. Normal sweat gland function.," *Journal of the American Academy of Dermatology,* vol. 20, no. 4, pp. 537-563., 1989.

[31] N. De Giovanni and N. Fucci, "The current status of sweat testing for drugs of abuse: a review.," *Current medicinal chemistry,* vol. 20, no. 4, pp. 545-561., 2013.

[32] D. A. Kidwell, J. C. Holland and S. Athanaselis, "Testing for drugs of abuse in saliva and sweat.," *Journal of Chromatography B: Biomedical Sciences and Applications*, vol. 713, no. 1, pp. 111-135., 1998.

[33] A. Mena-Bravo and M. L. De Castro, "Sweat: a sample with limited present applications and promising future in metabolomics.," *Journal of pharmaceutical and biomedical analysis,* vol. 90, pp. 139-147., 2014.

[34] S. Anastasova, B. Crewther, P. Bembnowicz, V. Curto, H. M. Ip, B. Rosa and G. Z. Yang, "A wearable multisensing patch for continuous sweat monitoring.," *Biosensors and Bioelectronics, , ,* vol. 93, pp. 139-145., 2017.

[35] H. Y. Y. Nyein, W. Gao, Z. Shahpar, S. Emaminejad, S. Challa, K. Chen and A. Javey, "A wearable electrochemical platform for noninvasive simultaneous monitoring of Ca2+ and pH.," *ACS nano, (), ,* vol. 10, no. 7, pp. 7216-7224., 2016.

[36] M. J. Patterson, S. D. Galloway and M. A. Nimmo, "Variations in regional sweat composition in normal human males.," *Experimental physiology,* vol. 85, no. 6, pp. 869-875., 2000.

[37] T. Guinovart, A. J. Bandodkar, J. R. Windmiller, F. J. Andrade and J. Wang, "A potentiometric tattoo sensor for monitoring ammonium in sweat.," *Analyst,* vol. 138, no. 22, pp. 7031-7038., 2013.

[38] A. Abellán-Llobregat, I. Jeerapan, A. Bandodkar, L. Vidal, A. Canals, J. Wang and E. Morallon, "A stretchable and screen-printed electrochemical sensor for glucose determination in human perspiration.," *Biosensors and Bioelectronics,* vol. 91, pp. 885-891, 2017.

[39] J. Kim, I. Jeerapan, S. Imani, T. N. Cho, A. Bandodkar, S. Cinti and J. Wang, "Noninvasive alcohol monitoring using a wearable tattoo-based

iontophoretic-biosensing system.," *ACS Sensors,* vol. 1, no. 8, pp. 1011-1019., 2016.

[40] W. Gao, H. Y. Nyein, Z. Shahpar, H. M. Fahad, K. Chen, S. Emaminejad and J. Bullock, "Wearable microsensor array for multiplexed heavy metal monitoring of body fluids.," *Acs Sensors,* vol. 1, no. 7, pp. 866-874., 2016.

[41] J. R. Windmiller, A. J. Bandodkar, G. Valdés-Ramírez, S. Parkhomovsky, A. G. Martinez and J. Wang, "Electrochemical sensing based on printable temporary transfer tattoos.," *Chemical Communications,* vol. 48, no. 54, pp. 6794-6796., 2012.

[42] J. B. Shields, B. C. Johnson, T. S. Hamilton and H. H. Mitchell, "The excretion of ascorbic acid and dehydroascorbic acid in sweat and urine under different environmental conditions.," *Journal of Biological Chemistry,,* vol. 161, pp. 351-356., 1945.

[43] W. Gao, H. Y. Nyein, Z. Shahpar, H. M. Fahad, K. Chen, S. Emaminejad and J. Bullock, "Wearable microsensor array for multiplexed heavy metal monitoring of body fluids.," *Acs Sensors,* vol. 1, no. 7, pp. 866-874., 2016.

[44] D. Kinnamon, R. Ghanta, K. C. Lin, S. Muthukumar and S. Prasad, "Portable biosensor for monitoring cortisol in low-volume perspired human sweat.," *Scientific reports,* vol. 7, no. 1, p. 13312., 2017.

[45] T. Kilic, V. Brunner, L. Audoly and S. Carrara, "Smart e-Patch for drugs monitoring in schizophrenia.," in *In Electronics, Circuits and Systems (ICECS), 2016 IEEE International Conference* , Monte Carlo, Monaco, 2016, December.

[46] J. Lieberman, "Cyclic fluctuation of sweat electrolytes in women: Effect of polythiazide upon sweat electrolytes.," *JAMA,* vol. 195, no. 8, pp. 629-635., 1966.

[47] J. I. Medbø and O. M. Sejersted, "Plasma potassium changes with high intensity exercise.," *The Journal of Physiology,* vol. 421, no. 1, pp. 105-122., 1990.

[48] S. R. Newmark and R. G. Dluhy, "Hyperkalemia and hypokalemia.," *JAMA,* vol. 231, no. 6, pp. 631-633., 1975.

[49] K. Sato and F. Sato, "Individual variations in structure and function of human eccrine sweat gland.," *American Journal of Physiology-Regulatory, Integrative and Comparative Physiology,* vol. 245, no. 2, pp. R203-R208., 1983.

[50] N. A. Taylor and C. A. Machado-Moreira, "Regional variations in transepidermal water loss, eccrine sweat gland density, sweat secretion rates and electrolyte composition in resting and exercising humans.," *Extreme physiology & medicine,* vol. 2, no. 1, p. 4, 2013.

[51] D. P. Rose, M. E. Ratterman, D. K. Griffin, L. Hou, N. Kelley-Loughnane, R. R. Naik and J. C. Heikenfeld, "Adhesive RFID sensor patch for monitoring of sweat electrolytes.," *IEEE Transactions on Biomedical Engineering, (), ,* vol. 62, no. 6, pp. 1457-1465., 2015.

[52] Z. Sonner, E. Wilder, T. Gaillard, G. Kasting and J. Heikenfeld, "Integrated sudomotor axon reflex sweat stimulation for continuous sweat analyte analysis with individuals at rest.," *Lab on a Chip,* vol. 17, no. 15, pp. 2550-2560., 2017.

[53] D. H. Choi, A. Thaxton, I. cheol Jeong, K. Kim, P. R. Sosnay, G. R. Cutting and P. C. Searson, "Sweat test for cystic fibrosis: Wearable sweat sensor vs. standard laboratory test.," *Journal of Cystic Fibrosis.,* 2018.

[54] J. Kim, I. Jeerapan, S. Imani, T. N. Cho, A. Bandodkar, S. Cinti and J. Wang, "Noninvasive alcohol monitoring using a wearable tattoo-based

iontophoretic-biosensing system.," *ACS Sensors,* vol. 1, no. 8, pp. 1011-1019., 2016.

[55] A. Koh, D. Kang, Y. Xue, S. Lee, R. M. Pielak, J. Kim, M. C. Manco and R. J. A., "A soft, wearable microfluidic device for the capture, storage, and colorimetric sensing of sweat.," *Science translational medicine,* vol. 8, no. 366, p. 366ra165, 2016.

[56] S. Nakata, T. Arie, S. Akita and K. Takei, "Wearable, flexible, and multifunctional healthcare device with an ISFET chemical sensor for simultaneous sweat pH and skin temperature monitoring.," *ACS sensors,* vol. 2, no. 3, pp. 443-448., 2017.

[57] A. Cazalé, W. Sant, J. Launay, F. Ginot and P. Temple-Boyer, "Study of field effect transistors for the sodium ion detection using fluoropolysiloxane-based sensitive layers.," *Sensors and Actuators B: Chemical,* vol. 177, pp. 515-521., 2013.

[58] M. Douthwaite, N. Moser, E. Koutsos, D. Yates, P. Mitcheson and P. Georgiou, "A CMOS ISFET array for wearable thermoelectrically powered perspiration analysis.," in *Biomedical Circuits and Systems Conference (BioCAS)*, Shanghai, 2016.

[59] A. J. &. W. J. Bandodkar, "Non-invasive wearable electrochemical sensors: a review.," *Trends in biotechnology,* vol. 32, no. 7, pp. 363-371., 2014.

[60] Q. P. Yan, S. G. B., B. E. Cohan, T. C. Major and M. E. Meyerhoff, "Measurement of tear glucose levels with amperometric glucose biosensor/capillary tube configuration.," *Analytical chemistry*, vol. 83, no. 21, pp. 8341-8346., 2011.

[61] M. Nakatsukasa, C. Sotozono, K. Shimbo, N. Ono, H. Miyano, A. Okano and S. Kinoshita, "Amino acid profiles in human tear fluids analyzed by high-

performance liquid chromatography and electrospray ionization tandem mass spectrometry.," *American journal of ophtalmology,* 2011.

[62] C. K. M. Choy, P. Cho, W. Y. Chung and I. F. Benzie, "Water-soluble antioxidants in human tears: effect of the collection method.," *Investigative ophthalmology & visual science,* vol. 42, no. 13, pp. 3130-3134., 2001.

[63] N. J. Van Haeringen and E. Glasius, "Collection method dependant concentrations of some metabolites in human tear fluid, with special reference to glucose in hyperglycaemic conditions.," *Albrecht von Graefes Archiv für klinische und experimentelle Ophtalmologie,* vol. 202, no. 1, pp. 1-7, 1977.

[64] H. Yao, Y. Liao, A. R. Lingley, A. Afanasiev, I. Lähdesmäki, B. P. Otis and B. A. Parviz, "A contact lens with integrated telecommunication circuit and sensors for wireless and continuous tear glucose monitoring.," *Journal of Micromechanics and Microengineering,* vol. 22, no. 7, p. 075007, 2012.

[65] A. Aguirre, L. A. Testa-Weintraub, J. A. Banderas, G. G. Haraszthy, M. S. Reddy and M. J. Levine, "Sialochemistry: a diagnostic tool?," *Critical Reviews in Oral Biology & Medicine,* vol. 4, no. 3, pp. 343-350., 1993.

[66] A. Vasudev, A. Kaushik, Y. Tomizawa, N. Norena and S. Bhansali, "An LTCC-based microfluidic system for label-free, electrochemical detection of cortisol.," *Sensors and Actuators B: Chemical,* vol. 182, pp. 139-146., 2013.

[67] A. J. Preston and W. M. Edgar, "Developments in dental plaque pH modelling. Journal of dentistry,," vol. 33, no. 3, pp. 209-222., 2005.

[68] H. Graf and H. R. Mühlemann, "Oral telemetry of fluoride ion activity.," *Archives of oral biology,* vol. 14, no. 3, pp. 259-IN3., 1969.

[69] J. Kim, G. Valdés-Ramírez, A. J. Bandodkar, W. Jia, A. G. Martinez, J. Ramírez and J. Wang, "Non-invasive mouthguard biosensor for continuous

salivary monitoring of metabolites.," *Analyst,* vol. 139, no. 7, pp. 1632-1636., 2014.

[70] M. S. Mannoor, H. Tao, J. D. Clayton, A. Sengupta, D. L. Kaplan, R. R. Naik and M. C. McAlpine, "Graphene-based wireless bacteria detection on tooth enamel.," *Nature communications,* vol. 3, p. 763, 2012.

[71] R. Piosik, R. Peper and W. Jansen, "The Centenary of the Glass Electrode.," *CHEMKON,* vol. 17, no. 1, pp. 19-24., 2010.

[72] A. A. Belyustin, "The centenary of glass electrode: from Max Cremer to FGK Baucke.," *Journal of Solid State Electrochemistry,* vol. 15, no. 1, pp. 47-65., 2011.

[73] F. G. Baucke, "Fundamental and applied electrochemistry at an industrial glass laboratory—an overview.," *Journal of Solid State Electrochemistry,* vol. 15, no. 1, pp. 23-46., 2011.

[74] M. J. Madou and S. R. Morrison, Chemical sensing with solid state devices, London: Elsevier, 1988.

[75] P. Bergveld, "Thirty years of ISFETOLOGY: What happened in the past 30 years and what may happen in the next 30 years," *Sensors and Actuators B: Chemical,* vol. 88, pp. 1-20, 2003.

[76] P. Bergveld, "Development of an ion-sensitive solid-state device for neurophysiological measurements.," *IEEE Transactions on Biomedical Engineering,* vol. 1, pp. 70-71, 1970.

[77] R. Stoop, "Understanding silicon nanowire field-effect transistors for biochemical sensing," *(Doctoral dissertation, University of Basel),* 2015.

[78] R. van Hal, "A general model to describe the electrostatic potential at electrolyte oxide interfaces," *Advances in Colloid and Interface Science,* vol. 69, pp. 31-62, 1996.

142

[79] R. van Hal, "A novel description of ISFET sensitivity with the buffer capacity and double-layer capacitance as key parameters," *Sensors and Actuators,* vol. 24, pp. 201-205, 1995.

[80] P. a. A. S. Bergveld, Analytical and biomedical applications of ion-selective field-effect transistors., Amsterdam : Elsevier, 1988.

[81] L. Shepherd and C. Toumazou, "Weak inversion ISFETs for ultra-low power biochemical sensing and real-time analysis.," *Sensors and Actuators B: Chemical,* vol. 107, no. 1, pp. 468-473., 2005.

[82] P. Georgiou and C. Toumazou, "ISFET characteristics in CMOS and their application to weak inversion operation.," *Sensors and Actuators B: Chemical,* vol. 143, no. 1, pp. 211-217., 2009.

[83] L. M. Shepherd and C. Toumazou, "A biochemical translinear principle with weak inversion ISFETs.," *IEEE Transactions on Circuits and Systems I: Regular Papers,* vol. 52, no. 12, pp. 2614-2619., 2005.

[84] S. Rigante, "Sensing with Advanced computing technology: fin field-effect transistors with high-k gate stack on bulk silicon.," *ACS nano,* vol. 9, no. 5, pp. 4872-4881, 2015.

[85] K. Rajendran and G. S. Samudra, "Modelling of transconductance-to-current ratio (gm/ID) analysis on double-gate SOI MOSFETs.," *Semiconductor science and technology,* vol. 15, no. 2, p. 139, 2000.

[86] J. P. Colinge and C. A. Colinge, Physics of semiconductor devices., Springer Science & Business Media., 2005.

[87] J. Bobacka, A. Ivaska and A. Lewenstam, "Potentiometric ion sensors.," *Chemical reviews,* vol. 108, no. 2, pp. 329-351., 2008.

[88] S. Rigante, High-K Dielectric FinFETs on Si-Bulk for Ionic and Biological Sensing Integrated Circuits. (Doctoral Dissertation), 2014.

[89] E. Accastelli, P. Scarbolo, T. Ernst, P. Palestri, L. Selmi and C. Guiducci, "Multi-wire tri-gate silicon nanowires reaching milli-pH unit resolution in one micron square footprint.," *Biosensors*, vol. 6, no. 1, p. 9, 2016.

[90] S. Holler, Label-Free Sensing., Basel: Shu-Kun Lin, 2016.

[91] J. S. Wright, W. Lim, D. P. Norton, S. J. Pearton, F. Ren, J. L. Johnson and A. Ural, "Nitride and oxide semiconductor nanostructured hydrogen gas sensors.," *Semiconductor Science and Technology*, vol. 25, no. 2, p. 024002, 2010.

[92] R. Yan, D. Gargas and P. Yang, "Nanowire photonics.," *Nature photonics*, vol. 3, no. 10, p. 569, 2009.

[93] V. F. Curto, C. Fay, S. Coyle, R. Byrne, C. O'Toole, C. Barry and F. Benito-Lopez, "Real-time sweat pH monitoring based on a wearable chemical barcode micro-fluidic platform incorporating ionic liquids.," *Sensors and Actuators B: Chemical*, vol. 171, pp. 1327-1334, 2012.

[94] S. C. Russell, G. Czerwieniec, C. Lebrilla, P. Steele, V. Riot, K. Coffee and E. E. Gard, "Achieving high detection sensitivity (14 zmol) of biomolecular ions in bioaerosol mass spectrometry.," *Analytical chemistry*, vol. 77, no. 15, pp. 4734-4741., 2005.

[95] P. Song, N. D. Hershey, O. S. Mabrouk, T. R. Slaney and R. T. Kennedy, "Mass spectrometry "sensor" for in vivo acetylcholine monitoring.," *Analytical chemistry*, vol. 84, no. 11, pp. 4659-4664., 2012.

[96] J. Zhang, H. P. Lang, F. Huber, A. Bietsch, W. Grange, U. Certa and C. Gerber, "Rapid and label-free nanomechanical detection of biomarker transcripts in human RNA.," *Nature nanotechnology*, vol. 1, no. 3, p. 214.

[97] T. P. Burg, M. Godin, S. M. Knudsen, W. Shen, G. Carlson, J. S. Foster and S. R. Manalis, "Weighing of biomolecules, single cells and single nanoparticles in fluid.," *Nature,* vol. 446, no. 7139, p. 1066, 2007.

[98] I. L. Medintz, A. R. Clapp, H. Mattoussi, E. R. Goldman, B. Fisher and J. M. Mauro, "Self-assembled nanoscale biosensors based on quantum dot FRET donors.," *Nature materials,* vol. 2, no. 9, p. 630, 2003.

[99] G. U. Lee, D. A. Kidwell and R. J. Colton, "Sensing discrete streptavidin-biotin interactions with atomic force microscopy.," *Langmuir,* vol. 10, no. 2, pp. 354-357., 1994.

[100] J. Kong, M. G. Chapline and H. Dai, "Functionalized carbon nanotubes for molecular hydrogen sensors.," *Advanced Materials,* vol. 13, no. 18, pp. 1384-1386., 2001.

[101] J. J. Gooding, "Nanostructuring electrodes with carbon nanotubes: A review on electrochemistry and applications for sensing," *Electrochimica Acta,* vol. 50, no. 15, pp. 3049-3060., 2005.

[102] A. J. Haes and R. P. Van Duyne, "A nanoscale optical biosensor: sensitivity and selectivity of an approach based on the localized surface plasmon resonance spectroscopy of triangular silver nanoparticles.," *Journal of the American Chemical Society,* vol. 124, no. 35, pp. 10596-10604, 2002.

[103] Y. Teramura and H. Iwata, "Label-free immunosensing for α-fetoprotein in human plasma using surface plasmon resonance.," *Analytical biochemistry,* vol. 365, no. 2, pp. 201-207., 2007.

[104] D. E. Yates, S. Levine and T. W. Healy, "Site-binding model of the electrical double layer at the oxide/water interface.," *Journal of the Chemical Society, Faraday Transactions 1: Physical Chemistry in Condensed Phases.,* vol. 70, pp. 1807-1818., 1974.

[105] A. van den Berg, P. Bergveld, D. N. Reinhoudt and E. J. Sudhölter, "Sensitivity control of ISFETs by chemical surface modification.," *Sensors and Actuators,* vol. 8, no. 2, pp. 129-148., 1985.

[106] A. Tarasov, M. Wipf, R. L. Stoop, K. Bedner, W. Fu, V. A. Guzenko and C. Schönenberger, "Understanding the electrolyte background for biochemical sensing with ion-sensitive field-effect transistors.," *ACS nano,* vol. 6, no. 10, pp. 9291-9298, 2012.

[107] H. J. Modi and D. W. Fuerstenau, "Streaming Potential Studies on Corundum in Aqueous Solutions of Inorganic Electrolytes," *J. Phys. Chem. ,* vol. 61, p. 640– 643, 1957.

[108] R. J. Hunter and H. J. L. Wright, "The Dependence of Electrokinetic Potential on Concentration of Electrolyte," *J. Colloid Interface Sci.,* vol. 37, p. 564– 580, 1971.

[109] C.-P. Huang and W. Stumm, "Specific Adsorption of Cations on Hydrous γ-Al2O3," *J. Colloid Interface Sci. ,* vol. 43, p. 409– 420, 1973.

[110] R. E. Sprycha, "Double Layer at Alumina/Electrolyte Interface," *J. Colloid Interface Sci.,* vol. 127, p. 1– 11, 1989.

[111] S. B. Johnson, P. J. Scales and T. W. Healy, "The Binding of Monovalent Electrolyte Ions on α-Alumina. I. Electroacoustic Studies at High Electrolyte Concentrations," *Langmuir,* vol. 15, p. 2836– 2843, 1999.

[112] M. Kosmulski, "Confirmation of the Differentiating Effect of Small Cations in the Shift of the Isoelectric Point of Oxides at High Ionic Strengths," *Langmuir,* vol. 18, p. 785– 787, 2002.

[113] F. G. K. Baucke, "Fundamental and Applied Electrochemistry at an Industrial Glass Laboratory—An Overview," *J. Solid State Electrochem.* , vol. 15, p. 23– 46, 2011.

[114] C. D. Fung, P. W. Cheung and W. H. A. Ko, "Generalized Theory of an Electrolyte-Insulator-Semiconductor Field-Effect Transistor," *IEEE Trans. Electron Devices* , vol. 33, p. 8– 18, 1986.

[115] L. Bousse, N. F. de Rooij and P. Bergveld, "Operation of Chemically Sensitive Field-Effect Sensors as a Function of the Insulator-Electrolyte Interface," *IEEE Trans. Electron Devices* , vol. 30, p. 1263– 1270, 1983.

[116] J. A. Davis, R. O. James and J. O. Leckie, "Surface ionization and complexation at the oxide/water interface: I. Computation of electrical double layer properties in simple electrolytes.," *Journal of colloid and interface science*, vol. 63, no. 3, pp. 480-499., 1978.

[117] J. &. H. H. Westall, "A comparison of electrostatic models for the oxide/solution interface.," *Advances in Colloid and Interface Science*, vol. 12, no. 4, pp. 265-294., 1980.

[118] E. Stern, R. Wagner, F. J. Sigworth, R. Breaker, T. M. Fahmy and M. A. Reed, "Importance of the Debye screening length on nanowire field effect transistor sensors.," *Nano letters*, vol. 7, no. 11, pp. 3405-3409, 2007.

[119] J. Janata, "Chemical sensors," *Analytical Chemistry*, vol. 64, no. 12, pp. 196-219, 1992.

[120] J. Robertson, "High dielectric constant oxides.," *The European Physical Journal-Applied Physics*, vol. 28, no. 3, pp. 265-291, 2004.

[121] J. Robertson, "Band offsets of wide-band-gap oxides and implications for future electronic devices.," *Journal of Vacuum Science & Technology B:*

Microelectronics and Nanometer Structures Processing, Measurement, and Phenomena, vol. 18, no. 3, pp. 1785-1791., 2000.

[122] G. Brezeanu, M. Brezeanu and F. & Bernea, "High-K Dielectrics in Nano & Microelectronics.," Nat'l Seminar of Nanoscience & Nanotechnology, 2010.

[123] E. Buitrago, G. Fagas, M. F. B. Badia, Y. M. Georgiev, M. Berthomé and A. M. Ionescu, "Junctionless silicon nanowire transistors for the tunable operation of a highly sensitive, low power sensor.," *Sensors and Actuators B: Chemical,* vol. 183, pp. 1-10., 2013.

[124] M. Gutowski, J. E. Jaffe, C. L. Liu, M. Stoker, R. I. Hegde, R. S. Rai and P. J. Tobin, "Thermodynamic stability of high-K dielectric metal oxides ZrO 2 and HfO 2 in contact with Si and SiO 2.," *Applied Physics Letters,* vol. 80, no. 11, pp. 1897-1899., 2002.

[125] S. Chen, J. G. Bomer, E. T. Carlen and A. van den Berg, "Al2O3/silicon nanoISFET with near ideal Nernstian response.," *Nano letters,* vol. 11, no. 6, pp. 2334-2341, 2011.

[126] S. D. Zafar, C. Emic, A. Afzali, B. Fletcher, Y. Zhu and T. (. Ning, "Optimization of pH sensing using silicon nanowire field effect transistors with HfO2 as the sensing surface.," *Nanotechnology,* vol. 22, no. 40, pp. 405-501, 2011.

[127] R. E. G. Van Hal, E. J. C. and P. Bergveld, "A novel description of ISFET sensitivity with the buffer capacity and double-layer capacitance as key parameters.," *Sensors and Actuators B: Chemical,* vol. 24, no. 1-3, pp. 201-205., 1995.

[128] S. Kim, T. Rim, K. Kim, U. Lee, E. Baek, H. Lee and J. S. Lee, "Silicon nanowire ion sensitive field effect transistor with integrated Ag/AgCl

148

electrode: pH sensing and noise characteristics.," *Analyst,* vol. 136, no. 23, pp. 5012-5016., 2011.

[129] T. Rim, K. Kim, N. K. W. Hong, C. K. Baek, S. Jeon and J. S. Lee, "Investigation of the electrical stability of Si-nanowire biologically sensitive field-effect transistors with embedded Ag/AgCl pseudo reference electrode.," *RSC Advances,* vol. 3, no. 21, pp. 7963-7969, 2013.

[130] M. G. Nikolaides, S. Rauschenbach and A. R. Bausch, "Characterization of a silicon-on-insulator based thin film resistor in electrolyte solutions for sensor applications.," *Journal of applied physics,* vol. 95, no. 7, pp. 3811-3815., 2004.

[131] Y. H. Kim and J. C. (. Lee, "Hf-based high-k dielectrics: process development, performance characterization, and reliability.," *Synthesis Lectures on Solid State Materials and Devices,* vol. 1, no. 1, pp. 1-92., 2006.

[132] F. Bellando, E. Garcia-Cordero, F. Wildhaber, J. Longo, H. Guérin and A. M. Ionescu, "Lab on skin™: 3D monolithically integrated zero-energy micro/nanofludics and FD SOI ion sensitive FETs for wearable multi-sensing sweat applications," *Electron Devices Meeting (IEDM) ,* vol. 1, no. 4, pp. 1-18, 2017.

[133] J. P. Colinge, 2008, New York: Springer, FinFETs and other multi-gate transistors .

[134] J. H. Ahn, J. Y. Kim, M. L. Seol, D. J. Baek, Z. Guo, C. H. Kim and Y. K. Choi, "A pH sensor with a double-gate silicon nanowire field-effect transistor.," *Applied Physics Letters,* vol. 102, no. 8, p. 083701, 2013.

[135] N. KV and e. al, "In vitro and in vivo evaluation of SU-8 biocompatibility.," *Materials Science and Engineering: C,* vol. 33, no. 7, pp. 4453-4459, 2013.

[136] M. Zimmerman, "Valves for autonomous capillary systems," *Microfluidics and Nanofluidics,* vol. 5, no. 3, pp. 395-402, 2008.

[137] R. Safavieh and D. Juncker, "Capillarics: pre-programmed, self-powered microfluidic circuits built from capillary elements," *Lab on a Chip,* no. 13, pp. 4180-4189, 2013.

[138] H. Bruss, Theoretical microfluidics, Oxford: Oxford University Press, 2008.

[139] P. G. de Gennes, "Wetting: statics and dynamics," *American Physical Society,* vol. 57, no. 3, 1985.

[140] D. Juncker, "Autonomous Microfluidic Capillary System," *Anal. Chem. ,* no. 74, pp. 6139-6144, 2002.

[141] J. Won Suk, "Capillary flow control using hydrophobic patterns," *Journal of micromechanics and microengineering,* no. 17, pp. 11-15, 2007.

[142] E. Delamarche, J. D. and S. H., "Microfluidics for Processing Surfaces and Miniaturizing Biological Assays," *Advanced Materials,* no. 17, pp. 2911-2933, 2005.

[143] J. L. Garcia-Cordero, L. Basabe-Desmonts, J. Ducrée and A. J. Ricco, "Liquid recirculation in microfluidic channels by the interplay of capillary and centrifugal forces.," *Microfluidics and nanofluidics,* vol. 9, no. 4-5 , pp. 695-703., 2010.

[144] E. W. Washburn, "The dynamics of capillary flow.," *Physical review,* vol. 17, no. 3, p. 273., 1921.

[145] F. 9. Bellando, Design and realization of a microfluidic capillary channel for zero power delivery of sweat to a pH sensing chip (Master's thesis)., Politecnico di Torino, Torino, Italy., 2015.

[146] A. Vorobyev and C. Guo, "Direct femtosecond laser surface nano/microstructuring and its applications," *Laser & photonics reviews,* vol. 7, no. 3, pp. 385-407, 2012.

[147] F. Benito-Lopez and D. Diamond, "Pump less wearable microfluidic device for real time pH sweat monitoring.," *Procedia Chemistry,* vol. 1, no. 1, pp. 1103-1106, 2009.

[148] J. R. Philip, "The theory of infiltration: 4. Sorptivity and algebraic infiltration equations," *Soil science,* vol. 84, no. 3, pp. 257-264, 1957.

[149] K. Y. Lee, "Micromachining applications of a high resolution ultrathick photoresist," *Journal of Vaccum Science & Technology,* pp. 3012-3016, 1995.

[150] A. Bertsch and P. Renaud, "Special Issue: 15 years of SU8 as MEMS Material," *micromachines,* vol. 6, pp. 790-792, 2015.

[151] M. J. Madou, Fundamentals of microfabrication, CRC Press, 2002.

[152] P. Maoddi, "SU-8 as a material for microfabricated particle physics detectors," *Micromachines,* vol. 5, no. 3, pp. 594-606, 2014.

[153] C. Lee and e. al, "Sidewall roughness characterization," *Materials Characterization,* vol. 58, pp. 603-609, 2007.

[154] J. Melai and e. al., "The electrical conduction and dielectric strength," *Journal of Micromechanics and Microengineering,* vol. 19, 2009.

[155] L. Gervais, "Capillary Microfluidic Chips for Point-of-Care Testing: from Research Tools to Decentralized Medical Diagnostics," *(Doctoral dissertation, EPFL),* 2011.

[156] D. Laser, "A review of micropumps," *Journal of micromechanics and microengineering,* vol. 14, no. 6, p. R35, 2004.

[157] M. Zimmermann and e. al, "Capillary pumps for autonomous capillary systems," *Lab on a Chip*, no. 7, pp. 119-125, 2007.

[158] L. Gervais, M. Hitzbleck and E. Delamarche, "Capillary-driven multiparametric microfluidic chips for one-step immunoassays.," *Biosensors and Bioelectronics*, vol. 27, no. 1, pp. 64-70., 2011.

[159] V. Jokinen, "Microstructured surfaces for directional wetting," *Advanced Materials*, vol. 21, no. 47, pp. 4835-4838, 2009.

[160] P. Maoddi, "SU-8 as a material for microfabricated particle physics detectors," *Micromachines*, vol. 5, no. 3, pp. 594-606, 2014.

[161] G.-C. E., W. F., B. F., L. J, F. B. M, G. H. and I. A. M., "Embedded passive nano-liter micropump for sweat collection and analysis," in *IEEE Micro Electro Mechanical Systems (MEMS)*, Belfast, 2018.

[162] A. Ulman, An Introduction into Ultrathin Organic Films, San Diego, CA: Academic Press, 1991.

[163] J. J. Hickman, D. Ofer, P. E. Laibinis, G. M. Whitesides and M. S. Wrighton, "Molecular self-assembly of two-terminal, voltammetric microsensors with internal references," *Science*, vol. 252, no. 5006, pp. 688-691., 1991.

[164] I. Willner, M. Lion-Dagan, S. Marx-Tibbon and E. Katz, "Bioelectrocatalyzed amperometric transduction of recorded optical signals using monolayer-modified Au-electrodes1.," *Journal of the American Chemical Society*, vol. 117, no. 24, pp. 6581-6592., 1995.

[165] S. Flink, F. C. J. M. van Veggel and D. N. Reinhoudt, "Recognition of cations by self-assembled monolayers of crown ethers.," *J. Phys. Chem. B*, vol. 103, pp. 6515-6520; , 1999.

[166] L. Sun, R. M. Crooks and A. J. Ricco, "Molecular interactions between organized, surface-confined monolayers and vapor-phase probe molecules. 5. Acid-base interactions.," *Langmuir,* vol. 9, no. 7, pp. 1775-1780., 1993.

[167] J. Spinke, M. Liley, F. J. Schmitt, H. J. Guder, L. Angermaier and W. Knoll, "Molecular recognition at self-assembled monolayers: Optimization of surface functionalization.," *The Journal of Chemical Physics,* vol. 99, no. 9, pp. 7012-7019., 1993.

[168] K. Motesharei and D. C. Myles, "Molecular recognition on functionalized self-assembled monolayers of alkanethiols on gold.," *Journal of the American Chemical Society,* vol. 120, no. 29, pp. 7328-7336., 1998.

[169] I. Rubinstein, S. Steinberg, Y. Tor, A. Shanzer and J. & Sagiv, "Ionic recognition and selective response in self-assembling monolayer membranes on electrodes. ,," *Nature,* vol. 332, no. 6163, p. 426., 1988.

[170] G. G. Ting, O. Acton, H. Ma, J. W. Ka and A. K. Y. Jen, "Study on the Formation of Self-Assembled Monolayers on Sol– Gel Processed Hafnium Oxide as Dielectric Layers.," *Langmuir,* vol. 25, no. 4, pp. 2140-2147., 2009.

[171] G. J. Zhang, A. Agarwal, K. D. Buddharaju, N. Singh and Z. Gao, "Highly sensitive sensors for alkali metal ions based on complementary-metal-oxide-semiconductor-compatible silicon nanowires.," *Applied physics letters,* vol. 90, no. 23, p. 233903, 2007.

[172] M. Wipf, Chemical and Biochemical Sensors Based on Silicon Nanowire Field-Effect Transitor Arrays (Doctoral Dissertation)), Basel , 2014.

[173] D. Y. Petrovykh, H. Kimura-Suda, A. Opdahl, L. J. Richter, M. J. Tarlov and L. J. Whitman, "Alkanethiols on platinum: Multicomponent self-assembled monolayers.," *Langmuir ,* vol. 22, pp. 2578-2587, 2006.

[174] M. A. F. Addato, A. A. Rubert, G. A. Benitez, M. H. Fonticelli, J. Carrasco, P. Carro and R. C. Salvarezza, "Alkanethiol Adsorption on Platinum: Chain Length Effects on the Quality of Self-Assembled Monolayers.," *J. Phys. Chem. C* , vol. 115, pp. 17788-17798, 2011.

[175] J. Zhu, Y. Qin and Y. Zhang, "Preparation of all solid-state potentiometric ion sensors with polymer-CNT composites.," *Electrochemistry Communications,* vol. 11, no. 8, pp. 1684-1687., 2009.

[176] E. Bakker and E. Pretsch, "Nanoscale potentiometry.," *TrAC Trends in Analytical Chemistry,* vol. 27, no. 7, pp. 612-618., 2008.

[177] M. Fibbioli, W. E. Morf, M. Badertscher, N. F. de Rooij and E. Pretsch, "Potential drifts of solid-contacted ion-selective electrodes due to zero-current ion fluxes through the sensor membrane.," *Electroanalysis: An International Journal Devoted to Fundamental and Practical Asptects of Electroanalysis,* vol. 12, no. 16, pp. 1286-1292, 2000.

[178] S. D. Moss, J. Janata and C. C. Johnson, "Potassium ion-sensitive field effect transistor.," *Analytical Chemistry,* vol. 47, no. 13, pp. 2238-2243., 1975.

[179] A. J. Bard and L. R. .. Faulkner, ELECTROCHEMICAL METHODS: Fundamentals and applications, Phoenix, USA: Wiley, 2001.

[180] P. Bergveld and A. Sibbald, Analytical and Biomedical Applications of Ion-Sensitive Field-Effect Transistors., Amsterdam: Elsevier, 1988.

[181] T. Matsumoto, a. Ohashi and N. Ito, "Development of a micro-planar Ag/AgCl quasi-reference electrode with long-term stability for an amperometric glucose sensor.," *Analytica Chimica Acta,* vol. 462, no. 2, p. 253–259. , 2002.

[182] M. Waleed Shinwari, D. Zhitomirsky, I. a. Deen, P. R. Selvaganapathy, M. Jamal Deen and D. Landheer, "Microfabricated reference electrodes and their biosensing applications.," *Sensors,* vol. 10, no. 3, p. 1679–1715. , 2010.

[183] P. R. Griffiths, "Standard hydrogen electrode challenge.," *Analytical and Bioanalytical Chemistry,* vol. 392, no. 1-2, p. 9–10. , 2008.

[184] U. Guth, F. Gerlach, M. Decker, W. Oelßner and W. Vonau, "Solid-state reference electrodes for potentiometric sensors.," *Journal of Solid State Electrochemistry,* vol. 13, no. 1, p. 27–39, 2009.

[185] G. Gritzner, "Reference Redox Systems in Nonaqueous Systems and the Relation of Electrode Potentials in Nonaqueous and Mixed Solvents to Standard Potentials in Water," in *Handbook of Reference Electrodes*, Berlin, Springer, 2013, pp. 25-31.

[186] J. Ghilene, P. Haplot and A. J. Bard, "Metal/polypyrrole quasi-reference electrode for voltammetry in nonaqueous and aqueous solutions.," *Analytical Chemistry,* vol. 78, no. 19, p. 6868–6872, 2006.

[187] H. Suzuki, T. Hirakawa, S. Sasaki and I. Karube, "Micromachined liquid-junction Ag / AgCl reference electrode," *Sensors and Actuators B,* vol. 46, p. 146–154., 1998.

[188] B. J. Polk, A. Stelzenmuller, G. Mijares, W. MacCrehan and M. .. Gaitan, "Ag/AgCl microelectrodes with improved stability for microfluidics.," *Sensors and Actuators, B: Chemical,* vol. 114, no. 1, p. 239–247. , 2006.

[189] J. Zhou, K. Ren, Y. Zheng, J. Su, Y. Zhao, D. Ryan and H. & Wu, "Fabrication of a microfluidic Ag/AgCl reference electrode and its application for portable and disposable electrochemical microchips.," *Electrophoresis,* vol. 31, no. 18, pp. 3083-3089, 2010.

[190] A. Mroz, "Disposable reference electrode.," *The Analyst,* vol. 123, no. 6, p. 1373–1376., 1998.

[191] J. S. Lee, S. D. Lee, G. Cui, H. J. Lee, J. H. Shin, G. S. Cha and H. Nam, "Hydrophilic Polyurethane Coated Silver/Silver Chloride Electrode for the Determination of Chloride in Blood.," *Electroanalysis,* vol. 11, no. 4, p. 260–267. , 1999.

[192] M. a. Nolan, S. H. Tan and S. P. Kounaves, "Fabrication and Characterization of a Solid State Reference Electrode for Electroanalysis of Natural Waters with Ultramicroelectrodes.," *Analytical Chemistry*, vol. 69, no. 6, p. 1244–1247. , 1997.

[193] Y. C. Tang and A. J. Davenport, "Magnetic field effects on the corrosion of artificial pit electrodes and pits in thin films.," *Journal of the Electrochemical Society,* vol. 154, no. 7, pp. C362-C370., 2007.

[194] E. Garcia-Cordero, "Ultra-Low Power Ion-Sensing Smart Platform for Noninvasive Healthcare Applications," in *Smart Systems Applications*, Munich, 2016.

[195] X. Xu, "Effect of chromium intermediate layer on properties of silver coatings.," *Optical Engineering,* vol. 43, no. 4, p. 971, 2004.

[196] G. J. and K. J.K., "Effects of surface treatments on the adhesion of Cu and Cr/Cu metallizations to a multifunctional photoresist.," *J. Appl. Phys,* vol. 92, p. 3007–3015, 2002.

[197] M. Nordström, A. Johansson, E. S. Noguerón, B. Clausen, M. Calleja and A. Boisen, "Investigation of the bond strength between the photo-sensitive polymer SU-8 and gold.," *Microelectronic Engineering,,* Vols. 78-79, no. (1-4), p. 152–157, 2005.

[198] E. Garcia-Cordero, H. Guerin, A. Muhech, F. Bellando and A. M. & Ionescu, "Heterogeneous integration of low power pH FinFET sensors with passive capillary microfluidics and miniaturized Ag/AgCl quasi-Reference Electrode.," *European Solid-State Devide Research Conference (ESSDERC)*, pp. 452-455, 2016.

[199] F. Bellando, E. Garcia-Cordero, F. Wildhaber, J. Longo, H. Guérin and A. M. Ionescu, "Lab on skin™: 3D monolithically integrated zero-energy micro/nanofludics and FD SOI ion sensitive FETs for wearable multi-sensing sweat applications," in *IEDM*, San Francisco, USA, 2017.

[200] N. Aliakbarinodehi, P. Jolly, N. Bhalla, A. Miodek, G. De Micheli, P. Estrela and S. Carrara, "Aptamer-based Field-Effect Biosensor for Tenofovir Detection.," *Scientific reports*, vol. 7, p. 44409, 2017.

[201] M. O. E. Ahmed, C. X. Li and W. K. Leong, "Luminescent silver nanoparticles stabilised by a crown ether capped with an organometallic cluster.," *J. Organomet. Chem.*, vol. 692, pp. 3474-3478., 2007.

[202] L. Sun, L. J. Kepley and R. M. Crooks, "Molecular interactions between organized, surface-confined monolayers and vapor-phase probe molecules: hydrogen-bonding interactions.," *Langmuir*, vol. 8, no. 9, pp. 2101-2103., 1992.

[203] T. Matsumoto, a. Ohashi and N. Ito, "Development of a micro-planar Ag/AgCl quasi-reference electrode with long-term stability for an amperometric glucose sensor.," *Analytica Chimica Acta*, vol. 462, no. 2, p. 253–259. , 2002.

[204] W. Shinwari, Z. D. M., I. a. Deen, P. R. Selvaganapathy, M. Jamal Deen and D. Landheer, "Microfabricated reference electrodes and their biosensing applications.," *Sensors*, vol. 10, no. 3, p. 1679–1715. , 2010.

[205] U. Guth, F. Gerlach, M. Decker, W. Oelßner and W. Vonau, "Solid-state reference electrodes for potentiometric sensors.," *Journal of Solid State Electrochemistry,* vol. 13, no. 1, p. 27–39, 2009.

[206] M. Waleed Shinwari, D. Zhitomirsky, I. a. Deen, P. R. Selvaganapathy, M. Jamal Deen and D. Landheer, "Microfabricated reference electrodes and their biosensing applications.," *Sensors,* vol. 10, no. 3, p. 1679–1715., 2010.

[207] Z. Sonner, E. Wilder, J. Heikenfeld, G. Kasting, F. Beyette, D. Swaile and R. Naik, "The microfluidics of the eccrine sweat gland, including biomarker partitioning, transport, and biosensing implications.," *Biomicrofluidics,* vol. 9, no. 3, p. 031301., 2015.

[208] R. Rushmer, K. J. K, J. Buettner-Short and G. Odland, "The Skin.," *Science,* vol. 154, no. 3747, pp. 343-348., 1966.

[209] I. Y. Huang, R. S. Huang and L. H. Lo, "Improvement of integrated Ag/AgCl thin-film electrodes by KCl-gel coating for ISFET applications.," *Sensors and Actuators, B: Chemical,* vol. 94, no. 1, p. 53–64., 2003.

Erick Antonio García-Cordero

Electronics and Computer Engineer, DOB 29.06.1990
Chemin du Stade 1, CH-1007 Lausanne, Switzerland
Cell Ph. +41 78 783 3731
erickgc@gmail.com

Skills

- Versatile experience in different phases of product development for the wearable technology sector: research, development, manufacturing, validation and quality assurance, technical documentation, project management.
- Expertise in industrialization and heterogeneous integration of biomedical systems to enable healthcare products.
- Experienced with Project Management. (B2B & B2C) Stakeholder and customer management experienced.
- Solid analytical skills for problem solving, and excellent communication skills. Fast learner, excellent for working under pressure.
- Experienced in multicultural environments. Collaborated and worked for/with people from different regions of the world such as America, LATAM, Western/Eastern Europe, Middle East, India & China.

Experience

R&D Engineer   **April 2014 - August 2018**
EPFL-Nanolab / XSensio   **Lausanne, Switzerland**

- Development of a state-of-the-art wearable device for Healthcare applications. The development considers biocompatibility of the product and beyond, aiming to have a Human-Centered Design to create a product attractive to the market, investors and to the potential customers.

Project Manager   **July 2013 - April 2014**
Cisco Systems   **Mexico City, Mexico**

- Performed Project Manager and Business Analyst tasks for Central and South US Enterprise Area of Cisco Systems. Revenue under my supervision reached 4M USD per quarter. Main clients in Atlanta, GA, Houston, TX and Chicago, IL.
- Development of the Service Catalog for the Project Specialist Role of Mexico's GSP team. Development of a Business plan to optimize the use of Project Management resources across the GSP groups of Bangalore, Dalian and Mexico.
- Identification of potential revenue pull in and analyzed the cost of several accounts to maximize the profit margin (+100 active projects). Responsible for accurate cost and revenue forecasting.

Education

Doctoral Program in Microelectronics and Microsystems   **April 2014 - August 2018**
École Polytechnique Fédéral de Lausanne   **Lausanne, Switzerland**

Nanoelectronic Devices Laboratory, *Mentor: Prof. Adrian M. Ionescu*

Thesis Topic: Ultra-Low Power Ion-Sensing Smart Platform for Noninvasive Healthcare Applications

- Development of miniaturized point of care devices with polymeric substrates, for on-chip integration with a sweat pH wearable sensor. The sweat pH sensing system is to be incorporated to a physiological parameter sensing system. Main activities include research on materials and fabrication protocols in clean room, microfluidic design, electronic design, and integration of technology to the IoE.
- Results: Several demos & prototypes presented to stakeholders & investors, 4 conference papers and a US patent (pending).

Master Thesis for Exchange Students   **May-December 2011**
École Polytechnique Fédéral de Lausanne   **Lausanne, Switzerland**

Laboratory of Nanoscale Biology, *Mentor: Prof. Aleksandra Radenovic*

Thesis Topic: Software for Nanopore Signals

- Development of a computer program to analyze nanopore translocation experiments using a statiscal algorithm for abrupt change detection. Algorithm allowed automated detection of RNA-p in DNA strands.
- Research resulted in a publication in the Nanoletters journal.

BS Electronic and Computer Engineering   **August 2008 - May 2013**
Tecnológico de Monterrey (ITESM-CEM)   **Atizapán, México**

- *Student projects:* Certified Associate Project Management Training. Designed and developed a smart car for a Freescale contest (3rd place). Designed and fabricated a digital clock and a bank token display for a Mexican NGO that helps people with intellectual disability. Designed and implemented a network for monitoring the humidity and temperature of a greenhouse for a Mexican NGO that aids kids with Downs syndrome.

Additional Experience

Summer internship, Research Assistant   **Summer 2009**
Dublin City University   **Dublin, Ireland**

National Centre for Sensor Research, *Mentor: Dr. Stephen O'Driscoll*

○ Development of a software algorithm embedded in a cellphone program to read the color of a litmus paper (pH paper) to deliver diagnoses depending on pH levels of a biological buffer.

Technical Skills

○ **Micro & Nanoelectronics:** Device fabrication in Cleanroom (ISO 5,6,7). Experience in photolitograhy, thin-film deposition, etching, packaging (full SU-8 devices, PDMS line).

○ **Electronics:** Analog and digital electronics. Hardware design and implementation. Microsystem design experienced for wearable products. Focused in ultra-low power consumption, miniaturization and cost optimization. Experienced with flexible electronics.

○ **Lab Automation:** LabVIEW programming to enable automatized characterization of ISFET devices. Electro-chemical measurement setup design.

○ **Analytical Methods:** Image and signal processing (Matlab), Scanning Electron Microscopy (Zeiss LEO & Merlin).

○ **Software Programming:** iOS programming (iPhone/iPad), LabVIEW, Matlab, C, CISCO Packet Tracer, UNIX.

Professional Certifications

Cisco Systems   **September 2013**
Cisco Certified Network Associate   **Atizapán, México**

National Instruments   **November 2012**
Certified LabVIEW Associate Developer   **Atizapán, México**

IBM   **October 2012**
Embedded System Design with IBM Rational Rhapsody   **Atizapán, México**

Awards/Honours/Achievements

○ 2017, Lausanne, Switzerland - Winner, Comission for Technology and Innovation, Swiss Confederation - CTI Entrepreneurship Training, CLEX start-up Business Development.
"CLEX is a start-up that provides an innovative hydrogel technology enabling fine control of gelation with stable pH and temperature conditions, allowing inexpensive and scalable high tech applications in microfluidics, 3D bio-printing, and injectables"

○ 2016, Lausanne, Switzerland - Chief of Staff in the European Solid-State Circuits Conference. Leader of 40 volunteers. Responsible for the organization of the staff and perfect execution of their tasks. Close to 1,000 people attended the conference.

○ 2013, Mexico City, Mexico - Cisco Systems, 2 Cisco Achievement Program Awards for performance.

Languages

Spanish, native speaker. *English*, fluent (TOEFL, 101 points, 2014). *French*, fluent. *Italian*, advanced. *German*, A1.

Publications

Journal papers:

1. Raillon, C., Cousin, P., Traversi, F., <u>Garcia-Cordero, E</u>., Hernandez, N., & Radenovic, A. (2012). Nanopore detection of single molecule RNAP–DNA transcription complex. Nano letters, 12(3), 1157-1164.

Conference papers:

1. Zhang, J., <u>Garcia-Cordero E</u>., Bellando F., Wildhaber F., Longo J., Ebejer, N., Guerin H., Ionescu A. M., "CMOS compatible energy autonomous wearable sensor system for in situ sweat analysis," to be presented in *2018 Micro and Nano Engineering (MNE)*, Copenhagen.

2. Zhang, J., Bellando F., Rupakula, M., <u>Garcia-Cordero E</u>., Ebejer, N., Longo J. , Wildhaber F., Guerin H., Ionescu A. M., "CMOS 3D-Extended Metal Gate ISFETs with Near Nernstian Ion Sensitivity," to be presented in *2018 Device Research Conference (DRC)*, Santa Barbara.

3. <u>Garcia-Cordero E</u>., Wildhaber F., Bellando F., Longo J. Fernandez Bolanos M. Guerin H., Ionescu A. M., "Embedded passive nano-liter micropump for sweat collection and analysis," *2018 IEEE Micro Electro Mechanical Systems (MEMS)*, Belfast, 2018, pp. 1217-1220.

4. Bellando F, <u>Garcia-Cordero E.</u>, Wildhaber F., Longo J., Guérin H. and Ionescu A. M., "Lab on skin™: 3D monolithically integrated zero-energy micro/nanofluidics and FD SOI ion sensitive FETs for wearable multi-sensing sweat applications," *2017 IEEE International Electron Devices Meeting (IEDM)*, San Francisco, CA, 2017, pp. 18.1.1-18.1.4.

5. <u>Garcia-Cordero, E</u>., Guerin, H., Muhech, A., Bellando, F., & Ionescu, A. M. (2016, September). Heterogeneous integration of low power pH FinFET sensors with passive capillary microfluidics and miniaturized Ag/AgCl quasi-Reference

Electrode. In *Solid-State Device Research Conference (ESSDERC), 2016 46th European* (pp. 452-455).

6. Garcia-Cordero, E., Guérin, H. M., Muhech, A., Bellando, F., & Ionescu, M. A. (2016). Ultra-Low Power Ion-Sensing Smart Platform for Noninvasive Healthcare Applications. In Smart Systems Applications (No. EPFL-CONF-221663).

Patents

1. M. A. Ionescu, H. M. Guerin, E. Garcia-Cordero, F. Bellando. (2017) Capillary flow device for bio-fluid collection with semiconductor sensors, PCT Application No. PCT/IB2017/055456

2. M. A. Ionescu, H. M. Guerin, E. Garcia-Cordero, Wildhaber F., Longo J. , F. Bellando (2018) Apparatus for non-invasive sensing of biomarkers in human sweat, US Patent Application No. 15/913714

3. M. A. Ionescu, Zhang J., E. Garcia-Cordero, Bellando F. (2018). Field effect transistor device and method for sensing ions and biomarkers in a fluid. U.S. Patent Application No 62/688,413